



City Research Online

City, University of London Institutional Repository

Citation: Hosseinpour, A. (2018). An investigation into electric supercharging for emission reduction by means of engine downsizing. (Unpublished Doctoral thesis, City, University of London)

This is the accepted version of the paper.

This version of the publication may differ from the final published version.

Permanent repository link: <https://openaccess.city.ac.uk/id/eprint/19787/>

Link to published version:

Copyright: City Research Online aims to make research outputs of City, University of London available to a wider audience. Copyright and Moral Rights remain with the author(s) and/or copyright holders. URLs from City Research Online may be freely distributed and linked to.

Reuse: Copies of full items can be used for personal research or study, educational, or not-for-profit purposes without prior permission or charge. Provided that the authors, title and full bibliographic details are credited, a hyperlink and/or URL is given for the original metadata page and the content is not changed in any way.

City University of London



**An investigation into electric supercharging for emission reduction by means
of engine downsizing**

by
Amir Hosseinpour

A thesis submitted for the degree of
Doctor of Philosophy of the University of London
2018

Academic supervisors:

Professor Keith Pullen

Dr Maria Tomas-Rodriguez

Industrial supervisor:

Mr Alessandro Renna (AVL)

Dr Alex Darlington (AVL)

School of Mathematics, Computer Science and Engineering

ABSTRACT

This thesis describes an investigation into the operation and performance of internal combustion engines boosted by an electric supercharger (eSC) in combination with a turbocharger.

Engine downsizing offers one of the most effective ways to meet increasingly demanding CO₂ reduction targets set for the automotive vehicles. The addition of a turbocharger has enabled significant downsizing but the loss of torque at low engine speeds remains a key barrier to further downsizing. A known solution to this problem is to additionally boost the engine using a supercharger. However, until recently, this was very difficult to implement economically on engines with modest engine power suitable for small to medium sized vehicles due to the low air mass flow rates for such engines. Now, a new turbo-machinery innovation, the high forward swept TurboClaw compressor, allows significant boosting to be done at low flow rates yet with moderate compressor shaft speeds.

Since this compressor can be driven at a moderate speeds, the electric motor which drives for the electric supercharger (eSC) is more affordable. The research objective was to assess this new eSC system by means of a theoretical and experimental investigation.

There are two possible combinations in terms of whether the (eSC) goes before the turbocharger (ETC), or after (TEC). Employing the eSC after turbocharger generally has the advantage of broadening the eSC map, towards higher-mass flows since a denser air exits the turbo-compressor as the turbocharger provides boosted air to the system. This augments the overlap of the two operating maps for the two devices. However the real benefit of eSC in each layout depends on the engine (baseline). In this research ETC and TEC produce basically the same

torque increase; the real eSC benefit is at low speed where the nominal maximum torque is recovered for all the range. However since the current drawn from the battery is a key factor for this application, the investigation shows that the thermodynamic power requested by eSC is less than 1.5kW for ETC layout while this value is 2.5kW for TEC layout. Therefore ETC layout was chosen as the final configure to be implemented on the selected vehicle for the dyno test purposes since it requires less power.

Theoretical models for the engine, turbocharger and TurboClaw eSC including electric motor were created and validated. The system of all components was designed including control system and strategy. A key result showed that the eSC was found to boost the torque of a 1.0 litre turbocharged engine by 125% and 58% for 1000 rpm and 1200 rpm respectively.

ACKNOWLEDGEMENTS

Firstly, I would like to express my sincere gratitude to my supervisor Prof. Keith Pullen for the continuous support of my Ph.D study and related research, for his patience, motivation, and immense knowledge. His guidance helped me in all the time of research and writing of this thesis. I could not have imagined having a better advisor and mentor for my Ph.D study.

My sincere thanks also go to Mr Alessandro Renna, Dr Alex Darlington and Dr Shahram Etemad. Without their precious support it would not be possible to conduct this research.

Last but not the least, I would like to thank my family for supporting me spiritually throughout writing this thesis and my my life in general.

TABLE OF CONTENTS

ABSTRACT	ii
ACKNOWLEDGEMENTS	v
LIST OF FIGURES	xi
LIST OF ABBREVIATIONS.....	xix
CHAPTER 1	21
1 Introduction.....	21
1.1 The emission challenge and downsizing	21
1.2 Legislation.....	24
1.3 Brief history of supercharging	29
1.4 Background on Engine Technologies	30
1.4.1 4-stroke spark ignition and cycles.....	30
1.4.2 Engine Knock	33
1.4.3 Techniques to improve engine efficiency.....	36
1.4.4 Direct Fuel Injection	37
1.5 The Boost concept.....	39
1.5.1 Variable valve timing.....	40
1.5.2 Twin charged engine (eSC+TC).....	48
1.5.3 The Hybrid Electric Vehicle (HEV).....	49
1.6 Research Question	52
1.7 Outline.....	53
CHAPTER 2.....	55
2 Literature Review	55
2.1 Supercharged engine systems.....	57
2.1.1 Eaton’s Electrically Assisted Variable Speed Supercharger	57
2.1.2 CPT COBRA water cooled electric supercharger	62
2.1.3 HyBoost – An intelligently electrified optimised downsized gasoline engine concept.....	65
2.1.4 The MAHLE Downsizing demonstrator engine.....	69
2.2 Aeristech’s eSupercharger	70
2.2.1 E-Supercharging for Heavily Downsized Gasoline Engines	72
Engine Test Results	73
2.3 Summary	75
CHAPTER 3.....	76
3 An investigation into small compressors including scaling.....	76

3.1 Turbo compressors	76
3.2 The TurboClaw compressor	79
3.2.1 Experimental Testing for Electric Supercharger	81
3.3 Positive Displacement Compressors.....	83
3.4 Rotary positive displacement compressor investigation	84
3.5 Background.....	84
3.6 Screw compressor modelling	85
3.7 Geometry of screw compressor rotors.....	85
3.8 Screw Compressor Downscaling Investigation	86
3.9 Summary	88
CHAPTER 4.....	90
4 Engine, turbocharger and electric supercharger models.....	90
4.1 Model description.....	93
4.1.1 Engine block model.....	95
4.1.2 Engine performance	95
4.1.3 Engine cylinders modelling	97
4.1.4 Volumetric efficiency modelling	101
4.1.5 Restriction modelling	102
4.1.6 Adiabatic pipe modelling.....	104
4.1.7 Air cooler modelling	107
4.1.8 Shaft modelling.....	108
4.1.9 Charging components.....	108
4.1.10 Waste-gate controller	119
4.1.11 eSC Control System	119
4.2 Summary	122
CHAPTER 5.....	123
5 Simulation results- Mean Value Engine model.....	123
5.1 Naturally Aspirated (NA) Engine Simulation Results.....	123
5.2 eSC effect on Steady State simulation.....	126
5.2.1 Boost condition evaluation.....	128
5.2.2 Charging layout comparison	133
5.3 eSC effect on Transient simulation.....	136
5.4 eSC effect on Vehicle simulation	138
5.5 Summary about MVEM simulation.....	142
CHAPTER 6.....	144
6 Hardware in the Loop (HiL) Test.....	144

6.1 Test Rig.....	145
6.2 National Instrument Modules	147
6.2.1 NI 9205	147
6.2.2 NI 9264	148
6.2.3 NI 9211	148
6.2.4 NI 9217	148
6.2.5 NI 9215	149
6.2.6 NI 9234	149
6.3 Flowmeter (ABB TRIO-WIRL Flowmeter).....	149
6.4 Pressure Sensors	153
6.5 Temperature sensors	154
6.6 The steady state HiL test results.....	156
6.7 Dyno Test Results	162
6.8 Summary.....	165
Chapter 7.....	166
7 Conclusion	166
7.1 Future work.....	168
8 References	169
9 Appendices	180
9.1 Detailed transient response	180
9.2 Matlab M-File transcript to control the simulations.....	187
9.3 Simulation blocks and flowcharts	195
9.3.1 Summary of Cylinder Block.....	195
9.3.2 Summary of Connecting Volume Blocks	199

LIST OF FIGURES

Figure 1: New car registrations by Vehicle Excise Duty (VED) band.....	21
Figure 2: New car CO ₂ emissions, UK 2001 - Q4 2015.....	22
Figure 3: Total global CO ₂ emissions in 2014.....	25
Figure 4: Emissions and fuel consumption plots for the NEDC drive cycle.....	28
Figure 5: Emissions and fuel consumption plots for the WLTP drive cycle.....	28
Figure 6: Basic geometry of the reciprocating IC engine-the four-stroke operating cycle	31
Figure 7: P-V diagram of Otto cycle.....	32
Figure 8: Auto ignition sites	35
Figure 9: knocking cycle pressures trace	35
Figure 10: Passenger vehicles with turbocharged engines.....	36
Figure 11: Direct injection (left) vs Port fuel injection system (right)	38
Figure 12: Variable Timing Electronic Control system (VTEC)	41
Figure 13: A turbocharger schematic and flow movement	43
Figure 14: Pumping loop for a turbocharged engine	44
Figure 15: A belt drive mechanical supercharger (TSI engine).....	46
Figure 16: Schematic diagram of the left: parallel turbocharged system with two unequal-size turbochargers, and right: series turbocharged system	47
Figure 17: A Twin charged engine layout (eSC before TC).....	49
Figure 18: Normal cruising power flow diagram	50
Figure 19: Operating data map and driving resistance curve.....	52
Figure 20: Air mass flow rate vs engine speed for different engine sizes- Pressure ratio 1.4.....	56
Figure 21 : Brake power vs engine speed for different engine sizes	56
Figure 22: A conventional compressor map	57
Figure 23: EAVS with start/stop architecture and 3D model	58

Figure 24: EAVS operating mode vs vehicle speed example	59
Figure 25: 8. Diametral rotor leakage locations (left) and air leakage between the rotor lobe tip and rotor housing	60
Figure 26 : Leakage between rotors and end plates.....	60
Figure 27: Supercharger performance map	61
Figure 28: Measured engine torque output	61
Figure 29: Water cooled electric supercharger; C88	62
Figure 30: Cobra C88 characteristics	63
Figure 31 : Efficiency vs Pressure ratio for Cobra C88	64
Figure 32: Scheme of the concept with the 2.0L NA.....	66
Figure 33: Ford 2.0 L Duratec vs HyBoost torque curves comparison	68
Figure 34: Two-stage turbocharger arrangement	70
Figure 35: E-Supercharger 2012 Model.....	71
Figure 36: Aeristech’s supercharger performance map	71
Figure 37: Schematic of the twin-turbocharger arrangement, Post turbocharger compressor.....	73
Figure 38: Schematic of the twin-turbocharger arrangement, Pre-turbocharger compressor.....	73
Figure 39: Test results from the MAHLE downsized engine with combined eSupercharger and turbocharger; a) BMEP, b) power and c) eSupercharger power.....	74
Figure 40 : Specific Speed vs Efficiency	77
Figure 41: Turbocharger speed for different engines at PR 1.4.....	78
Figure 42: Compressor systems	79
Figure 43: The TurboClaw Geometry and rotor exit velocity triangle	80
Figure 44 : TurboClaw	81
Figure 45: TurboClaw for supercharger application	81
Figure 46: TurboClaw compressor map for an 85mm rotor.....	82

Figure 47: Common types of positive displacement compressor.....	83
Figure 48 : Cross Section of a Representative Rotary Screw Compressor.....	85
Figure 49: Rotor N profile diagram.....	87
Figure 50: Efficiency vs Mass flow rate for different sizes at pressure ratio 1.4.	88
Figure 51: Efficiency vs Mass flow rate for different sizes at pressure ratio 1.6.	88
Figure 52: Sketch of a turbo charged SI-engine. The figure illustrates how the engine is divided into subsystems to enable physical modelling of the engine	91
Figure 53: Simulink MVEM with Turbocharger and eSC.....	94
Figure 54: Engine block.....	97
Figure 55: Cylinder block overview	98
Figure 56: Output temperature as a function of exhaust mass flow rate, 1000-6000 rpm.....	99
Figure 57: Cylinder flow-charts	100
Figure 58: Volumetric efficiency map as a function of manifold pressure and engine speed.....	102
Figure 59: Ψ function for restriction modelling, as a combination of three models	104
Figure 60: Connecting volumes (adiabatic pipe) block overview	105
Figure 61: Connecting volumes (adiabatic pipe) flow-chart	106
Figure 62 : Intercooler block overview	107
Figure 63 : Intercooler flow-chart	108
Figure 64: TurboClaw mass flow rate map as a function of compressor speed and pressure ratio	111
Figure 65 : TurboClaw efficiency map as a function of speed and mass flow rate	111
Figure 66 : TurboClaw mass flow rate and efficiency blocks layout	112
Figure 67: eSC compressor block overview	112
Figure 68 : eSC compressor flow-chart	113

Figure 69 : Turbo-compressor mass flow rate map	115
Figure 70 : Turbo-compressor efficiency map	115
Figure 71 : Turbine efficiency as a function of turbine speed and mass flow rate	116
Figure 72 : Turbine mass flow rate as a function of speed and pressure ratio .	116
Figure 73 : Turbine Simulink block	117
Figure 74: eSC controller flow-chart	121
Figure 75: PID controller performance	121
Figure 76: Left: Torque vs engine speed - right: cylinder mass flow rate as a function of engine speed.....	123
Figure 77 : 1.0 L NA engine validation plot.....	124
Figure 78: 1.0 L NA engine validation plot- 1000-2000 rpm.....	125
Figure 79 : Simulation vs measured data, eSC+TC (ETC layout)	126
Figure 80: eSC + TC System Layout (ETC).....	127
Figure 81: TC + eSC System Layout (TEC).....	127
Figure 82 : Compressor PR Design Of Experiment	128
Figure 83 : simplified MVEM for boost condition evaluation	129
Figure 84 : ETC operating points at 1200 rpm (cyan lines on EDS map approximate the surge and choke limits).....	131
Figure 85 : TEC operating points at 1200 rpm (cyan lines on EDS map approximate the surge and choke limits).....	132
Figure 86 : Chosen final setpoint PRs and resulting overall boost pressure for each engine speed	133
Figure 87 : steady-state WOT results for ETC and TEC models and comparison with TC model- Torque vs Engine speed.....	134
Figure 88 : steady-state WOT results for ETC and TEC models and comparison with TC model- Boost pressure vs Engine speed	134
Figure 89 : steady-state WOT results for ETC and TEC models and comparison with TC model- Compressor temperature vs Engine speed	134

Figure 90 : steady-state WOT results for ETC and TEC models and comparison with TC model- eSC power required be Engine speed.....	135
Figure 91 : Operating points on compressors map for steady-state simulation of TEC and ETC	136
Figure 92 : Common turbocharger inertia values [www.dieselnet.com]	136
Figure 93: transient torque evolution for TC, ETC and TEC.....	137
Figure 94: Time evolution of compressors operating point for ETC and TEC .	138
Figure 95: MVEM connected to a fixed gear vehicle	139
Figure 96: vehicle dynamic balance block.....	139
Figure 97: block for resistances calculation.....	140
Figure 98: block for traction calculation	141
Figure 99: tip-in vehicle simulation results for TC, ETC and TEC models	142
Figure 100: Test rig layout	145
Figure 101: Phase 1 -Test cell.....	146
Figure 102: ABB Flowmeter	150
Figure 103: PTX 1400 Pressure sensor	153
Figure 104: Omegadyne PXM 219 Pressure sensor	154
Figure 105: PT100 RTD.....	154
Figure 106: Test Cell- TurboClaw installation.....	155
Figure 107: Left: Fast valve, Right: dSPACE unit.....	155
Figure 108: Left: ABB Flow meter, Right: NI units	156
Figure 109: TurboClaw mass flow rate vs engine speed for eSC+TC layout....	157
Figure 110: Torque vs engine speed for eSC+TC layout	158
Figure 111: Compressor speed (eSC) vs engine speed for eSC+TC layout	158
Figure 112: TurboClaw pressure ratio vs engine speed for eSC+TC layout	159
Figure 113: TurboClaw temperature vs engine speed for eSC+TC layout.....	160
Figure 114: Inlet turbine temperature vs engine speed for eSC+TC layout	160

Figure 115: example of operation points on compressor map	161
Figure 116: Selected vehicle for the dyno test.....	163
Figure 117: Dyno test room	163
Figure 118: eSC mounted on the vehicle	164
Figure 119: eSC mounted on the vehicle-2.....	164
Figure 120: 1.0 L Turbocharged engine with and without eSC	165
Figure 121: Torque vs time- transient response	181
Figure 122: Torque vs time- transient response	181
Figure 123: Torque vs time- transient response	182
Figure 124: Torque vs time- transient response	182
Figure 125: Torque vs time- transient response	183
Figure 126: Torque vs time- transient response	183
Figure 127: Torque vs time- transient response	184
Figure 128: Torque vs time- transient response	184
Figure 129: Torque vs time- transient response	185
Figure 130: Torque vs time- transient response	185
Figure 131: Torque vs time- transient response	186
Figure 132: Torque vs time- transient response	186
Figure 133: Cylinder block overview	195
Figure 134: Cylinder flow-charts	196
Figure 135: Throttle block overview	197
Figure 136: Throttle valve flowchart.....	198
Figure 137: Connecting volumes (adiabatic pipe) block overview	199
Figure 138: Connecting volumes (adiabatic pipe) flow-chart	200
Figure 139: eSC compressor block overview	201
Figure 140 : eSC compressor flow-chart.....	202
Figure 141 : eSC Engine simulation layout	203

Figure 142: TurboClaw 2-D mass flow rate map as a function of compressor speed and pressure ratio..... 205

Figure 143: Figure 142: TurboClaw 2-D efficiency as a function of compressor speed and pressure ratio- 2D map 206

LIST OF TABLES

Table 1: Mandatory CO ₂ emissions and fuel consumption targets for light duty vehicles.....	26
Table 2 : The main differences between the NEDC and WLTP	27
Table 3: Some of the Variable Valve Timing technologies used by different automotive companies.....	40
Table 4 : EAVS operation modes	58
Table 5: Cobra C88 Characteristics - 2kW line.....	64
Table 6 : Cobra C88 Characteristics – 3.5kW line.....	65
Table 7: MAHLE Specifications	69
Table 8: e-Supercharger specification summary	71
Table 9: Boost pressure set points [kPa] as a function of engine speed and throttle position - Throttle position: 0 and 1 are fully closed, and fully open throttle respectively.....	120
Table 10: Desired HiL test outcome- Performance matrix.....	147
Table 11: NI modules summary	152
Table 12: PTX 1400 specifications	153
Table 13: Omegadyne PXM 219 specifications	154

LI ST OF ABBREVIATIONS

Symbol	Quantity (explanation)	Unit
W_{cyl}	Air mass flow into the cylinder	kg/s
C_p	Air specific heat	J kg ⁻¹ K ⁻¹
λ	Air-fuel ratio	-
CD	Discharge coefficient	-
$A(\Phi th)$	Effective throttle area	m ²
eSC	Electric supercharger	-
V_d	Engine displacement	L
P_{net}	Engine power	kw
N	Engine speed	RPM
N_{eng}	Engine type number (2 for a four stroke engine)	-
W_f	Fuel mass flow rate	kg/s
R	Ideal gas constant	J kg ⁻¹ K ⁻¹
P_{in}	Inlet pressure	kPa
T_{in}	Inlet temperature	K
P_m	Manifold pressure	kPa
T_m	Manifold temperature	K
V_m	Manifold volume	m ³
H_f	Net calorific value	kJ/kg
N_{cyl}	Number of cylinder	-
W_{tc}	Out mass flow rate	kg/s
P_{out}	Outlet pressure	kPa
T_{out}	Outlet temperature	K
P_{loss}	Power loss	kw
Pr	Pressure ratio	-
γ	Specific heat ratio (cp/cv)	-
L_{th}	Stoichiometric normalisation factor	-
Ψ	The non- linear function of the pressure ratio	-
η_t	Thermal efficiency	-
Trq	Torque	Nm
Eff	Turbo-compressor efficiency	-
W_{tc}	Turbo-compressor speed	rad-/s
η_{vol}	Volumetric efficiency	-
Screw compressors study		
$GapA$	Axial Clearance	mm
$GapI$	Interlobe clearance	mm
$GapR$	Radial clearance	mm
$R3$	Radius on the female rotor tooth	mm
$R4$	Radius on the female rotor tooth	mm
R	Radius on the female rotor tooth	mm
Ra	Radius on the male rotor tooth	mm
$R1$	Radius on the male rotor tooth	mm

<i>R2</i>	Radius on the male rotor tooth	mm
<i>A</i>	Rotor centre distance	mm
<i>L/D</i>	Rotor relative length	-
Simulation symbols		
<i>T_{ac}</i>	After-cooler temperature	K
<i>P_{amb}</i>	Ambient pressure	kPa
<i>T_{amb}</i>	Ambient temperature	K
<i>A_{eff}</i>	Effective area	m ²
<i>eta</i>	Efficiency	-
<i>n_{eds}</i>	Electric supercharger speed	rpm
<i>P_b</i>	Engine inlet pressure (Boost pressure)	kPa
<i>eng_speed</i>	Engine speed	rpm
<i>TQ_{eng}</i>	Engine torque	Nm
<i>T_{ic}</i>	Inter-cooler temperature	K
<i>W</i>	Mass flow rate	Kg/s
<i>PR</i>	Pressure ratio	-
<i>ETC</i>	Supercharger + Turbocharger (Series)	-
<i>Turb</i>	Turbine	-
<i>TEC</i>	Turbocharger + Supercharger (Series)	-
<i>p_{tcom}</i>	Turbo-compressor outlet pressure	kPa
<i>n_{tc}</i>	Turbo-compressor speed	rpm
<i>W_{wg}</i>	Waste-gate controller	-

CHAPTER 1

1 Introduction

1.1 The emission challenge and downsizing

Recent increases in sales of lower emissions vehicles in the UK indicate that the last five years there has been a dramatic change in the buying behaviour of UK motorists, Figure 1, and consequently on the rate of CO₂ emissions reduction (1). Since the recession struck the UK in 2008, new car buyers have prioritised fuel efficiency more than ever, and vehicle manufacturers have redoubled efforts to enhance efficiency and reduce emissions across all vehicle types (2) .

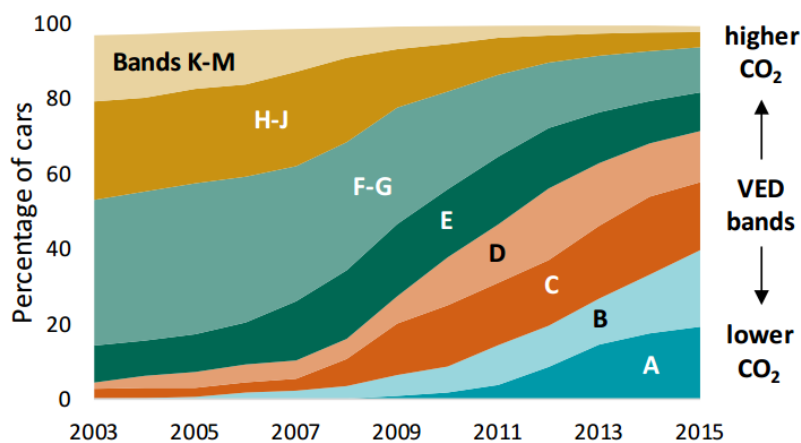


Figure 1: New car registrations by Vehicle Excise Duty (VED) band, 2003 – 2015 (3)

Global warming and volatile fuel prices are increasing public concern, and legislation is adding to the pressures experienced by the automotive industry (4). As a result, the automotive industry reduced average new car CO₂ emissions to 133.1 g/km in 2012, 130 g/km in 2015 and they plan to reduce it to 95 g/km by 2020. As shown in Figure 2 (3). The 2015 and 2020 targets represent

reductions of 18% and 40% respectively compared with the 2007 fleet average of 158.7g/km. The average emissions level of a new car sold in 2014 was 123.4 g CO₂/km (provisional data), well below the 2015 target. Since monitoring started under current legislation in 2010, emissions have decreased by 17 g CO₂/km (12 %). The European commission is presently working on consultations involving new emission targets that will begin being effective within the next ten years as a way of lowering carbon releases as well as the reduction of toxic waste within the cities (5), (2).

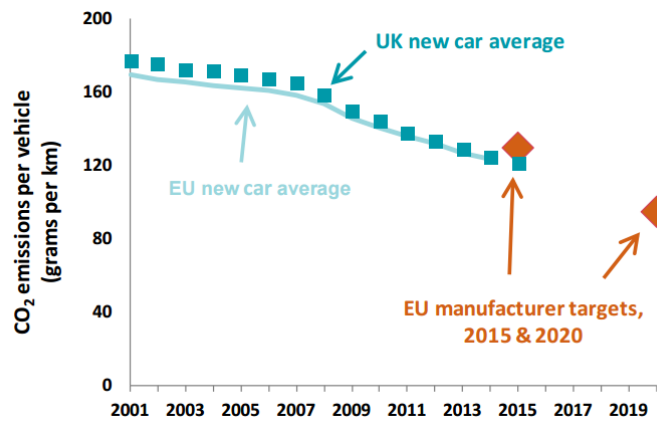


Figure 2: New car CO₂ emissions, UK 2001 - Q4 2015 (3)

Scandals from the emissions deceptions by the Volkswagen diesel and Mitsubishi energy exposed the extent the vehicle manufacturers' are willing to try when facing challenges in their endeavours to achieve the set standards on emissions. Some of these manufacturers, therefore, result to unscrupulous ways by fabricate the tests results (6). For instance, the Volkswagen Company was cornered implementing erudite systems within the engines of their vehicles so as to cheat the tests by the U.S. Federal authorities. This led to their diesel automobiles emanating a NO_x pollution level of about 40 times that of these required by the regulations. Volkswagen has acknowledged that there are

about 10 million vehicles internationally fitted with this defective algorithm of which about 1.1 m diesel cars were purchased in the United Kingdom alone (7). The Mitsubishi Company acknowledged that it had manipulated its fuel proficiency facts for the engines fixed in their vehicle models as well as others that were fixed in certain Nissan models (8). Around 624,000 vehicles that were purchased in Japan reported this error (in overall, four models). This has resulted to the suspension of the affected models (9). The Mitsubishi Company, during the test on fuel efficiency overinflated their tyres which successfully realized positive outcomes (10). CNN informed the public that the Mitsubishi Company was on the verge of inspecting the fabricated fuel efficiency investigations on an additional eight models. There has been a major public backlash particularly against diesel and many automotive manufacturers have announced aggressive timescale for release of more electric vehicles and more downsizing on gasoline engines.

Fuel consumption improvements, climate change, and impact of transport are some of the main drivers for engine development within the automotive industry (11). The current status of the EU fleet indicates that significant work is still required to achieve this target, particularly in the field of gasoline spark ignition engines. Furthermore, recent proposed legislation in California indicates that the US market will follow the EU's lead. Drivers are aware that a car with a smaller engine provides lower fuel consumption than the same model with a larger engine, assuming the same level of engine modernity. The problem with the smaller engine is lack of power for accelerating (12) or hill climbing particularly if there is a headwind. It is noted that this high power requirement is very intermittent, so a large engine has to be operated at low power when most of the time a smaller engine would be sufficient. One solution is to use an electric supercharger which is a small device containing an

electric motor and compressor to pressurize the intake air. By pressurizing the air available to the engine intake system, the air becomes denser, and is matched with more fuel, producing increased power to the wheels. Using an electric motor is beneficial since the boost pressure can be easily controlled, and power is supplied from the battery thus maximising available engine power at the time of demand. The battery can be recharged when full engine power is not needed. When operating, this system is not particularly efficient but since it operates over short time periods, the benefit of having a small engine over a large engine far outweighs this inefficiency leading to an overall improved fuel economy; the best of both worlds. However, it is vital that the device is low cost particularly for vehicles of low to medium engine powers (up to C class) where manufacturer's margins are relatively small.

1.2 Legislation

The downsizing of engines, especially SI petrol, has now become firmly established as a proven approach for reduction in CO₂ emitted from vehicles, and it delivers significant fuel economy benefits. The pressures to reduce CO₂ emissions and fuel consumption have grown stronger and more urgent in recent years; however, the desire to have vehicles with increasingly better performance has never waned. Transport is the only major sector in the EU where greenhouse gas emissions are still rising despite decrease of CO₂ emission for each vehicle and this is due to increased number of vehicles in the road. 15.9 percent of the global total emitted carbon dioxide (CO₂) was due to the road transport in 2014 as shown in Figure 3 (13). CO₂ emissions from road transport increased by nearly 23 percent between 1990 and 2010, and without the economic downturn, growth could have been even higher. Light-duty vehicles, cars and vans, are one of the major sources of greenhouse gas emissions, producing around 15 percent of the EU's emissions of CO₂.

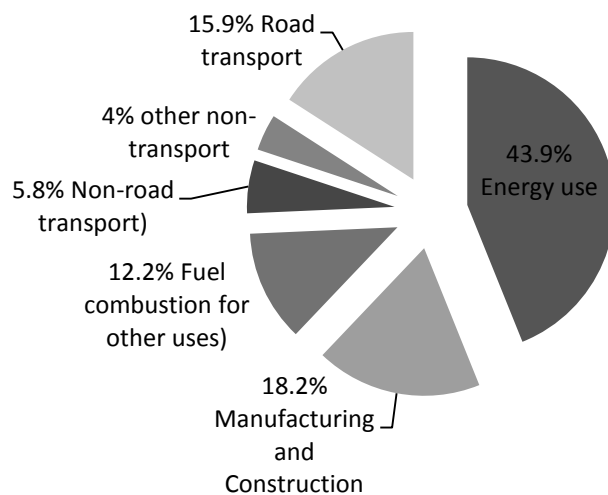


Figure 3: Total global CO₂ emissions in 2014 (13)

From the resulting European commission strategy agreed in 2007, the EU has agreed a comprehensive legal framework to reduce CO₂ emissions from new light duty vehicles in order to guarantee it meets its greenhouse gas emission reduction targets under the Kyoto Protocol and beyond. The legislation sets compulsory emission targets for new car and van fleets, therefore, the average emissions are falling each year due to these obligations and targets.

Car manufacturers are required to ensure that their new car fleet does not produce more than an average of 130 grams of CO₂ per kilometre (g CO₂/Km) for 2015 and 95 g by 2021. 175 g CO₂/km by 2017 and 147g by 2020 is the mandatory target for vans. This compares with an average of 203g in 2007 and 180.2g in 2012. The 2017 fuel consumption's target is almost equivalent to 7.5 litres per 100 km (l/100 km) of gasoline or 6.6 l/100 km of diesel. The 2020 target is approximately 6.3 l/100 km of gasoline or 5.5 l/100 km of diesel. Table 1 gives a summary of the CO₂ emissions and fuel consumption targets for light duty vehicles.

Mandatory targets for Light Duty Vehicles			
		Fuel consumption targets	
	CO ₂ Emission's target (g/km)	gasoline (l/100 km)	Diesel (l/100 km)
2007	160		
2012	132.2		
2015	130	5.6	4.9
2021	90	4.1	3.6

Table 1: Mandatory CO₂ emissions and fuel consumption targets for light duty vehicles

As of September 2017, the old NEDC lab test for cars will gradually be replaced by the new WLTP test (14). The old lab test – called the New European Driving Cycle (NEDC) – was designed in the 1980s and became outdated today due to several evolutions in technology and driving conditions. The UNECE has therefore prepared a new test, called the Worldwide Harmonised Light Vehicle Test Procedure (WLTP) that applied from September 2017. WLTP is based on real-driving data while the NEDC was based on theoretical driving (15).

WLTP has many benefits such as more realistic driving behaviour, higher average and maximum speed, CO₂ values and fuel consumption are provided for individual vehicles as built, a greater range of driving situations (urban, suburban, main road, motorway), longer test distance, shorter stops and etc (15). Because of all these improvements, WLTP will provide a much more accurate basis for calculating a car's fuel consumption and emissions. Table 2 shows the main differences between the two test procedures (14).

	NEDC	WLTP
Test cycle	Single test cycle	Dynamic cycle more representative of real driving
Cycle time	20 minutes	30 minutes
Cycle distance	11 kilometre	23.25 kilometre
Driving phases	2 phases, 66% urban and 34% non-urban driving	4 more dynamic phases, 52% urban and 48% non-urban
Average speed	34 kilometre per hour	46.5 kilometre per hour
Maximum speed	120 kilometre per hour	131 kilometre per hour
Influence of optional equipment	Impact on CO ₂ and fuel performance not considered under NEDC	Additional features (which can differ per car) are taken into account
Gear shifts	Vehicles have fixed gear shift points	Different gear shift points for each vehicle
Test temperatures	Measurements at 20-30°C	Measurements at 23°C, CO ₂ values corrected to 14°C

Table 2 : The main differences between the NEDC and WLTP

Figures 4 and 5 were produced by using ADVISOR software to illustrate the differences between NEDC and WLTP cycles. The purpose of this was to compare the fuel consumption and tailpipe emissions of six normally aspirated C-segment conventional vehicles with increasing engine capacities simulated on selected drive cycles. Each vehicle is driven from a cold condition (all vehicle components at 20°C). Simulation input data used in ADVISOR can be found in tables 15-17 in page 209.

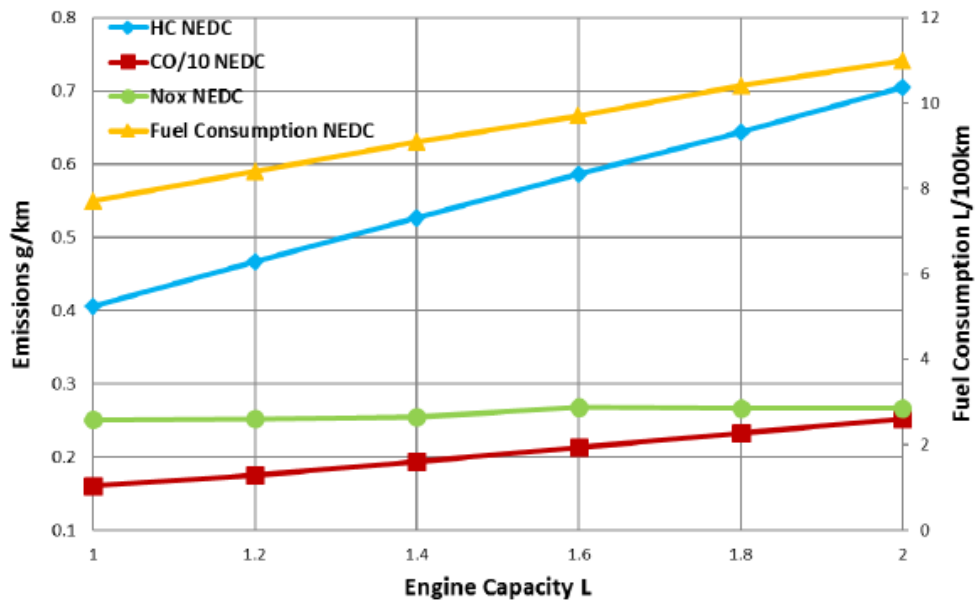


Figure 4: Emissions and fuel consumption plots for the NEDC drive cycle

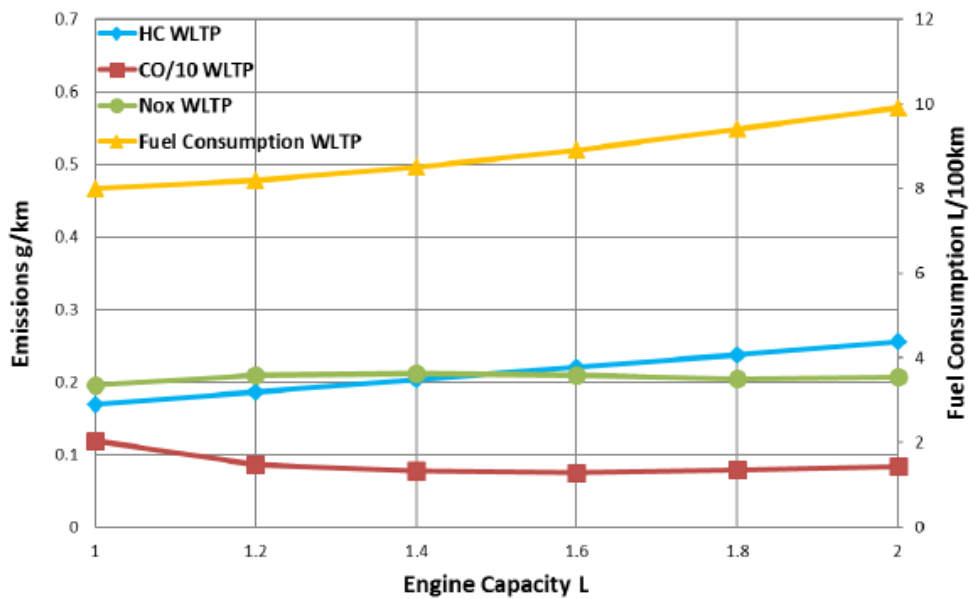


Figure 5: Emissions and fuel consumption plots for the WLTP drive cycle

The principle of doing this analysis was to show that engine downsizing reduces fuel consumption. The graphs show how much fuel consumption will be gained for the same model of car with different size of engine.

1.3 Brief history of supercharging

In 1860, brothers Philander and Francis Marion Roots of Connersville, Indiana, patented the design for an air mover, for use in blast furnaces and other industrial applications. By the late 1800s, it had made its way to Germany, where an engineer called Krigar invented an air pump that utilized twin rotating shafts that compressed air. The combination of the pair of inventions resulted in a third, with the first functional supercharger attributed to German engineer Gottlieb Daimler, who received a German patent for supercharging an internal combustion engine in 1885. Louis Renault patented a centrifugal supercharger in France in 1902. An early supercharged race car was built by Lee Chadwick of Pottstown, Pennsylvania in 1908, which, it was reported, reached a speed of 100 miles per hour (160 km/h). Supercharging of larger engines has been performed by the late 1800s (16), but supercharging a small engine (order 1.0 L) has presented a major problem particularly at low engine speeds (2000 rpm or less) since the volume flow rates of air required are very low, in the order of 40-80 m³/hr (13-27 g/s). The speeds required for a standard backswept turbo-compressor are very high (well in excess of 100,000 rpm) creating challenges for the bearings and the electric motor. It is technically feasible but not acceptable due to potential costs and risks for the automotive industry. Speeds of over 100,000 rpm are not a problem for turbochargers; however, the drive is not an electric motor but a high speed turbine. Bearings are plain oil type and the configuration of pressurized compressor and turbine mitigates the sealing issue which is difficult to perform when the driver is an unpressurised electric motor.

1.4 Background on Engine Technologies

In this section, the important automotive engine technologies are reviewed. One of the main components to be simulated was the engine block therefore a sufficient level of understanding of the engines was essential. Knocking is an additional area which demanded consideration since it limits the engine charging pressure. The investigation into eSC was limited to 4-stroke petrol engines hence diesel was not considered. eSC can be applied to diesel but there is less need since low speed torque is much better for diesel and there may be issues with exhaust gas recirculation (EGR).

The EGR system is designed to reduce the amount of NO_x created by the engine during operating periods that usually result in high combustion temperatures. NO_x is formed in high concentrations whenever combustion temperature exceeds about 1645 K. It is common practice nowadays, to use EGR to reduce the formation of NO_x emissions by recirculating small amounts exhaust gases into the intake manifold where it mixes with the incoming air/fuel charge. The exhaust gas acts as an inert gas in the combustion chamber, it does not participate in the combustion reaction. This leads to a reduction of the combustion temperature by different effects (17).

1.4.1 4-stroke spark ignition and cycles

Internal combustion engines are designed to convert the fuel's chemical energy into mechanical energy. This energy is released by oxidizing the fuel by combustion inside the engine which expands the gasses. There are two types of working fluids involved in the oxidizing process; air-fuel mixture before combustion and the burned product after combustion. The amount of

combusted air and fuel into the cylinder is approximately proportional to the power output produced at crankshaft (18).

Most 4-stroke Spark Ignition (SI) petrol engines are reciprocating engines, the exception being the Wankle engine, no longer used in production vehicles. In this type of engine, the piston moves up and down in a cylinder and the drive shaft is driven via a connecting rod and crank shaft as shown in Figure 6. The crank movement produces a cyclical piston motion. Top-dead-centre and bottom-dead-centre refer to the piston position when it comes to rest at the top-centre (*TC*) crank position and bottom-centre (*BC*) crank position, when the cylinder has the minimum or maximum volume respectively. The cylinder has the minimum volume when the piston is at top-dead-centre which is known as clearance volume (V_c). Swept volume (V_d) is the difference between maximum volume (V_t) and the clearance volume. The ratio of the maximum volume to minimum volume is called compression ratio (r_c).

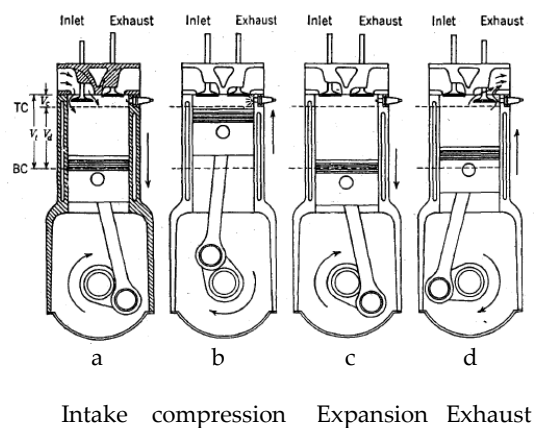


Figure 6: Basic geometry of the reciprocating IC engine-the four-stroke operating cycle (18)

Reciprocating engines mostly operate on four-stroke cycle regardless of the fuel type. This means that each cylinder requires four strokes or two revolutions of the crankshaft to complete the event.

This cycle is commonly described as the Otto cycle after its inventor, Nicolaus Otto, a German engineer who developed the first engine operating on these principles in 1876. The different processes of Otto cycle are shown on a P-V diagram in Figure 7.

1. Intake stroke, air and fuel drawn into engine (5 → 1)
2. Compression stroke, ρ, T increase (1 → 2)
3. Combustion (spark), short time, essentially constant volume (2 → 3).

Model: heat absorbed from a series of reservoirs at temperatures T_2 to T_3

4. Power stroke: expansion (3 → 4)
5. Valve exhaust: valve opens, gas escapes
6. (4 → 1) Model: rejection of heat to series of reservoirs at temperatures T_4 to T_1
7. Exhaust stroke, piston pushes remaining combustion products out of chamber (1 → 5)

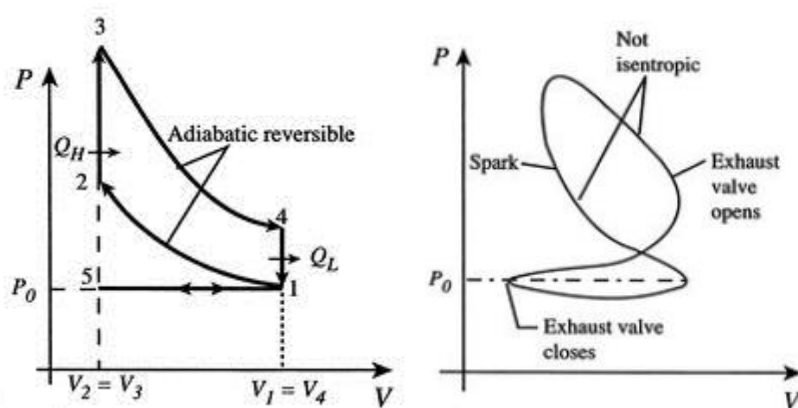


Figure 7: P-V diagram of Otto cycle (18)

Two stroke engines are the other type of internal combustion engines whereby the whole process of feeding the air-fuel to the cylinder and the exhaust occurs in two stroke; compression stroke and expansion stroke. Two stroke engines are normally found in low power vehicles, such as: garden equipment, jet skis and motorcycles (18) and are not considered in the research.

1.4.2 Engine Knock

Abnormal combustion, more commonly known as knock or detonation, has been the limiting factor in SI Internal Combustion engine power generation since the discovery of the Otto Cycle itself (19). It is important to understand and report this subject since engine boosting affects this phenomenon. Knocking, in a SI Internal-Combustion Engine, produces sharp sounds caused by premature combustion of part of the compressed air-fuel mixture in the cylinder. When the undesired flame front is initiated and how it is propagated define the cause of knocking. Any sort of abnormality in the combustion process has serious consequences in the power output, endurance and emissions generation of an engine. Auto-ignition causes rapid energy release at a rate about 5-25 times the characteristics of normal combustion. This rapid heat releases a pressure wave that oscillates across the cylinder bore to produce the sharp metallic sound (20).

Knocking is the reason for an uncontrolled combustion with multiple flame fronts, with only one of these flames being initiated by the spark plug. During knock, cylinder pressures experience an extremely rapid rise and spontaneous burning and release of the end gases' energy. Temperature rise or anything that will retain heat in the combustion chamber will endorse the auto-ignition. Sharp metal edges on the piston or in the combustion chamber are greatly

prone to super heating and will actually retain enough heat that it will start to glow. It is more likely to have another flame front if the fuel hits this glowing edge either prior to the lighting of the spark plug, or even after ignition. If this unintended ignition occurs very early in the compression stroke, then the piston will be forced up against the increased pressure of the burning gas and will result in a form of abnormal combustion referred to as pre-ignition. When this happens, the end result, if severe enough, is that the connecting rods bend. Turbocharged engines are specifically prone to this because the engine is running at high speeds for the turbocharger to produce boost for the engine. If the failure occurs at this range of speeds, the force acting on the connecting rod would be normally higher compared to low revs. Carbon deposits that build up in the combustion chamber or on the piston top have a similar effect, along with the decreased volume at TDC, which in turn raises the compression ratio.

As mentioned previously, anything that will raise the temperature in the cylinder will encourage knock. There are several reasons for the temperature raise such as a very lean air-fuel mixture, heating of the charge air prior to entering the combustion chamber, compression of the air from forced induction or poor heat dissipation through the cooling system. Increase of cylinder pressure will also prompt detonation. Camshaft profile, compression ratio and quench area can also affect the detonation.

When the intake air is compressed, the density of the air increases and subsequently the mass of air-fuel-mixture drawn into the cylinders during the intake stroke rises. As a result, the output torque of the engine is boosted. However, it is not possible to compress air without raising its temperature. This phenomenon is governed by the first law of thermodynamics ¹ and reduces to

¹ For any cycle of a closed system, the net heat transfer equals the net work

some extent the benefits of turbo and supercharging. One way to reduce the risk of knock in charged engines is to reduce the air temperature by using intercoolers, which is simply a heat exchanger (19), (21).

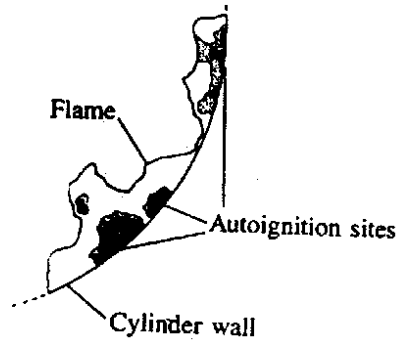


Figure 8: Auto ignition sites (21)

Figure 8 shows the potentially catastrophic pressure oscillations caused by knock. An in-cylinder pressure trace is plotted vs. Crank Angle Degree (CAD) after Bottom Dead Centre (aBDC) is shown in Figure 9. The peak cylinder pressures for Knocking and Non Knocking cycles are 95 and 78 bar respectively.

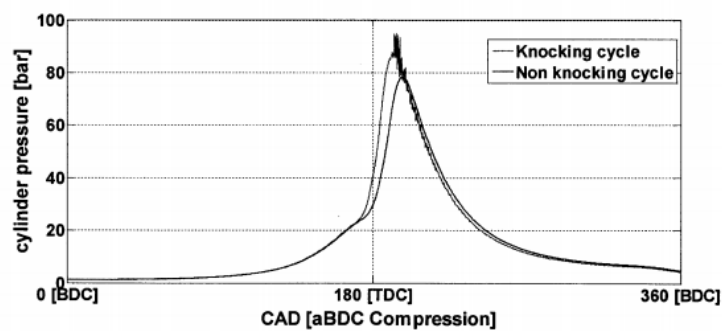


Figure 9: knocking cycle pressures trace (21)

1.4.3 Techniques to improve engine efficiency

In recent times, various technologies have been applied to gasoline engines to improve operating efficiency. Gasoline engine downsizing is the process whereby the speed / load operating point is shifted to a more efficient region through the reduction of engine capacity, whilst maintaining the full load performance via pressure charging in combination with other technologies. Passenger vehicles with turbocharged engines are expected to increase globally by more than 80 percent by 2017 in Europe and approximately 70 percent worldwide by 2020 (22) as shown in Figure 10.

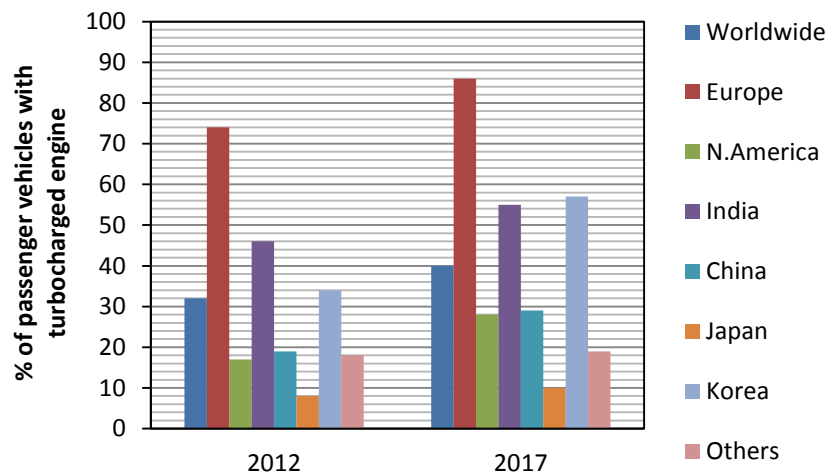


Figure 10: Passenger vehicles with turbocharged engines

However, it has long been known that pressure charging is one of the most effective technologies for immediate implementation. This has led to a significant increase in the number of downsized engines on the market today, with more engines to be introduced in the near future. This section will briefly clarify some of the technologies available in the market, and the advantages and disadvantages of each of them.

The most significant of these being:

- Direct injection (homogenous and stratified lean)

- Variable valve trains (profile switching, cylinder deactivation, fully variable lift and duration)
- Controlled auto-ignition or homogenous charge compression ignition
- Cylinder Deactivation
- Engine downsizing embedded by using charging
- Hybrid Electric Vehicles (HEV)
- Battery electric Vehicle (BEV)

1.4.4 Direct Fuel Injection

Bosch produced the first fully digital electronic injection system in 1982 and since then the automotive industry has been moving from traditional Port Fuel Injection (PFI) towards Direct Fuel Injection (DI) in Spark Ignition (SI) engines. As it can be seen from Figure 11 the main difference between the two technologies is that in DI the fuel is injected directly into the combustion chamber whereas in PFI the fuel sprayed in the intake port. The fuel injection system in a Gasoline Direct Injection (GDI) engine is a crucial component that must be carefully matched with the specific in cylinder flow field to provide the desired mixture cloud over the entire operating range of the engine.

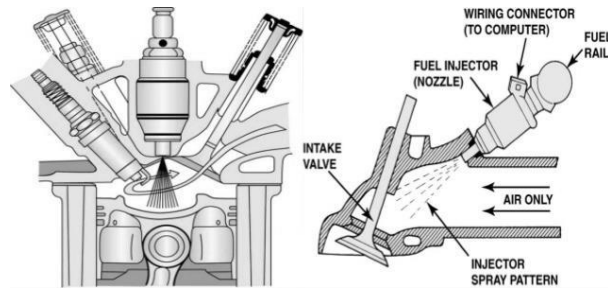


Figure 11: Direct injection (left) vs Port fuel injection system (right) (23)

A good atomized fuel spray must be produced for the operating condition. For the efficient combustion of a stratified mixture, stable and compact spray geometry is necessary. A GDI fuel system needs to provide for at least two, more distinct operating modes. For un-throttled, part-load operation, the injection system should provide the capability for rapid injection late in the compression stroke into an ambient pressure of up to 1.0 MPa, which requires a relatively high fuel injection pressure. The fuel injection pressure has been set to be very important for obtaining both effective spray atomization and the required level of spray penetration. Direct fuel injection has a few advantages over PFI, namely:

- **Charge Cooling:** the heat of vaporization of the fuel can be extracted in DI engines from the charge instead of walls, thus cooling it. Therefore, the result of this operation is volumetric efficiency improvement and power output compared to PFI. But more importantly, this benefit can be used to extend knock onset limits and therefore increase efficiency by allowing higher compression ratios, boost pressure and optimized spark timing.
- **Lean/stratified Operation:** Direct injection in cylinder is used to create a close stoichiometric mixture locally, while the overall mixture is lean

without any flammability problems, therefore this strategy is beneficial for efficiency.

- **Better mixture Preparation:** Injecting the fuel directly in cylinder improves transient response and reduces the over-fuelling in cold start.

The threat for DI engines is that fuel evaporation must take place on time, and adequate time should be allowed for mixing so that the fuel does not hit the walls or the piston, consequently, the mixture at the end should be truly homogeneous. The consequences of fuel hitting the wall include loss of potential charge cooling, and more importantly substantial increases in hydrocarbon and particulate matter emissions. One way to prevent this concern is to ensure that the injection pressures in DI engines are significantly higher than PFI (150bar compared to ~4bar). Higher injection pressures means better atomisation and evaporation but higher cost compared to PFI due to the more sophisticated fuel injection system (21).

1.5 The Boost concept

This section briefly describes the boost concept, engine downsizing techniques, the novelty and objectives of this research. There was no evidence of successful implementation of engine downsizing of small engines, (1.2 L or less) when this research started in August 2013 in the automotive industry and yet the lack of this technology can be felt in the industry. All of the proposed solutions have been studied and they are presented in Chapter 2. Most of the technologies are only suitable for a high power e.g Mahle Engine; they are too high flow to be used on a small engine.

There are two operating regimes which are important for this application, steady state and transient operation, the work done to date represents both operations (24), (25).

1.5.1 Variable valve timing

Most modern engines are now fitted out with Variable Valve Timing systems to improve engine performance. Variable valve timing increases an engine's flexibility under different conditions, which can result in increased fuel economy or better performance (26). The following table provides a breakdown of the most common technologies in the market, and which manufacturers use them.

Terms		Used By
VTEC	Variable Valve Timing and Lift Electronic Control	Honda
VVT-i or VVTL-i	Variable Valve Timing and Lift with Intelligence	Toyota
MIVEC	Mitsubishi Innovative Valve timing and lift Electronic Control	Mitsubishi
VVL	Variable Valve Lift	Nissan
VANOS	Variable Onckenwellen Steuerung	German-designed system used by BMW, Ford, Ferrari and Lamborghini

Table 3: Some of the Variable Valve Timing technologies used by different automotive companies

There are several other variable valve timing systems available from different manufacturers. Variable valve timing comprises of complex mechanical and

hydraulic processes inside the vehicle's engine. Each manufacturer technology differs slightly, but most of the functions obey the same basic rules (26). To get a fundamental understanding of the principals at work, Honda's VTEC system is explained in detail in, Figure 12. The system was the first of its kind and although most car makers worldwide started developing their own variable valve timing and lift control systems, the VTEC witnessed the biggest success becoming a trademark and an integral part of Honda's consumer perceived identity. Honda's system operates using three basic steps to regulate the functioning of the vehicle's engine.

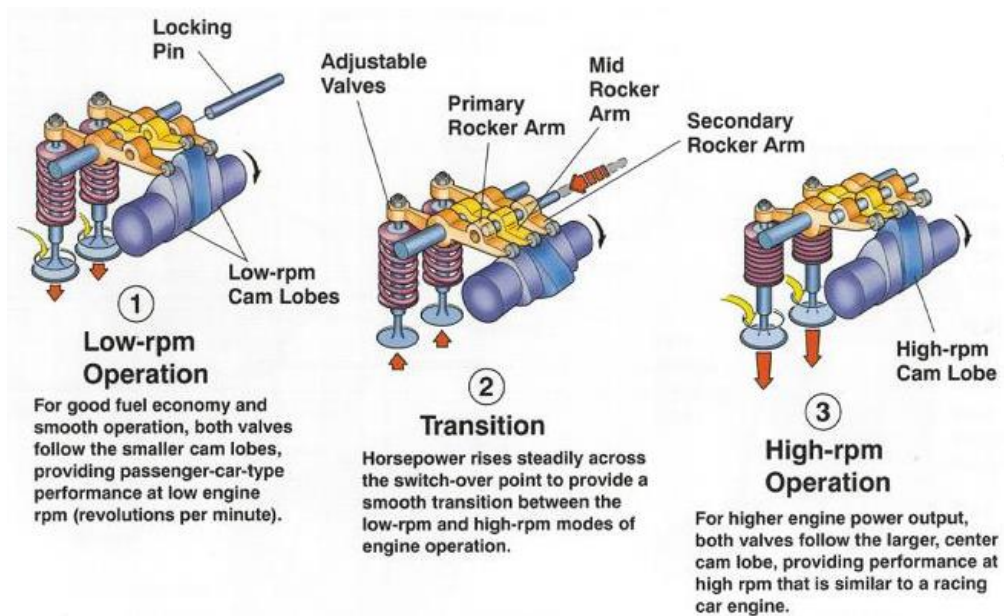


Figure 12: Variable Timing Electronic Control system (VTEC) (26)

Low RPM Drivability: When running at lower RPM, the VTEC engine uses a camshaft with a profile designed to provide a smooth idle, good fuel economy and better low end power and torque.

Electronic monitoring and switch: the engine's computer is responsible for monitoring the conditions under which the engine is operating, including the

position of the throttle pedal and the engine's speed or RPM, to decide when to switch to a different camshaft profile.

High RPM performance: An electronic switch is activated and hydraulic pressure is used to switch the valve operation to a different camshaft when high-performance camshaft is required. The high-performance camshaft provides the vehicle with considerably more power at high RPM's.

The purpose of variable valve timing systems is not only to increase the performance, but the manufacturers now offer it specifically to maximise the fuel economy of engines in vehicles that are less performance-oriented. (26)

Additional benefits of VVT include internal EGR and reduction in CO₂ emissions by allowing for more direction of internal gases, the variable valve timing system can reduce CO₂ emissions.

Better fuel economy: With more precise handling of engine valves, some auto makers have shown that VVT can produce better fuel economy for vehicles.

1.5.1.1 Turbocharging

A Turbocharger which is short for turbo driven supercharger consists of a compressor and a turbine coupled on a common shaft. The exhaust gases from the engine are directed by the turbine inlet casing on to the blades of the turbine, and consequently discharged into the atmosphere through a turbine outlet casing. The exhaust gases are utilised in the turbine to drive the compressor, which compresses the air and directs it to the engine induction inlet manifold. This supplies the engine cylinders with air of higher density than is available to a naturally aspirated engine.

Turbocharging increases power by increasing the torque due to increasing Indicated Mean Effective Pressure (IMEP). This is better than increasing power by increasing speed of the engine. Since the force on the rotating components of the engine scales by $\omega^2 r$, where ω is the rotational speed of the crankshaft and r is the radius of the crankshaft, and therefore the stress increases as the square of the engine speed. By turbocharging, indicated mean effective pressure (IMEP) is increased, so the speed of the engine does not have to increase to produce more power. Furthermore, a small increase in peak cylinder pressure leads to a larger increase in torque, since it is the average value that is felt (27).

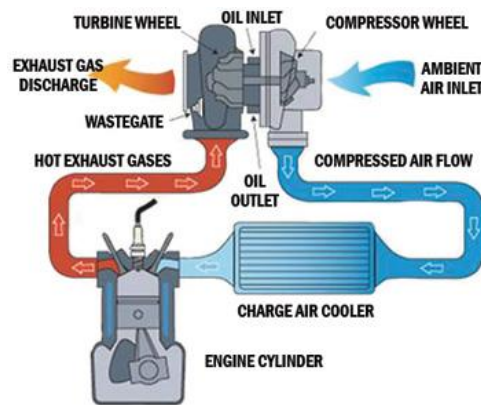


Figure 13: A turbocharger schematic and flow movement (27)

Another advantage of turbocharging is the effect it has on normal engine loss. Since the output is increased with increase of engine friction, and typically generating negative pump work (positive work out), efficiencies of turbocharged engines are generally higher. Figure 14 shows a typical pumping loop for a turbocharged engine. Since the intake pressure is higher than the exhaust pressure, work is done on the piston during the intake stroke (28). A turbocharger is powered by a turbine driven by the engine's exhaust gas. Below a certain rate of exhaust flow, the turbocharger produces insufficient boost because turbine is not producing enough power to drive the compressor. This

restricts boost at low engine speeds (800- 2000 rpm) regardless of exhaust gas pressure which is a major limitation (28).

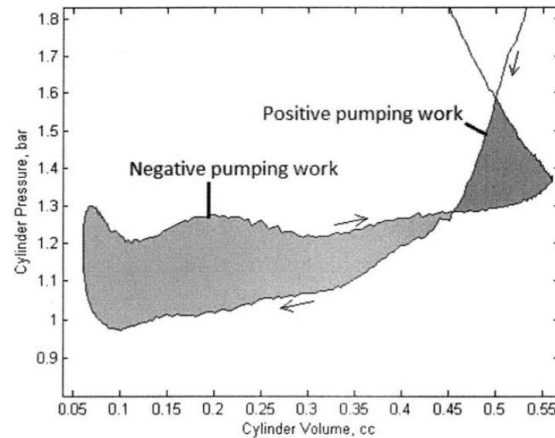


Figure 14: Pumping loop for a turbocharged engine (27)

1.5.1.2 Superchargers

In recent years, there has been an increased interest in the development of the supercharger with various types of technologies, to improve the performance of automotive engines (29). A supercharger can be considered as any boost compressor driven by a mechanical drive or electric motor. Need of the electric supercharger can be felt at low speeds. As electric supercharger's boost will be available in a fraction of a second upon drivers demand regardless of engine speed, and this feature makes the electric supercharger a novel approach to fill the lack of power at low engine speed where the turbocharger boost is impractical.

Mechanical superchargers and drives

A mechanical supercharger is driven by the engine crankshaft, belt, gears etc. Since the engine speed and supercharger speed are in a fixed ratio to each other, boost pressure changes with engine speed much more rapidly than in the case of a turbocharged engine. Therefore, a supercharged engine has no time lag needed to raise the boost pressure. But this system has a disadvantage in that there is a mechanical power drawn when driving the supercharger and additional impediment to engine acceleration due to the additional inertia (30).

Mechanically driven superchargers

There are four different varieties of conventional superchargers driven by the crank.

- Belt (V-belt, synchronous belt, flat belt)
- Gear drive
- Chain drive
- Continuously Variable Transmission drive (CVT)

A good example of this technology is TSI engines. The TSI engines from Volkswagen are impressive for their maximum efficiency and economy. Direct Gasoline Injection is combined with a turbocharger or charge compression, with a turbo and a supercharger working in tandem. This enhances the engine's combustion efficiency so the TSI engine power output is much higher than that of conventional, naturally aspirated engines. Superchargers in TSI engines are powered via a belt drive directly from the crankshaft, as shown in Figure 15. This provides high torque power on demand, even at very low engine speeds. However, TSI engines are designed to deliver maximum torque from engine speeds as low as 1500 or 1750 rpm while these numbers are from 800 to 2000

rpm for Electrically Driven Superchargers. This is one of the disadvantages of using mechanically driven superchargers since there is an insufficient amount of boost at very low speeds (31).

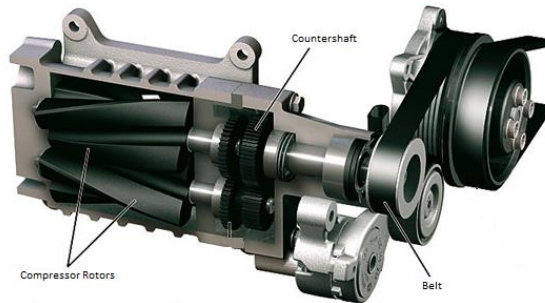


Figure 15: A belt drive mechanical supercharger (TSI engine)

Electric Superchargers

An Electric Supercharger (eSC) uses an electric motor to drive the compressor to pressurize the intake air. This will boost transient power reducing the requirement for a larger engine. For a start, the fact that the electric supercharger is not linked mechanically to engine speed means that the extra provision of power can be delivered when it is most needed without engine power within a fraction of a second (32).

Unlike a crankshaft driven supercharger or exhaust driven turbocharger, an electric supercharger operates independently of engine speed. This crucial difference means the technology is perfectly suited to maintaining vehicle transient performance and driveability - now widely recognised as a critical marketing issue for any car maker contemplating radical downsizing of an IC engine to maximise fuel efficiency (33).

1.5.1.3 Twin-turbo charged engines

Fuel economy improvement and CO₂ emission reduction led the automotive industry to develop the series and parallel turbocharging systems with two equal or unequal-size turbochargers. The concept of the parallel turbocharging system was presented at first by Brown Boveri at 1946, but the research did not begin to rise until the late 1970s due to technical limitations. The first published research was from Germany KHD Company, but this technique was not applied in any actual product. In the early 1980s, the first commercial application of the ST system was from Germany MTU Company (34). The first ST system application in car engine was from Borila Sweden Volvo Company (35).

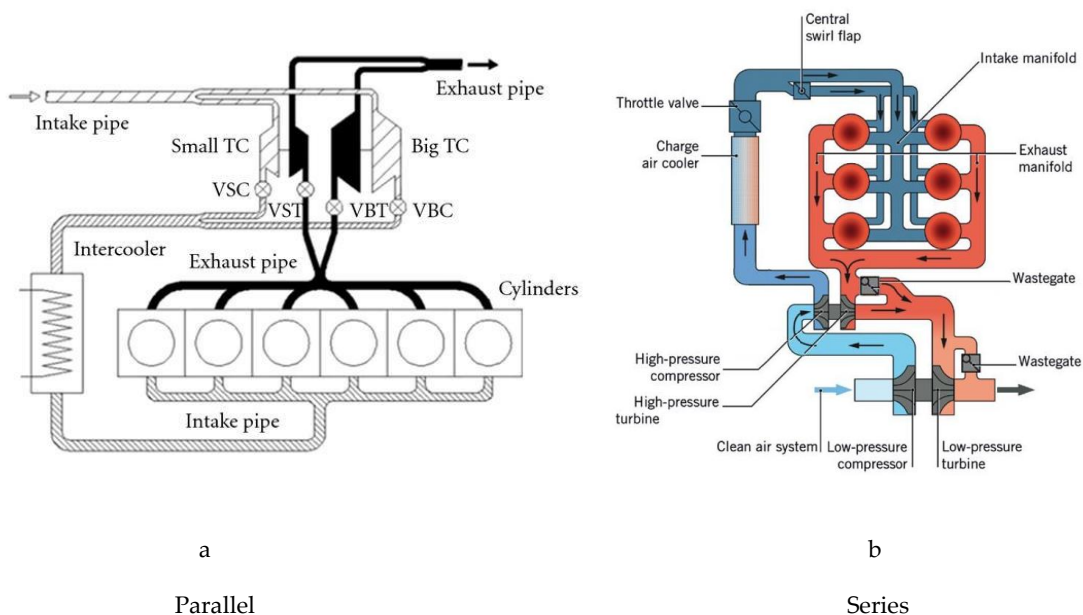


Figure 16: Schematic diagram of the left: parallel turbocharged system with two unequal-size turbochargers, and right: series turbocharged system (34)

The parallel turbocharging system consists of two or more turbochargers in parallel. This system can improve the turbochargers matching with the engine, therefore the efficiency of the turbocharger and boost pressure are both improved. The equivalent turbine flow area is capable of more than 50% variation in the ST system, so it significantly improves the performance of the engine with high brake mean effective pressure (BMEP) at low speed (34). Figure 16 shows the schematic diagram of a parallel turbocharging system.

Compared to other twin turbo system such as two-stage serial turbocharging system, the parallel system has advantages of packaging and costs due to smaller turbocharger size and it also has a wider range of applications such as locomotives, armoured vehicles, ships as well as sport car petrol engines.

1.5.2 Twin charged engine (eSC+TC)

An alternative method to boost an engine and to reduce CO₂ emission is to use combined supercharger and turbocharger. The combination of supercharger and turbocharger to increase the net power and torque of an engine is known as twin charging and the device use to increase the torque and power of engine is labelled as twin charger (36). A combination of turbocharger and supercharger either in series or parallel connection made a compressing device capable of compressing the atmospheric air to sufficient level and supplies them to the inlet valve of the engine. There are two possible combinations in terms of whether the eSC goes before the TC as shown in figure 17, or vice versa. Employing the eSC after turbocharger has the advantage of broadening the eSC map, towards higher-mass flows. Since a denser air exits the turbo-compressor as the turbocharger provides boosted air to the system which augments the overlap of the two operating maps for the two devices. However, in this layout, the eSC would be subjected to boost pressure from turbo-compressor which

means the turbo-compressor outlet air temperature could range from 100 to 120 °C, for a 1.0 L to 1.2 L engine, at full engine load. Furthermore, the eSC will have to withstand this temperature.

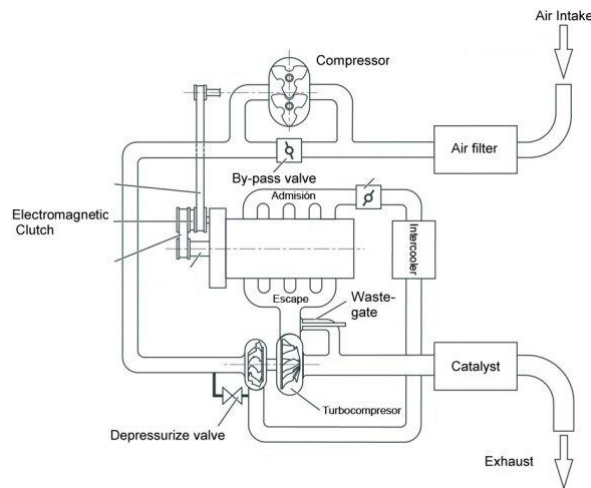


Figure 17: A Twin charged engine layout (eSC before TC) (37)

These two components mitigate the weaknesses of the other. An electrically driven supercharger offers exceptional response at low-rpms as it has relatively small lag (due to compressor inertia) time due to its independency of the exhaust gas while the turbocharger can be used at high-rpm since the high pressure gas is available to drive the turbine.

1.5.3 The Hybrid Electric Vehicle (HEV)

The concept of Hybrid Electric Vehicles (HEV) is nearly as old as the automobile itself (38). The main purpose, however, was not so much to lower the fuel consumption but rather to assist the IC engine to provide an acceptable level of performance. The first hybrid vehicles reported were shown at the Paris Salon of 1899 (39).

A hybrid car is an automobile that has two or more major sources of propulsion power. Most hybrid cars currently marketed to consumers have both conventional gasoline and electric motors, with the ability to power the vehicle by either one independently or in tandem.

At start-up and low-to mid-speed range, the electric motor operates with high energy efficiency and low-speed torque. In normal cruising from vehicle start up to the mid-speed range, where engine efficiency is poor, the engine is shut off and the vehicle operates with the high-output fuel engine alone.

Figure 18 represents the normal cruising diagram, which is the High fuel efficiency operation using the engine as the main power source. In this operation, the engine power is divided between two systems by a power split device. One of these systems drives the generator to produce electricity, which in turn drives the motor (b). The other directly powers the wheels (c). The relative power distribution between the two systems is controlled to ensure maximum efficiency.

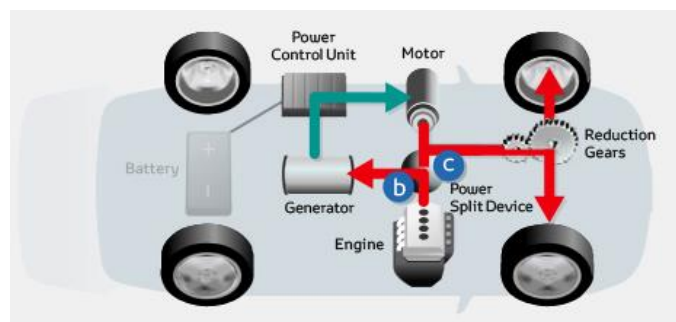


Figure 18: Normal cruising power flow diagram (40)

In Rapid Acceleration mode the two power sources provide the acceleration. The battery runs the electric motor during rapid acceleration. By adding the

electric power from battery to the engine, the vehicle delivers extremely responsive and smooth dynamic performance for additional superior acceleration.

The wheels drive the motor during the braking and deceleration. At this point, the high-output motor functions as a high-output generator in order to convert the braking energy into a source of electric power. This energy recovery process is known as regenerative braking, with the recovered electric power used to recharge the high-performance battery.

It is important to maintain a constant charge level for hybrid vehicles. When the battery charge level is low, starting the engine switches the generator on to recharge the battery (40).

1.5.3.1 Cylinder Deactivation

Cylinder Deactivation in automotive industry refers to the technology which allows the engine displacement to change by deactivating cylinders to minimise the fuel consumption and as a result to reduce the CO₂ emission (41).

Cylinder Deactivation or Temporary Downsizing offers an attractive compromise, as this allows the engine to shift its operating mode to achieve the specific consumption figures it is rated for, especially when low loads and operating speeds are encountered (41). One of the most consistent approaches to Cylinder Deactivation is to stop all moving parts (including the piston) as well as cutting the injection and ignition. This method utilizes the entire thermodynamic potential available and significantly reduces the frictions inside the engine.

The functioning cylinders following cylinder deactivation must generate a higher mean pressure when there is a specific performance requirement. The result of this load-point shifting results to throttle losses reduction as well as

fuel saving, as shown in Figure 19. Deactivating the valves also reduces friction loss in the cylinder head, which further minimizes consumption (42), (41) .

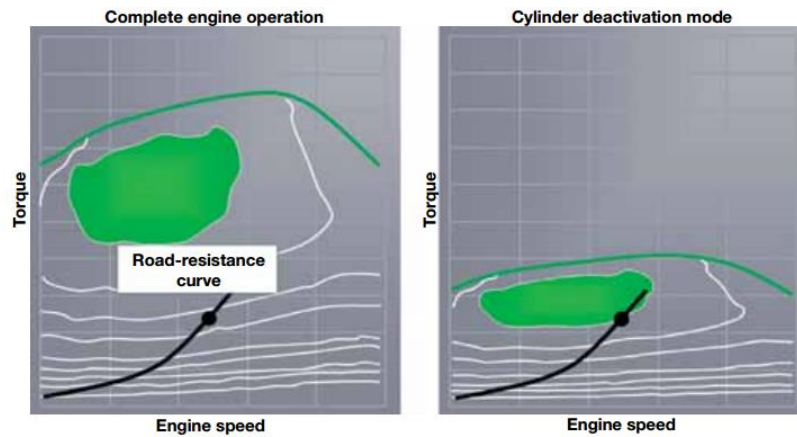


Figure 19: Operating data map and driving resistance curve (41)

The operating ranges associated with the lowest specific fuel consumption are approached in cylinder deactivation mode (Figure on the right)

1.6 Research Question

The research question which underpins the work described in this thesis is:
“Can eSC be feasibly implemented for small passenger cars (<1.2L) and what is the benefit in performance?”

Various technologies available in the market, which can lead to reduced CO₂ emissions, were discussed in detail. There are advantages and disadvantages to each approach but the question is which of these solutions are effective for the short term. The ultimate goal is to have zero emissions but what are the options in the meantime? What approaches can lead the society towards a greener environment?

Electric Vehicles look like a noble solution but there are number of barriers to fully adopt this technology at the moment such as infrastructure, charging strategies, battery range and reliability and more importantly the cost. Electric and Hybrid vehicles are expensive and cost is an important factor for the society. Therefore this option becomes limited for the time being. Meanwhile, the majority of vehicles are conventional and engine downsizing is a quick fix. It is the best way to reduce the CO₂ emission in vehicles.

In countries such as China, India, Iran and undeveloped countries where the cheap basic conventional cars with poor efficiency are used and majority of vehicle users can't afford expensive cars, eSC can cut the size of engines therefore vehicle fuel consumption can be reduced. This is even more applicable since lower cost vehicles are not boosted at all but are Naturally Aspirated. eSC might not be the best solution in long term but it is definitely an excellent short term solution to the problem.

1.7 Outline

The purpose of the introductory chapters was to introduce the topic, and place the research efforts of this thesis into the research field. The remaining of the thesis is dedicated to giving a description of the simulation and experimental work.

Chapter 2 describes the currently available technologies in the market which they are found to have limitations that are detrimental to the application of downsizing small engines.

An investigation of small compressors and devices is presented in Chapter 3. In this chapter TurboClaw and Screw Compressors are studied in detail and the reasons behind electing the TurboClaw compressor are also presented.

Chapter 4 describes the mean value engine model (MVEM) built within the Simulink environment. The focus of the research in this phase was to create a model which enables the user to vary system parameters in order to make a rapid assessment of several combinations of turbochargers and electric superchargers both in terms of steady-state full load operation and transient response. The results of the simulations are presented in Chapter 5.

Chapter 6 presents the experimental setup used for the measurements for the HiL boosting and the eSC package setup on the selected vehicle. Details of the sensors and measurements systems used are also given, along with general information on the testings.

Finally the motivation for the research was to provide pathway for success downsizing of small engines, one which is reliable and relatively cheap.

CHAPTER 2

2 Literature Review

As explained previously, there are well-known technologies available for larger engines but not for small engines, since a very small mass flow rate as low as 0.008g/s is required for low engine speeds where boosting is needed most. Figures 20 and 21 have been produced to show the required mass flow rate and break power for different capacities of engines for an assumed volumetric efficiency of 100% and intake conditions of 298 K, 1.01 bar. These graphs are produced just to demonstrate the generic trends which show more air flow is required as the engine gets larger and also the brake power increases as the engine gets bigger. Some of these options are not suitable for the automotive industry due to costly production or the need for a large electric motor such as backswept centrifugal compressors. Backswept centrifugal compressors need to run at high speeds and this is a costly feature of these machines, Figure 22. For instance as it can be seen on figure 22, MAHLE powertrain used a relatively large compressor to downsize a very small engine, the red triangle on the map shows the useful area which is needed for a 1.2L engine. Therefore, the following section demonstrates the findings on this subject in the literature.

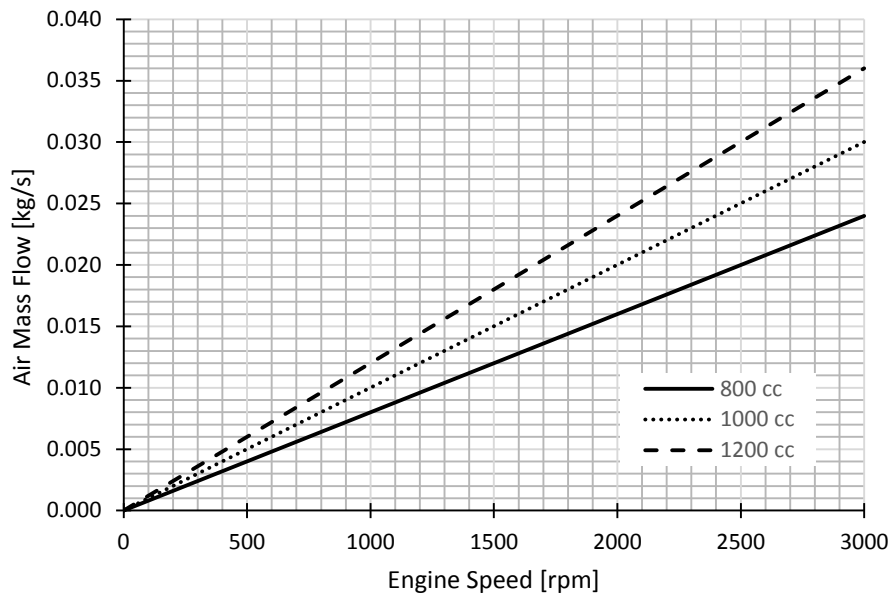


**Figure 20: Air mass flow rate vs engine speed for different engine sizes-
Pressure ratio 1.4**

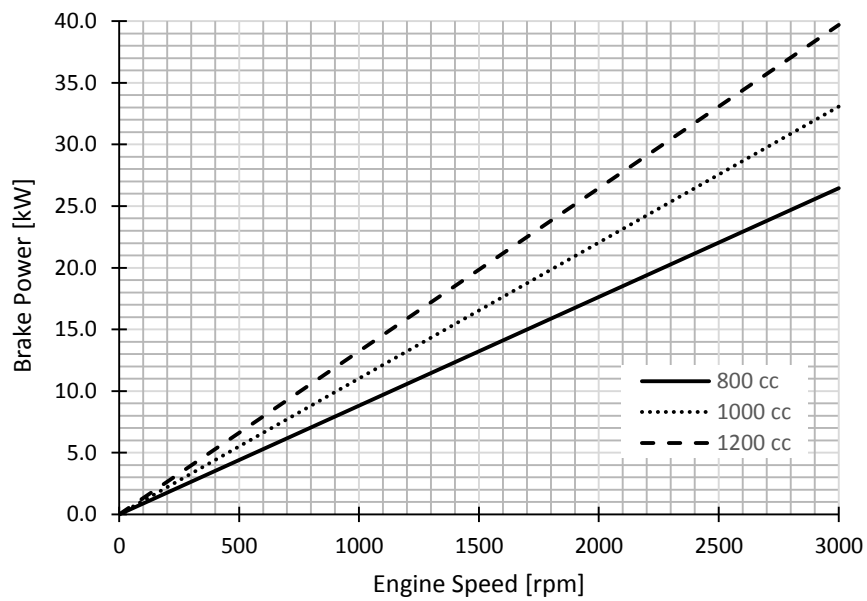


Figure 21 : Brake power vs engine speed for different engine sizes

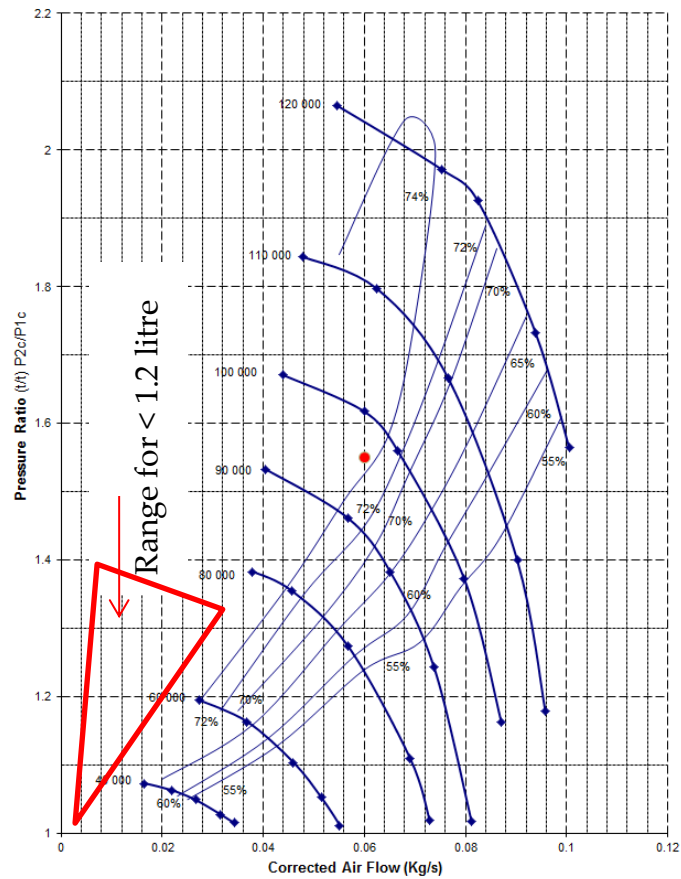


Figure 22: A conventional compressor map (43)

2.1 Supercharged engine systems

2.1.1 Eaton's Electrically Assisted Variable Speed Supercharger

According to Tsourapas and Benjey, 2013, Eaton's Electrically Assisted Variable Speed Supercharger (EAVS) combines all the advantages of a variable speed supercharger (SC) with engine off and engine starting functions, as well as regenerative (mild hybrid) capabilities using a planetary gear set to incorporate the engine, supercharger, and motor, as shown in Figure 23.

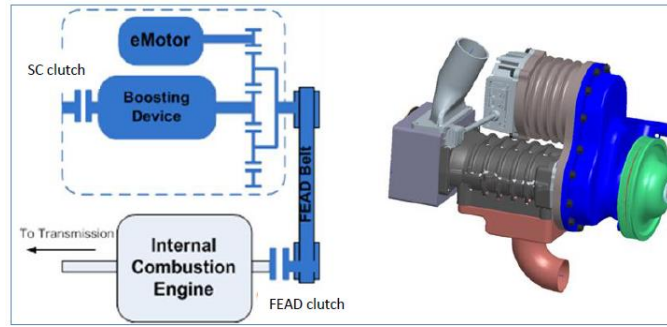


Figure 23: EAVS with start/stop architecture and 3D model (44)

EAVS have eight different operation modes depending on drive input and the power management strategy of the vehicle. These modes can be seen in the table 4.

operating mode	bypass position	Clutch 1 (SC brake)	Clutch 2 (FEAD)	Motor control	engine status
Boost	Closed	Open	Engaged	Pressure control	On
Naturally Aspirated	Open	Open	Engaged	Speed control	On
Engine start	Open	Engaged	Engaged	Speed control	On/Off
Brake Regen	Open	Engaged	Engaged	Torque control	On
Accessory	Open	Engaged	Open	Speed control	Off
Alternator	Open	Engaged	Engaged	Torque control	On
Torque Assist	Open	Engaged	Engaged	Torque control	On
Throttle Regen	Closed	Open	Engaged	Speed control	On

Table 4 : EAVS operation modes

Tsourapas and Benjey, 2013, focus on the boosting operation mode. When the driver torque demand exceeds the NA torque output of the engine, the EAVS is commanded to invoke boost operation. The bypass remains fully closed during boost since the variable speed control of the SC allows for accurate air flow control and does not require the bypass to modulate boost pressure. The SC

clutch is open and the FEAD clutch is engaged. The electric motor then controls the SC speed as a function of desired intake pressure which is calculated based on the torque demand map of the vehicle. A feed-forward and feedback control loop combination is used to ensure accurate SC speed control and compensation of the air flow dynamics. Figure 24 shows an example driving profile along with the potential modes of operation for each speed segment (44).

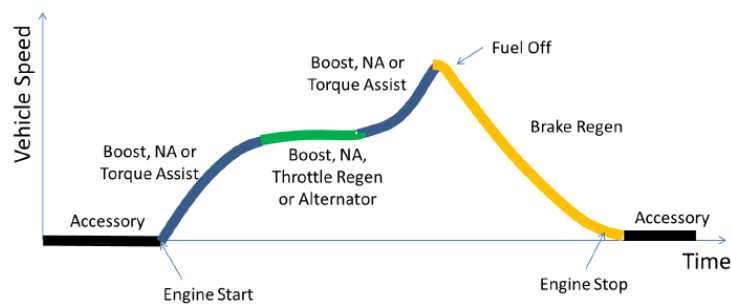


Figure 24: EAVS operating mode vs vehicle speed example (44)

Figures 27 and 28 show the supercharger performance map and the engine torque output respectively. The first observation from Figure 27 is the mass flow operating range and a scale of flow rate in g/s has been added to illustrate the issue. The lowest mass flow rate for this machine is somewhere around 22g/s with a 1.4 pressure ratio. Eaton successfully downsized a 2.8L NA to a 1.4L engine by using a TVS supercharger (Roots-type positive displacement compressor) but the SC has been pushed to operate in the corner of its map (red box on the map). The drawback of this approach is that a very large SC is operated at low speed to provide low mass flow rates. According to Hu (2017) “In conventional Roots-type positive displacement blowers, due to manufacturing tolerances, smaller clearances at multiple locations between two opposing supercharger rotors, between the rotor and housing (see Figure 25) and between the end plates and rotor ends (see Figure 26) cause leakage from

the outlet of the conventional series-production Eton TVS R-Series to the transfer volume and from the transfer volume to the inlet, resulting in reduced volumetric efficiency". The smaller TVS R-series devices, suitable for 0.5 L to 2.0 L displacement, suffer more from low speed volumetric efficiency due to the increased leakage area to displacement ratio (45) .

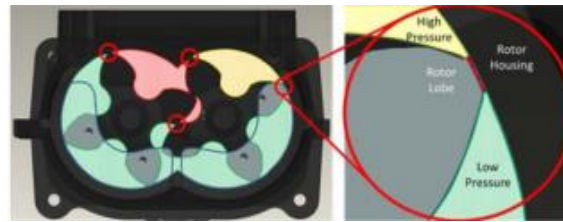


Figure 25: 8. Diametral rotor leakage locations (left) and air leakage between the rotor lobe tip and rotor housing (46)

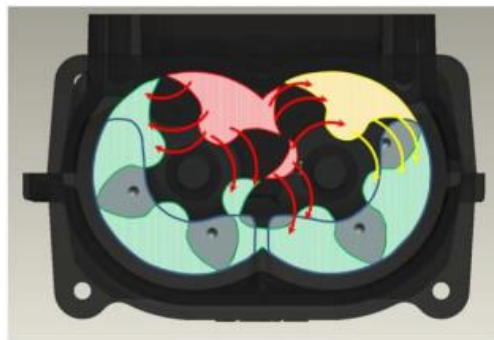


Figure 26 : Leakage between rotors and end plates (46)

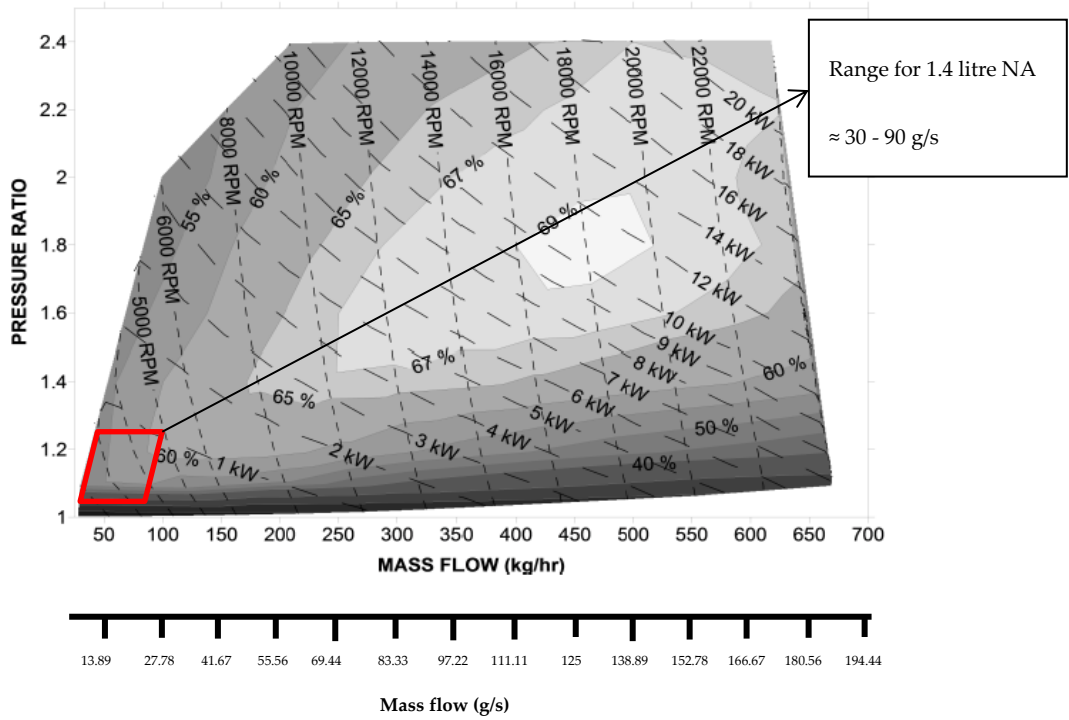


Figure 27: Supercharger performance map (44)

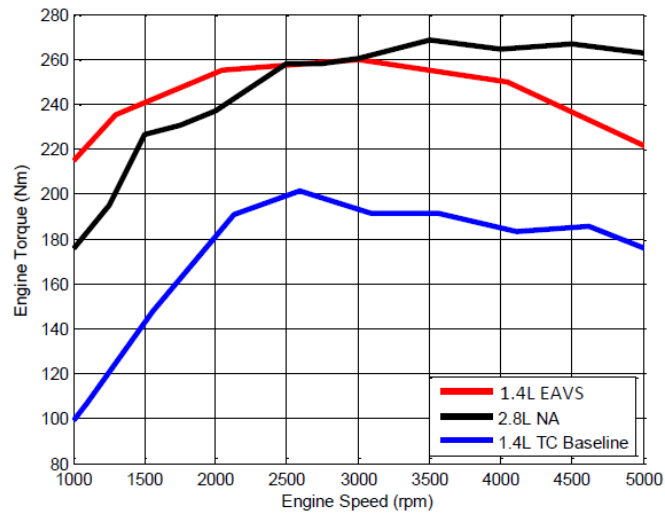


Figure 28: Measured engine torque output (44)

2.1.1.1 Critical review on Eaton's Electrically Assisted Variable Speed Supercharger

It is concluded from the paper, (44), that the solution appears to work for engines suitable for large or high performance cars and even for powerful engines the compressor is substantially oversized based on the supercharger performance map , Figure 27. This compressor does not cover the range of interest for engines < 1.2 litre. The range of interest is shown with a red box on the performance map.

2.1.2 CPT COBRA water cooled electric supercharger

Figure 30 shows the CPT COBRA (Controlled Boosting for Rapid Response) C88 compressor map. The C88 is a member of the electric supercharger family that CPOWER (Controlled POWER Technologies) have developed. The company claims that C88 is suitable for exhaust after treatment systems, fuel cell and air pressure up lift. C88 mass flow range is 10 -34 g/s. There are two other electric superchargers from the same family; C70 and C80 are both suitable for applications where large mass flow rates are required. C70 has a mass flow rate range of 27.78-83.33 g/s whereas C80 has a range of 83 -222 g/s (47).



Figure 29: Water cooled electric supercharger; C88 (47)

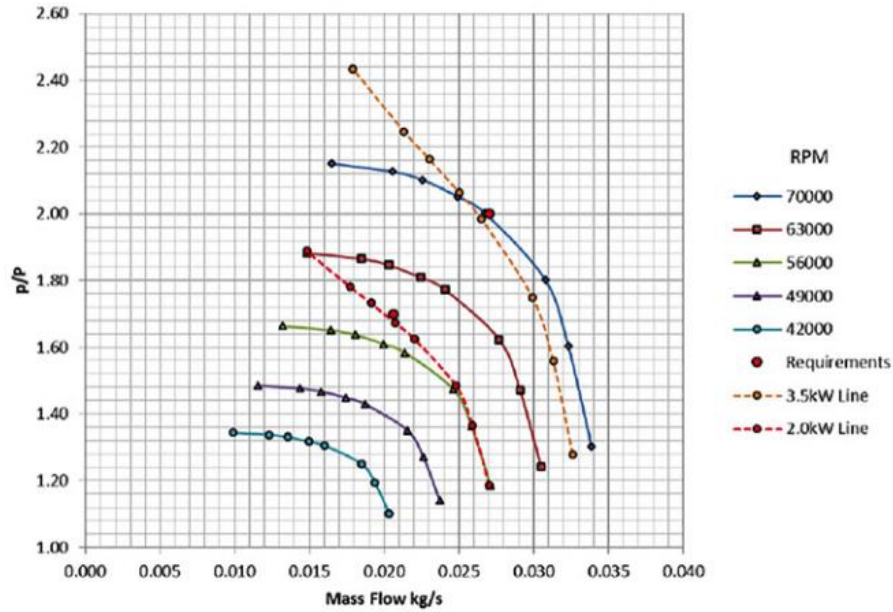


Figure 30: Cobra C88 characteristics (47)

There is limited information available on this product; however compressor efficiency could be calculated by using equation 1, derived from (48) :

$$\dot{W}_c = \frac{1}{\eta_c} C_p \dot{m} T_1 (Pr^{\frac{\gamma-1}{\gamma}} - 1) \quad [1]$$

Where W_c is power, \dot{m} is mass flow rate, T_1 is temperature, Pr is pressure ratio, η_c is compressor efficiency, C_p is specific heat capacity² and γ is specific heat ratio, 1.4. Figure 31 and tables 5&6 are produced based on the Equation 1 in order to draw a conclusion on this technology. The maximum efficiency for this compressor is around 45% at pressure ratios 1.68 and 1.98 for 2.0kW and 3.5 kW respectively which is a drawback. The expected efficiency for this application from industry would be 70% or more, some option will be discussed later on in this chapter with much higher efficiency. The other

² $C_p=1.005$ kJ/kg.K at 300 K

drawback to this technology is its coolant system which adds complexity to the system.

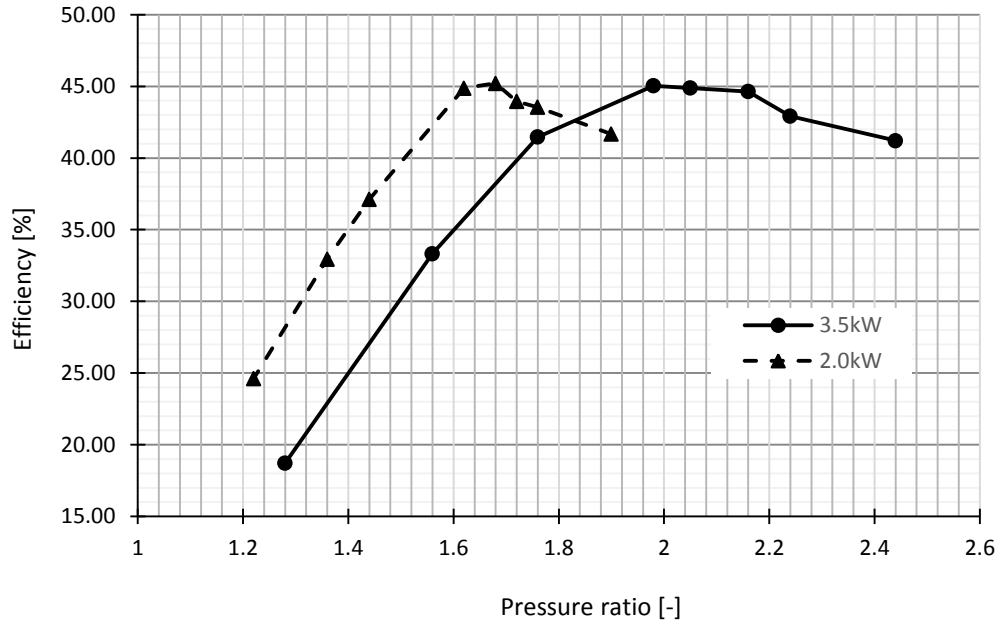


Figure 31 : Efficiency vs Pressure ratio for Cobra C88

2kW		
PR	Mass flow rate [kg/s]	Efficiency [-]
1.9	0.015	41.67
1.76	0.018	43.55
1.72	0.019	43.95
1.68	0.0205	45.20
1.62	0.022	44.87
1.44	0.0245	37.13
1.36	0.026	32.95
1.22	0.0305	24.61

Table 5: Cobra C88 Characteristics - 2kW line

3.5kW		
PR	Mass flow rate [kg/s]	Efficiency [-]
2.44	0.018	41.21
2.24	0.021	42.92
2.16	0.023	44.64
2.05	0.025	44.88
1.98	0.0265	45.04
1.76	0.030	41.47
1.56	0.0312	33.33
1.28	0.0325	18.73

Table 6 : Cobra C88 Characteristics – 3.5kW line

2.1.2.1 Critical review on CPT COBRA water cooled electric supercharger

The conclusion to this part is that this compressor is not an ideal solution for boosting small engines due to its poor efficiency. The car manufacturers are concerned about the current drawn from the battery and such a high pressure ratio is not required for such small engine.

2.1.3 HyBoost – An intelligently electrified optimised downsized gasoline engine concept

HyBoost targets were to deliver a C-segment model year 2011 (MY2011) Ford Focus demonstrating a 30-40 percent reduction in CO₂ emissions as measured over the NEDC (to below 100 g/km) versus a baseline MY2009 2.0L Naturally Aspirated (NA) gasoline engine version of the passenger car whilst maintaining the comparable vehicle performance and driveability attributes. Figure 32 shows a simple scheme of the concept with the 2.0L NA engine replaced with a downsized DI gasoline engine (1.0L 3-cylinder), and equipped with a

conventional fixed geometry turbocharger (FGT) delivering superior steady state power and torque levels. A Front End Accessory Drive (FEAD) mounted Belt Starter Generator (BSG) gave micro hybrid functionality of stop/start and more efficient motoring and generation enabled through the higher voltage "12+X" (typically between 18 – 27V) energy storage of an ultra-capacitor system. Energy recovered during deceleration events could be deployed in a sophisticated boosting system combining a 12+X electric supercharger "blowing through" the conventional turbocharger and/or the BSG torque assist system, using the electrical energy optimally to achieve good transient response or improved fuel consumption. The component systems have previously been demonstrated individually at 12 volts, but not brought together in this synergistic combination as a "12+X" system.

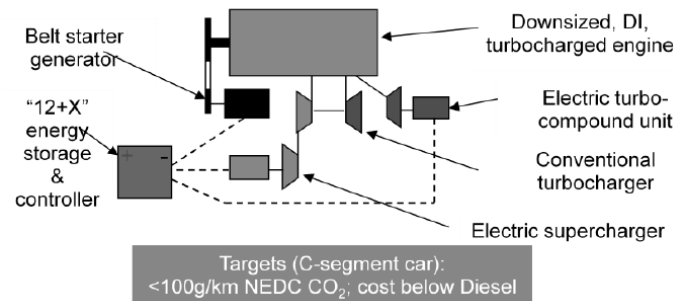


Figure 32: Scheme of the concept with the 2.0L NA (49)

HyBoost uses a modified near production Ford 1.0L 3-cylinder turbo GDI EcoBoost base engine. This gives 50 percent downsizing over the baseline 2L engine. Figure 33 shows the steady state torque curves of the two engines, and the superior performance of the HyBoost engine can be clearly seen. The Ford 2.0L Duratec engine produces peak power and torque levels of 107 kW at 6000

rpm and 185 Nm at 5000 rpm respectively. This compares to the HyBoost (with no electric supercharger assist) peak power and torque levels of 105 kW at 5500 rpm and 234 Nm at 2500 rpm respectively. This was achieved through re-optimisation of the boosting system, use of a new intake air path to include the electric supercharger, and fitment of a new high efficiency Valeo Water Charge Air Cooler (WCAC) system. The WCAC system was specified with a very high (relative to engine size and performance) heat rejection capability of between 16 – 18kW. This was key to enabling excellent charge cooling to mitigate knocking and maintain lambda 1 operation through to full load, resulting in excellent Brake Specific Fuel Consumption (BSFC) across the entire operating map (50).

As the engine becomes more aggressively downsized several potential issues arise with regards to perceived performance. Firstly, the main issue is turbocharger lag, where the device itself takes time to build up boost pressure, and the subsequent transient torque curve does not meet the steady state torque curve. Secondly, often there can be a large difference between the low engine speeds “NA” torque (typically 8 – 11 bar BMEP), where the Fixed Geometry Turbocharger (FGT) is not able to deliver any significant boost pressure even during steady state conditions, and peak torque, which can be as high as 34.5 bar BMEP in the case of HyBoost with a larger turbocharger fitted. This can also give a perceived turbocharger lag feel during vehicle launch even if the boosting system response is more than adequate (50) .

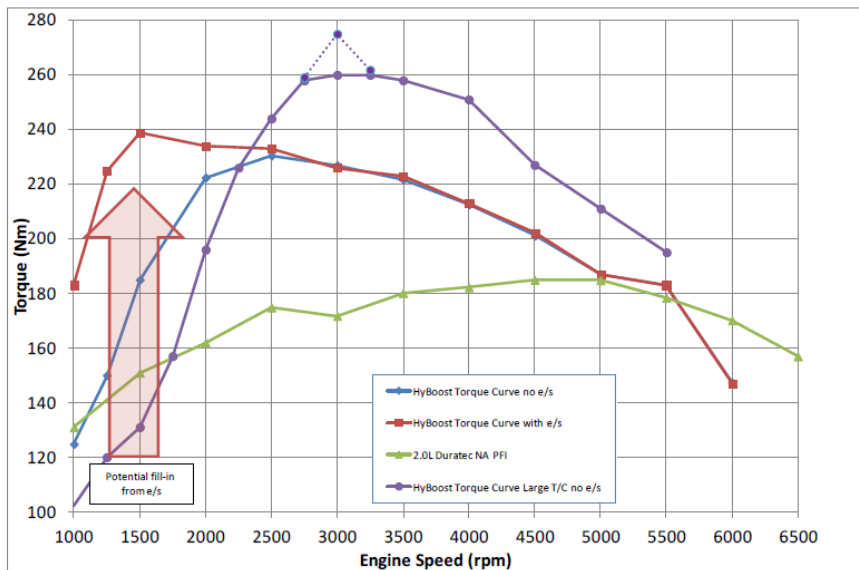


Figure 33: Ford 2.0 L Duratec vs HyBoost torque curves comparison (50)

Figure 33 also shows the full load torque curve of HyBoost with the electric supercharger running from 1000 to 2000 rpm engine speed. The following key benefits of the electric supercharger can be determined from the detailed analysis performed on the HyBoost project:

The electric supercharger provides additional boosting capability beyond the FGT and thus enables significant steady state and transient torque augmentation in the lower engine speed range. The FGT also behaves as a pressure ratio multiplier of the electric supercharger boost, so it is effectively an in-series, 2-stage compressor system.

At 1000 rpm, the torque rises from 125 to 183 Nm with the electric supercharger assistance, which is equivalent to a 6.1 kW increase in power at this speed (13.1 to 19.2 kW respectively). At 1500 rpm, the rise is from 185 to 239 Nm, which is an 8.48 kW increase, and both of these improvements were achieved with an input of only 1.8 kW to the electric supercharger. This equates to a 47 and 29 percent increase in engine torque at those speeds respectively, and transiently

the proportional increase in engine torque could be even higher dependant on the boost response without the electric supercharger assistance (50).

2.1.4 The MAHLE Downsizing demonstrator engine

The MAHLE engine is a 1.2 litre, 3 cylinder engine originally with two turbochargers (two-stage turbocharging), although later modified to just one turbocharger for a cost effective marketing approach.

Parameter	Value
Engine displacement	1.2 L
No. of Cylinders	3 in-line
Bore/stroke	83.0/ 73.9mm
Compression ratio	9.3:1
Fuel injection	Multi-hole central DI
Spark plug	M10
Engine Control	Mahle flexible ECU
Turbocharger	Bosch Mahle Turbo system

Table 7: MAHLE Specifications

MAHLE engineers aimed to produce a high torque, high output engine with two-stage turbocharging. This approach achieved a good transient response at all engine speeds, and exceeded 30 bar peak brake mean effective pressure (BMEP). The engine reached 6000 rpm and had an peak power engine of 144 kW (120 kW/litre). Furthermore, stoichiometric fueling was maintained over the full-load line. Figure 34 demonstrates the two-stage turbocharging arrangement used in the MAHLE engine (51) .

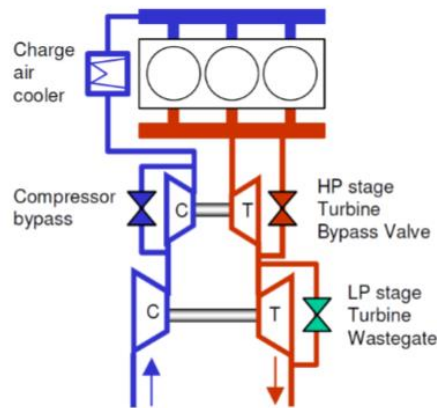


Figure 34: Two-stage turbocharger arrangement

2.1.4.1 Critical review on the MAHLE technology

The solution presented by MAHLE clearly shows improvement in engine output; However the argue is that this is a powerful engine. The engine is 1.2 L engine but it is not a small power engine as the peak power is 144 kW, it has small capacity but the power is high, therefore it is not an ideal solution for this project.

2.2 Aeristech's eSupercharger

Table 8 shows the Aeristech's eSupercharger specification summary used for Mahle's project . A centrifugal compressor with maximum operating speed of 140,000 rpm, the supercharger performance map is shown in Figure 36.



Figure 35: E-Supercharger 2012 Model

Parameter	Value
Compressor type	Centrifugal
Motor	High-speed PM
Max operating speed	120000 rev/min
Lubrication	Greased for life
Cooling	Liquid
Input voltage	48 V nominal
Unit mass	4.2 kg

Table 8: e-Supercharger specification summary

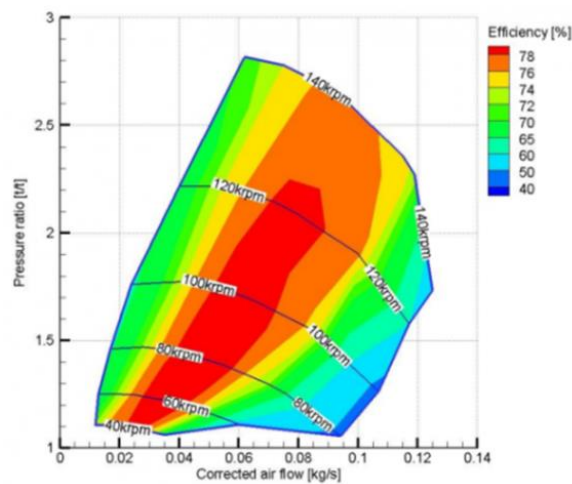


Figure 36: Aeristech's supercharger performance map (52)

2.2.1 E-Supercharging for Heavily Downsized Gasoline Engines

The e-Supercharger can be located upstream or downstream of the main turbocharger compressor, as shown schematically in Figure 37, or upstream, as shown in Figure 38. According to Bassett, 2015, In order to provide high-pressure air at low engine speeds, at flow rates below where there is sufficient exhaust energy for the larger main turbocharger to provide high-pressure air, the e-Supercharger is optimised for low flow rates. This means that the e-Supercharger will not be capable of passing the full air flow required by the engine at higher power outputs. Thus, the e-Supercharger must be bypassed when high engine power is required. Additionally, there must be sufficient overlap between the e-Supercharger operation map and the main turbocharger map to enable a seamless handover between the two devices in operation. This prevents any torque interruption which would give an undesirable torque dip for the driver (53).

Placing the e-Supercharger downstream of the main compressor has the advantage of effectively broadening the supercharger map, towards higher-mass flows. However, MAHLE Engineers have decided to place the e-Supercharger upstream of the turbocharger compressor, as shown in Figure 38, to protect the prototype as it will need to withstand a temperature of up to 180° C (51).

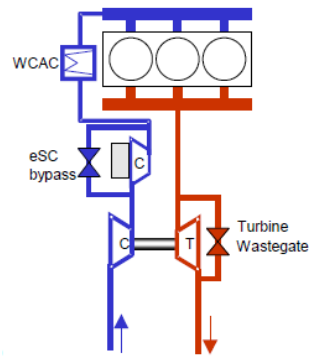


Figure 37: Schematic of the twin-turbocharger arrangement, Post turbocharger compressor (53)

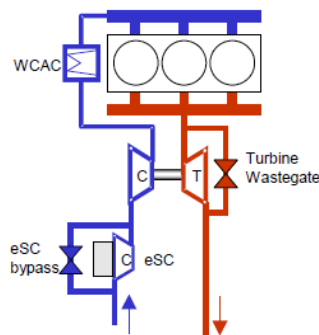


Figure 38: Schematic of the twin-turbocharger arrangement, Pre-turbocharger compressor (53)

Engine Test Results

The results, shown in Figure 39, show the significant improvement in peak power offered by the new turbocharger (increasing to 193 kW, from a baseline maximum of 120 kW). Equally, the penalty that this turbocharger imposes in terms of BMEP output, when operated without the e-Supercharger, at low speeds is evident from Figure 39. Without the e-Supercharger, the new turbocharger has almost no charging effect until engine speed is above 2,000 rpm, and peak torque is not achieved, operating with the turbocharger alone

until 3,000 rpm. If this configuration were to be used in a vehicle, a serious negative effect on the drivability would be anticipated, particularly in heavier vehicle applications (51).

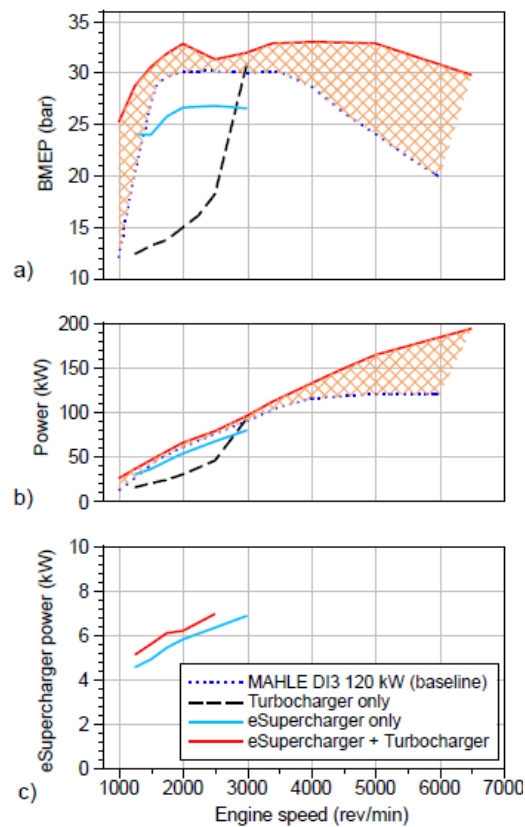


Figure 39: Test results from the MAHLE downsized engine with combined eSupercharger and turbocharger; a) BMEP, b) power and c) eSupercharger power (53)

2.2.1.1 Critical review on Aeristech’s supercharger

Based on the research done by Bassett, 2015, eSC boosted engine torque by 40% at 1200 rpm and 29% at 2000 rpm. This demonstrated eSC was very effective and feasible for high power engines.

There are many cases of boosting low capacity engines ; however, no solutions is offered for small power engines for small cars , <1.2L. Nonetheless, no engine points validation is provided by MAHLE to examine whether the engine is operating within the acceptable region or not. Based on the provided results , the eSC starts to operate at 1200 rpm but the graph shows that the eSC boosts the system from 1000 rpm, therefore a clarification is needed to explain this behaviour by the MAHLE engineers.

2.3 Summary

The critical review was done on each technology which was demonstrated earlier in this chapter. The common conclusion from these technologies is that there is a lack of supercharger for engine downsizing of small engines in the automotive industry. Different companies took different approaches but the common drawback is using a very powerful supercharger which is suitable for larger engines (>1.2L). Using a powerful supercharger leads to using a bigger and more powerful battery which leads into higher cost and a very powerful engine which is not the ideal for this project. Hence it was necessary to find a suitable compressor which can operate at lower speed (up to 50,000 rpm) when compared to conventional turbomachinery which can achieve low flow-rates for a range of pressure ratios.

CHAPTER 3

3 An investigation into small compressors including scaling

It was important to identify the most suitable compressors for small engine boosting application; therefore different types of compressors were identified and studied.

Centrifugal compressors are known for their high speed (54) therefore they cannot be a feasible solution for this application. The other two possible compressors were investigated in details, TurboClaw and Screw Compressors, and the results of this study are presented in sections 3.1 and 3.2.

3.1 Turbo compressors

As shown in the earlier chapters, supercharging has been demonstrated to be very effective in mitigating low engine torque in turbocharged engines for high power engines suitable for heavy and high performance passenger cars. However, for the mainstream passenger cars, a much smaller flow rate compressor is needed, with volume flow rate of 40-80 m³/hr ; whereas for all the examples of implemented eSC, the compressor flow rate required is between 150-400 m³/hr. It was hence necessary to investigate how compressors of both positive displacement and turbocompressors could be scaled down in flow and investigate the literature around small compressors.

According to Figure 40, axial turbo-compressors are the most efficient compressors available in the market. Nevertheless, it is not always possible to achieve the performance suggested by Figure 40 for small machines. Test results for numerous compressors lie within the shaded areas. The full lines

represent the envelopes of the different types. The dotted line is the suggested overall envelope.

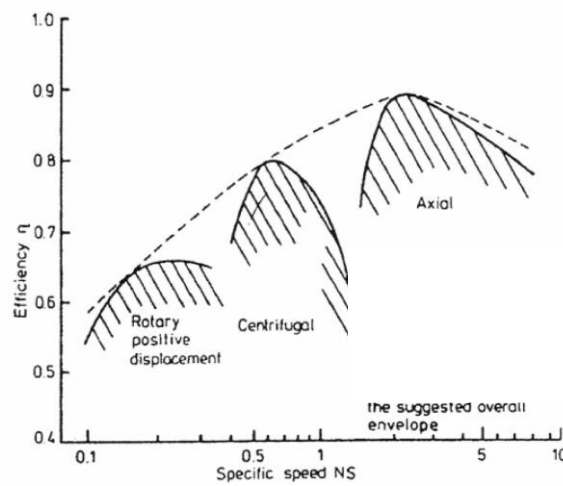


Figure 40 : Specific Speed vs Efficiency (55)

Non dimensional specific speed, N_s , defined by:

$$N_s = \omega \frac{\dot{Q}^{1/2}}{\Delta h^{3/4}} \quad [2]$$

Where ω , \dot{Q} and Δh are speed (rad/s), volumetric flow rate (m^3/s) and change in specific enthalpy (J/kg) respectively for isentropic compression. Figure 41 shows the specific speed line of 1.18 appropriate to conventional turbomachines. For a 1L engine size, calculation show a turbocharger operating in the range of 150,000 to 200,000 rpm to boost engine at high and low flow rates respectively (32).

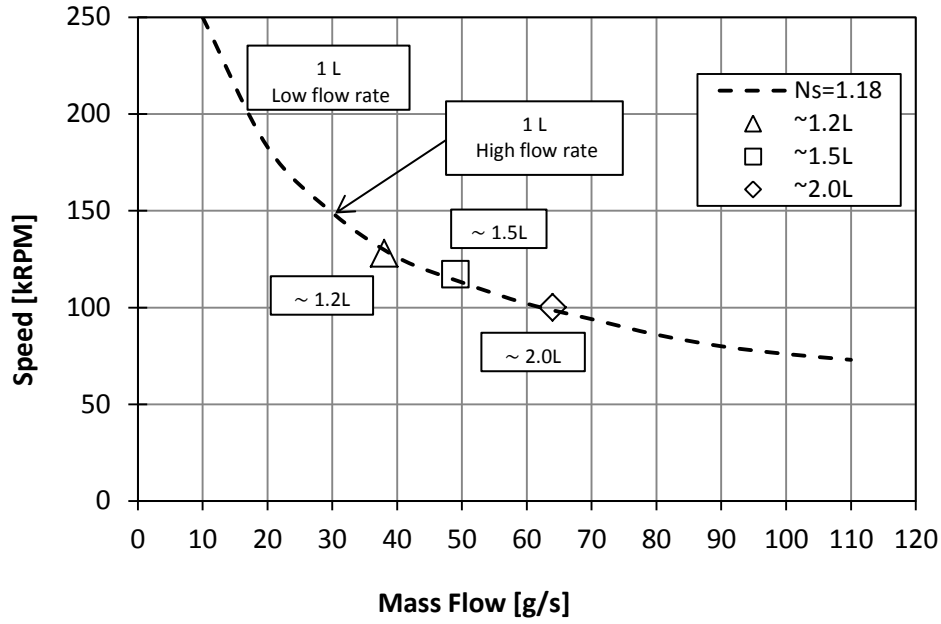


Figure 41: Turbocharger speed for different engines at PR 1.4 (32)

More accurate calculations may be performed considering that the turbocompressor pressure ratio p_{out}/p_{in} is governed by the thermodynamics relationship, Equation 3, (56).

$$\frac{P_{out}}{P_{in}} = \left(\frac{\eta_i \Delta h_o}{c_p T_{o,in}} + 1 \right)^{\gamma / \gamma - 1} \quad [3]$$

and the Euler Turbomachinery equation, equation 4 ;

$$\Delta h_o = U_{out} C_{\theta out} - U_{in} C_{\theta in} \quad [4]$$

Where Δh_o is the work input to the gas and U and C_θ , the blade speed and tangential velocities respectively.

The efficiency of turbo-machines reduces due to greater relative wall friction as they become smaller in size. This is a well-known phenomenon and semi-empirical methods based on the Reynolds number can be used to predict the efficiency penalty for scaling a turbo-machine down (57).

The speeds required for a standard backswept turbo-compressor are very high (150,000 rpm and above) creating challenges for the bearings and the electric motor. It is technically feasible but not acceptable due to potential costs and risks for the automotive industry. These speeds are not a problem for turbocharger since the drive is not an electric motor but a high speed turbine. Bearings are plain oil type and the configuration of pressurized compressor and turbine mitigates the sealing issue which is difficult to perform when the driver is an unpressurised electric motor. Pressurization could be done but this increases windage losses.

3.2 The TurboClaw compressor

TurboClaw is a new type of centrifugal compressor, Figure 42, developed by Dynamic Boosting Systems (DBS), where the flow is drawn axially, directed radially, and delivered axially. This technology brings the benefits of turbomachinery to low flow rate applications.

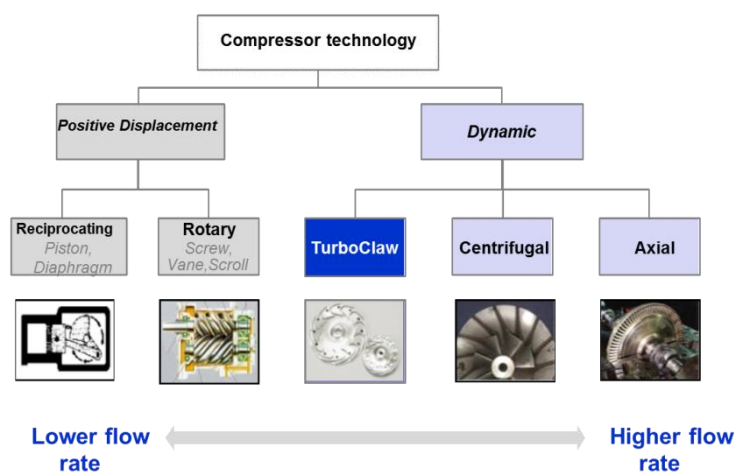


Figure 42: Compressor systems (58)

The use of forward sweep in order to increase Euler work (Equation 4), and to reduce blade speed has been understood for many years. However, it is seldom used because it was found that efficiency deteriorated and the flow range of the compressor was reduced. Added to this, it can lead to an unstable machine since the pressure ratio can rise with increased flow rate.

The innovation from DBS was to address this shortcoming by increasing forward sweep so substantially that the outlet blade angle becomes almost tangential. The design which ensues from this approach is shown in Figure 43 along with the velocity triangle for the rotor outlet (32).

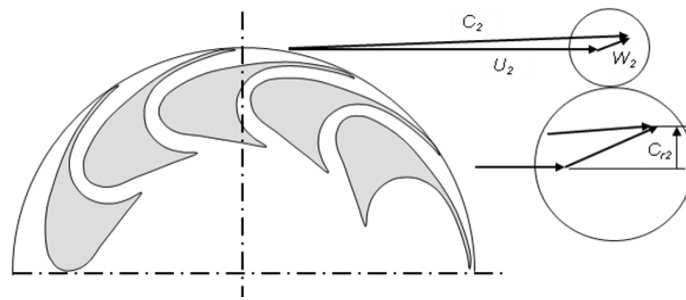


Figure 43: The TurboClaw Geometry and rotor exit velocity triangle (59)

TurboClaw based compressors have been tested extensively to supply low flow rates at moderate shaft speeds. A brushless DC electric motor designed and developed for testing purposes. The motor shaft drives a single stage TurboClaw compressor via a high speed torque sensor (58). TurboClaw achieves low flow-rates for a range of pressure ratios, at comparatively lower speeds of operation when compared to conventional turbomachinery. At low specific speed it achieves a similar or higher efficiency than both positive displacement and turbocompressor technologies at a fraction of the cost (60).



Figure 44 : TurboClaw (61)

3.2.1 Experimental Testing for Electric Supercharger

For the smaller size of machine suitable as an electric supercharger, a new design was produced driven directly by a specifically developed brushless DC electric motor. The specific speed of the machine was increased in order to provide compactness yet keep rotor speeds amenable for low cost bearings and motor (59).

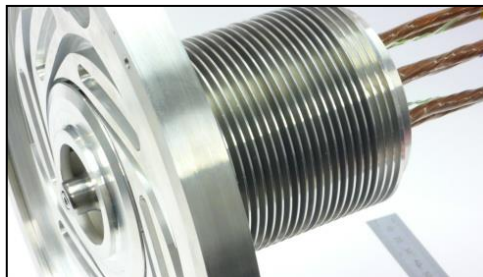


Figure 45: TurboClaw for supercharger application (59)

Figure 46 shows the compressor map for this machine. The characteristic of this compressor is similar to a conventional compressor but operates at significantly lower speed than a conventional turbocompressor.

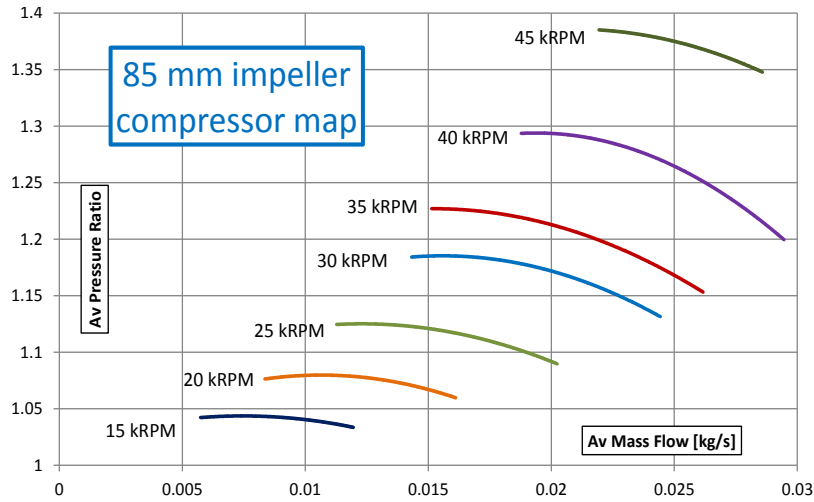


Figure 46: TurboClaw compressor map for an 85mm rotor (59)

Unlike the case of a turbocharger where a high speed turbine is available to drive an equally high speed conventional radial compressor, a supercharger must be driven by means of an electric motor or mechanical drive. TurboClaw supercharger operates intermittently at low engine speeds to restore acceleration torque of a smaller engine to the levels of the original size (59). Reducing the compressor speed allows the electric motor to operate at feasible speed not beyond 50,000 rpm, the cost of which is unsustainable for the automotive market (59).

To conclude, the TurboClaw compressor is a new form of radial turbo compressor. The innovation uniquely placed as it is amenable to being electrically driven at speeds substantially lower than conventional turbo compressors.

3.3 Positive Displacement Compressors

Typically a positive displacement machine will be chosen for low specific speed applications. These machines work by enclosing a fixed volume of gas, reducing its volume by a compression ratio that is fixed by the machine's geometry, and then exhausting the gas. The most common types of positive displacement compressors are shown in Figure 47 (62).

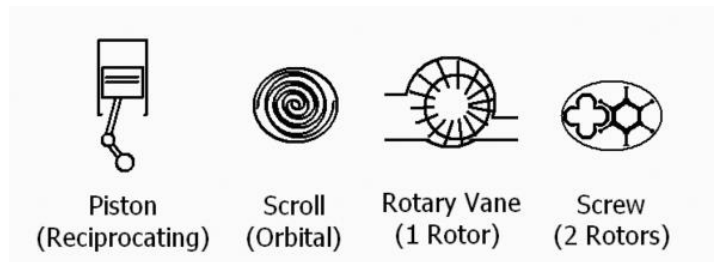


Figure 47: Common types of positive displacement compressor (63)

Reciprocating compressors are known to be the slowest and the largest positive displacement machines. Despite the fact that they require frequent maintenance, they operate efficiently. Oil ingesting designs require filtration and oil-free designs have a limited pressure ratio due to the temperature limits of the piston rings.

Scroll compressors are usually used for very low mass flow rate applications. These machines are used for fueling micro turbines. These machines have limited service life and non-established reliability since they are relatively new technology (54).

Rotary Vane compressors usually ingest oil give rubbing surfaces, which requires the usual removal process. They are reasonably reliable, cheap to manufacture, and require minimal maintenance. Their size is moderate when compared to other positive displacement machines (62).

3.4 Rotary positive displacement compressor investigation

It was important to evaluate potential alternatives to the TurboClaw for low mass flow rate superchargers rather than assume TurboClaw to be the only solution. Such positive displacement compressors have been used commercially as superchargers for many decades although mainly for large high performance engines. Low flow rate versions of these machines are not available and the reasons for this were not understood. Was it simply a cost issue or was it due to performance. A research study was hence carried out to answer this question.

3.5 Background

Screw compressors are rotary positive displacement machines of simple design with the moving parts comprising only two rotors rotating in four to six bearings. Screw compressors are well known for the efficient operation at high speeds over a wide range of operating pressures and flow rates. As a result these types of compressors are not suitable for the applications where the small mass flow rate is required. One of the main reasons for the high efficiency of these machines is the linear tolerance reduction to below 10 μm due to improvements in high accuracy profile milling and grinding. Therefore this allows rotors to be manufactured with interlobe clearances of 30-50 μm at an economic cost. The most common type of rotary compressor is the helical twin, screw compressor. Two mated rotors mesh together, trapping air, and reducing the volume of the air along the rotors. Depending on the air purity requirements, rotary screw compressors are available as lubricated or dry (oil free) types (64).

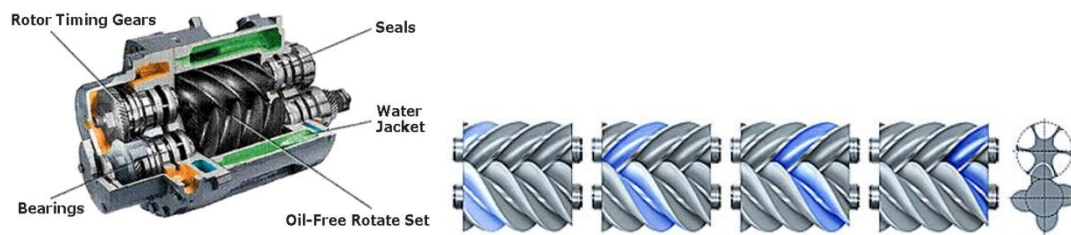


Figure 48 : Cross Section of a Representative Rotary Screw Compressor (64)

3.6 Screw compressor modelling

The software developed and used by the authors for the conceptual as well as the preliminary design of screw machines is called SCORPATH – Screw Compressor Rotor Profiling and Thermodynamics. It calculates and optimises compressor performance for a specified duty. To start the procedure of rotor profiling, the profile point coordinates in the transverse plane of one rotor, and their first derivatives, must be known. The full rotor and compressor parameters, in the form of rotor throughput, rotor displacement, size of leakage flow area, as well as suction and discharge port coordinates are calculated from the rotor transverse plane coordinates and rotor length and lead. They are later used as input parameters for the calculation of the thermodynamic and fluid flow processes within the screw compressor as well as for further design tasks, such as the generation of detailed drawings (64).

3.7 Geometry of screw compressor rotors

The rotor lobe profiles have to be defined together with the remaining rotor parameters before the rotor and housing geometry can be fully specified. To explain the rotor profiling principles, a default profile version is used, so called

Demonstrator, which can take any realistic combination of numbers of lobes in the main and gate screw rotors. However, any other known or a completely new profile can be generated, with little modification. Such profiles must, of course, satisfy geometrical constraints in order to obtain a realistic solution. The subroutines to calculate a majority of the existing screw compressor rotor profiles can be obtained upon request.

3.8 Screw Compressor Downscaling Investigation

The aim of this study is to determine the efficiency of smaller screw compressors and it was important to have as starting point a validated result. Therefore a relatively large (male and female outer diameter are 127 and 120 mm respectively) screw compressor was chosen for this purpose since this was the smallest compressor available on the rig. The compressor was tested in the test cell and results have been obtained and processed, then SCORPATH was used for the downscaling analysis.

The downscaling technique in this case was achieved by Importing the known compressor dimensions, geometry and thermodynamics conditions into the software then validating the software by comparing measured and simulated results. Once validated, use the software to perform direct scaling down .The result of this study can be found in the section 3.8

Five different sizes of screw machine were simulated and a summary of the results is given for two different pressure ratios in Figures 50 and 51. Compressors have asymmetric "N" profile with 3 and 5 lobes on the male and female rotor respectively, Figure 49. The compressor speeds ranging from 7000 to 40000 rpm and pressure ratio from 1.1 to 2. All the design data such as outer diameter, inner diameter, axis distance and etc have been scaled down

excluding clearances. 40 percent reduction in size represents 40 percent reduction in all the variables compared to the original compressor.

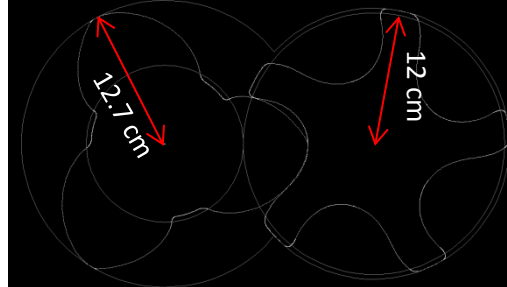


Figure 49: Rotor N profile diagram

Figures 50 and 51 show the efficiency vs mass flow rate for different compressor sizes at two different pressure ratios each for a range of speeds. As expected, the efficiency drops enormously as the size reduces. In overall the performance of these screw compressors are not close to the TurboClaw when it comes to small mass flow rate, Pressure ratio and low speeds. At both pressure ratios, efficiency of the smallest machine drops to lower than 10 percent, note that 80 percent reduction in size is producing the required amount of mass flow rate for this project and other sizes are too big for this application.

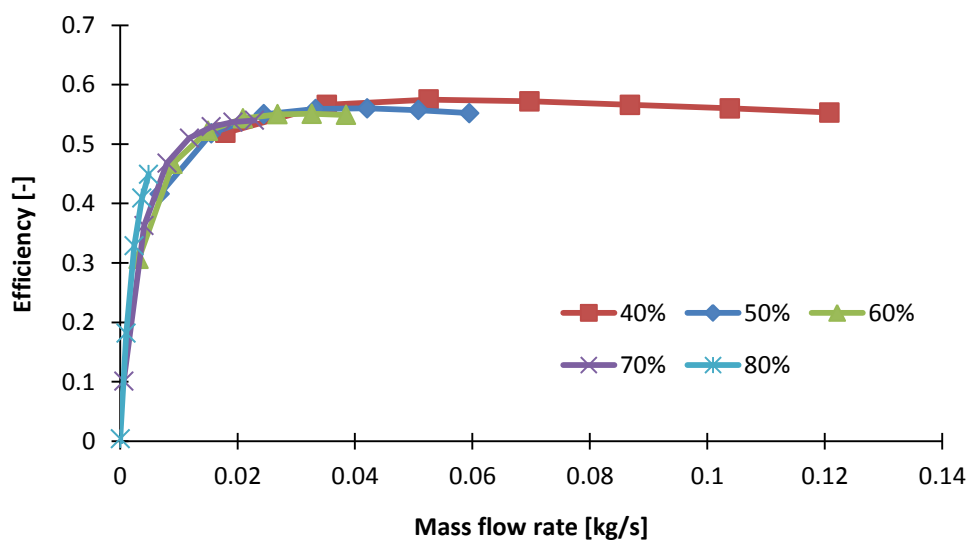


Figure 50: Efficiency vs Mass flow rate for different sizes at pressure ratio 1.4

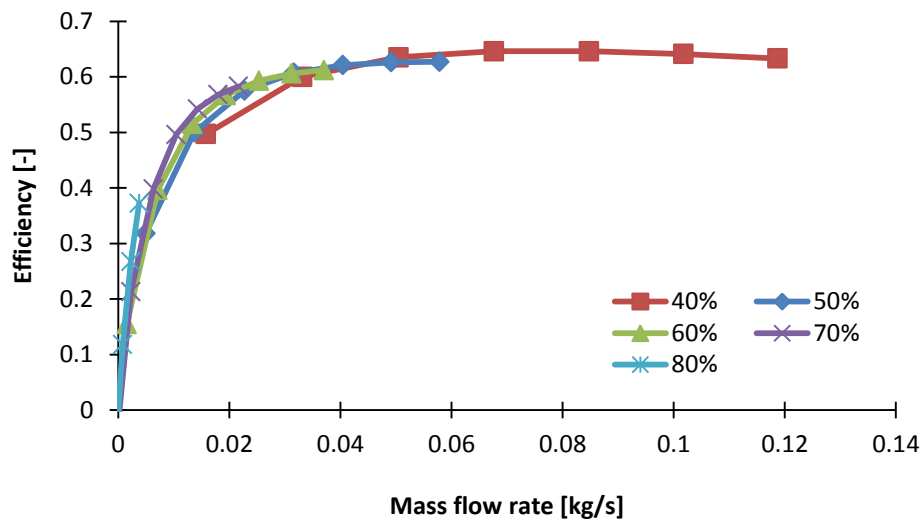


Figure 51: Efficiency vs Mass flow rate for different sizes at pressure ratio 1.6

Screw Compressors work at the higher end of the specific speed range for positive displacement machines, requiring much higher shaft speeds. They are more reliable and compact than other positive displacement machines and operate with reasonable efficiency. Oil ingesting designs require filtration. Oil-free designs require precision timing gears and very high manufacturing tolerances for a complex geometry (62). Screw compressors have the highest power density of the positive displacement machines. In summary, positive displacement machines have the disadvantages of large size and weight, high complexity, the requirement for frequent maintenance, oil ingestion, and high cost.

3.9 Summary

The conclusion to this chapter is that positive displacement compressors are not suitable for this application. Screw compressors have been used on air and various refrigeration and process applications for a great number of years. In

the past 20 years the machines have become very popular in the natural gas industry in booster and gas gathering applications with additional growth in the solution gas market in recent years (65) but due to poor efficiency at low flow rate they are not suitable options for small engines application. Rotary positive displacement, screw and roots suffer from low efficiency for feasible tolerances. On the other side TurboClaw may offer all the benefits of a turbo-compressor but at quarter the speed allowing lower precision rolling element or other low loss bearings to be used. Use of this new technology forms a core part of the research.

CHAPTER 4

4 Engine, turbocharger and electric supercharger models

This chapter explains the theory and equations applied to build the engine, turbocharger and the electric supercharger (eSC) models needed to assess the effect of eSC.

There are several ways to model the physical behaviour of a reciprocating machine such as an internal combustion engine: these can invoke fundamental laws from thermodynamics (such as heat transfer through cylinder walls), fluid-dynamics (flow through restrictions, momentum balance through pipe), chemical reactions (combustion process), mechanical dynamics (rotational inertias), etc.

In terms of spatial variables, one can distinguish between zero-dimensional (0D) or multi-dimensional (1D, 2D, 3D) modelling. In a 0D control volume all the state variables are assumed to be constant over x , y and z . In a 1D model all the state variables may vary over x (medium line of a pipe along its length and flow direction) but are assumed constant over y and z (cross sectional area of the flow). 0D models are of course less computing-demanding but also less accurate.

In terms of temporal variable the main distinction is between Mean Value Engine Model (MVEM) and Crank Angle Resolved Engine Model (CAREM): the first type is faster (larger simulation time step) and predicts the cycle averaged air flow and torque produced by the engine; the second type is slower, with an order of 10^{-6} second time step to capture the engine dynamics and predict the cyclic variations for air flow and torque.

In this work a 0D MVEM has been developed as a combinations of physics-based component models, which allow the physical parameter to be evaluated and controlled, and look-up table models, with fast response: these make the MVEM suitable for control applications and fast enough for Real Time (RT) analysis.

One benefit of this modelling strategy is that every component can be separately identified and then the engine model is built using the separate components. Each component is described in terms of equations, constants, parameters, states, inputs, and outputs.

Figure 52 shows all of the subsystems developed for the turbocharged engine. The diagram also shows the air flow within the system.

The air enters the compressor where both the pressure and temperature increases. Models for the compressor are developed in Section 4.1.8.

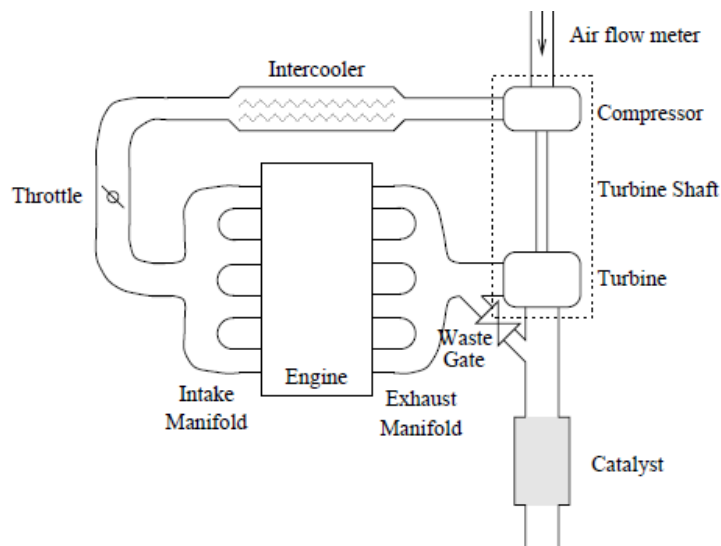


Figure 52: Sketch of a turbo charged SI-engine. The figure illustrates how the engine is divided into subsystems to enable physical modelling of the engine

The air temperature must be lowered to fill the cylinder with a greater amount of air charge (so more power with the same level of boost), to improve the materials durability and to avoid knock. This is done with an intercooler, described in Section 4.1.6. The next stage is the throttle. The mass flow into the cylinder is controlled by the throttle; the throttle opening depends on the accelerator pedal position and the mass flow through it, which is assumed to be fully opened for this investigation since the main issue of concern is maximum performance. The model is described in Section 4.1.4

Air then enters the intake manifold. The result of the simulation of the intake manifold can be found in Section 4.1.2. Combustion takes place in the cylinder which can also be found in Section 4.1.2

The hot exhaust gases then enter the exhaust manifold. From the exhaust manifold the exhaust gases proceed either through the turbine or through the waste gate. These subsystems are modelled in Sections 4.1.9 and 4.1.7 (67) (66).

The simulations were carried out in the Simulink environment. Simulink is a computational package within MATLAB that provides a way to model and simulate any system. Simulink is a block diagram environment whose graphical nature inherently illustrates the high-level structure of any system and how data flows within the system. Simulations in Simulink are performed using a series of discrete time steps until a final simulation time is reached. At each time step the blocks in the model update their output signal values to produce the simulation. It supports simulation, automatic code generation, and continuous test and verification of embedded systems. Simulink provides a graphical editor, customizable block libraries, and solvers for modelling and simulating dynamic systems. It is integrated with MATLAB, enabling the user to

incorporate MATLAB algorithms into models and export simulation results to MATLAB for further analysis.

4.1 Model description

MVEM construction in this section is based on the methodologies of (68) and (27).

Figure 53 shows the Simulink MVEM of a Turbocharged 1.0 litre gasoline engine.

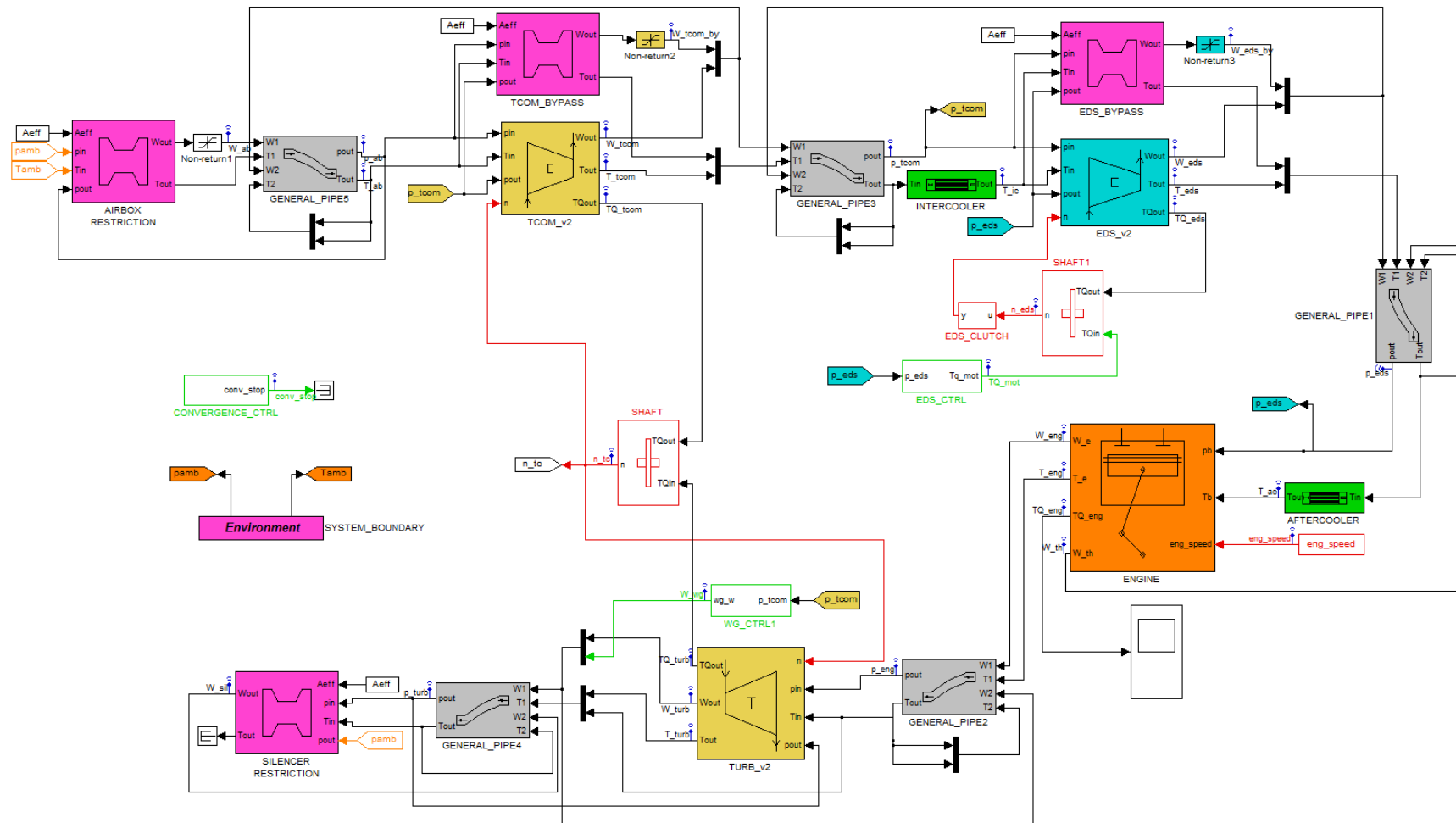


Figure 53: Simulink MVEM with Turbocharger and eS

The model consists of components such as air-box, compressor, intercooler, and so on. Between these components, there are pipes which can be considered as control volumes where the pressure and temperature states of the gas inside depend on the mass and energy flows into and out of the volume.

Massflows are determined by restrictions that are components in which pressure and temperature upstream and downstream are used to determine the massflow and temperature of the flow (i.e. airbox, bypass valve, throttle valve, silencer). Based on this definition cylinder, compressor and turbine can be considered as restrictions with energy exchange involved.

4.1.1 Engine block model

Engine block consists of throttle restriction, intake manifold, volumetric efficiency Look-Up Table (LUT) and cylinders block, in which fuel massflow is added to air system and then torque and exhaust gas temperature are calculated.

The compressor's by-pass is modelled through a restriction and a non-return saturation (only positive massflow is possible) block: in this way, back flow is avoided and flow through the valve is allowed only if compressor pressure ratio is less than 1.

4.1.2 Engine performance

The internal combustion engine is a machine that converts the chemical potential energy stored in a fuel into positive net mechanical energy available at the shaft through the combustion process between air and fuel.

The more the air mass flow, the more the fuel amount that can be burnt; hence the engine can deliver more power to the shaft as long as full combustion takes place.

The shaft or brake power available is the difference between the indicated power produced internally in the cylinders and the mechanical friction losses amount (always positive):

$$P_{brk} = P_{ind} - P_{loss} \quad [5]$$

The shaft dynamic (shaft speed ω_{eng} in rad/s) can be derived from the Newton's law for a given load torque (i.e. vehicle request for the propulsion against all the resistances) and shaft inertia as:

$$TQ_{brk} = \frac{P_{brk}}{\omega_{eng}} \quad [6]$$

$$TQ_{brk} - TQ_{load} = J \frac{d\omega_{eng}}{dt} \quad [7]$$

The thermodynamic quality of the energy conversion through the engine is commonly defined via the brake thermodynamic efficiency as:

$$\eta_{brk} = \frac{\text{final available power at shaft}}{\text{initial power source}} = \frac{P_{brk}}{W_{fuel} LHV} \quad [8]$$

Figure 54 represents the engine block in simulink environment. Each block will be explained in details within chapter 4.

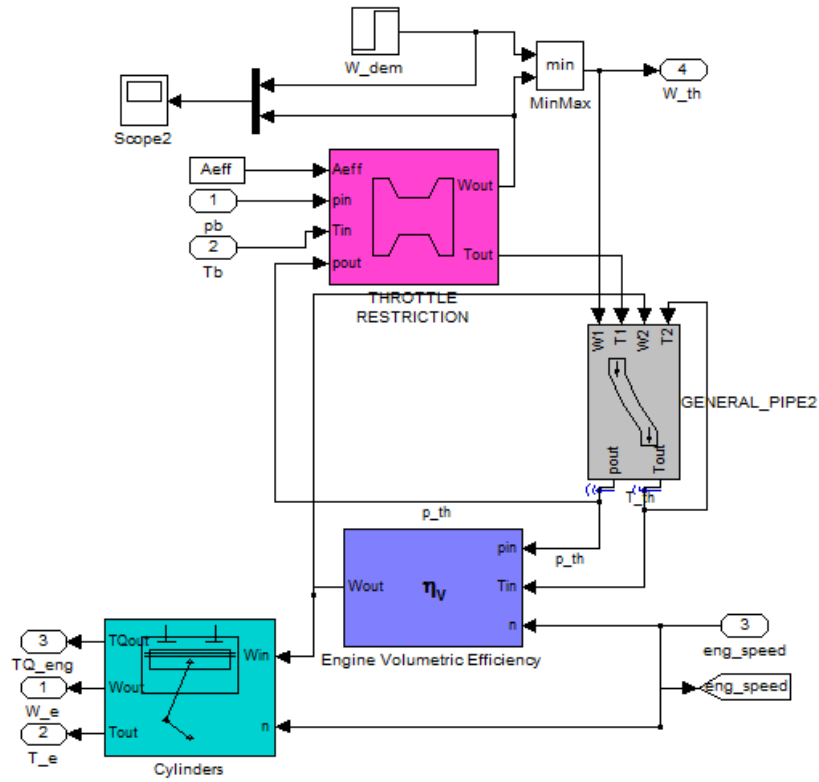


Figure 54: Engine block

4.1.3 Engine cylinders modelling

The engine cylinders block defines engine torque TQ_{eng} , exhaust temperature T_{eng} and massflow W_{eng} based on the following equations and input of engine speed n_{eng} , fuel Low Heat Value LHV, engine brake efficiency η_{brake} , air charge massflow W_a and fuel massflow W_f (and their ratio AFR):

$$TQ_{eng} = \frac{\eta_{brake} W_f LHV}{2\pi n_{eng} / 60} \quad [9]$$

$$W_{eng} = W_a + W_f = W_a + \frac{W_a}{AFR} \quad [10]$$

$$\begin{cases} AFR = LUT(n_{eng}) \\ \eta_{brake} = LUT(n_{eng}) \\ T_{eng} = LUT(W_{eng}) \end{cases} \quad [11]$$

Combustion process is neglected and LUTs are used to predict performance and they are based on experimental Wide Open Throttle (WOT) data. All the look-up tables were supplied by the engine manufacturer and are commercially confidential.

An overview of the Cylinder block is presented in Figure 55. As Mass flow rate and engine speed are the inputs, engine torque, mass flow rate-out and temperature are the outputs of the system. Figure 57 shows the cylinder flow-charts based on the declared equations in chapter 4.

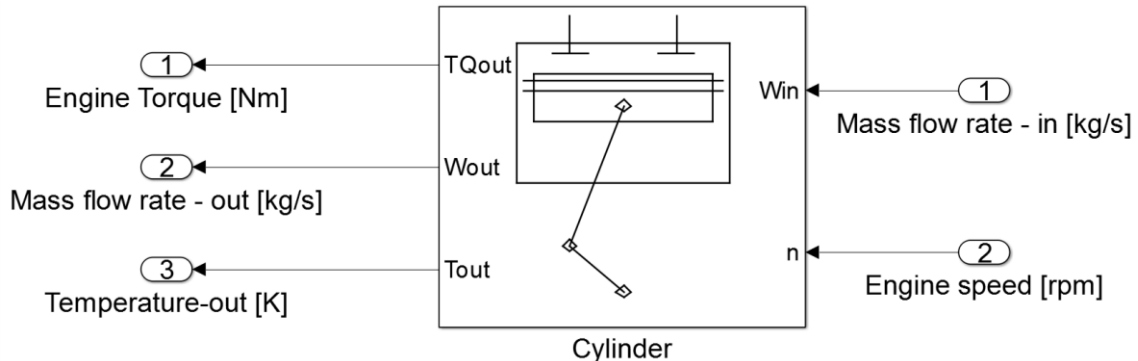


Figure 55: Cylinder block overview

Cylinder output temperature is calculated based on the exhaust mass flow rate and it is defined as a 1-D look up table in the cylinder block. Figure 56 is the graphical representation of the look up table.

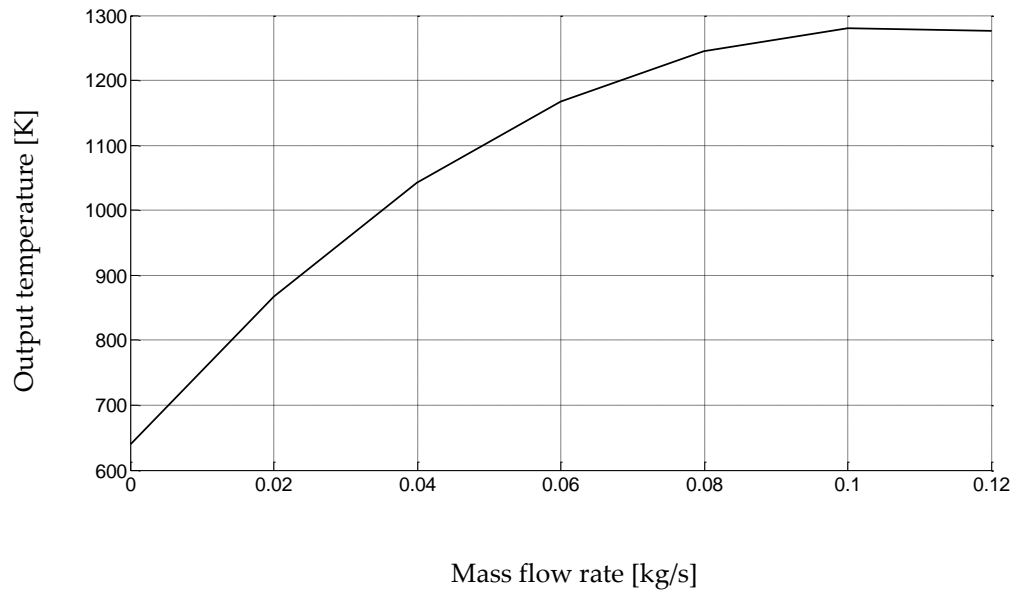


Figure 56: Output temperature as a function of exhaust mass flow rate, 1000-6000 rpm

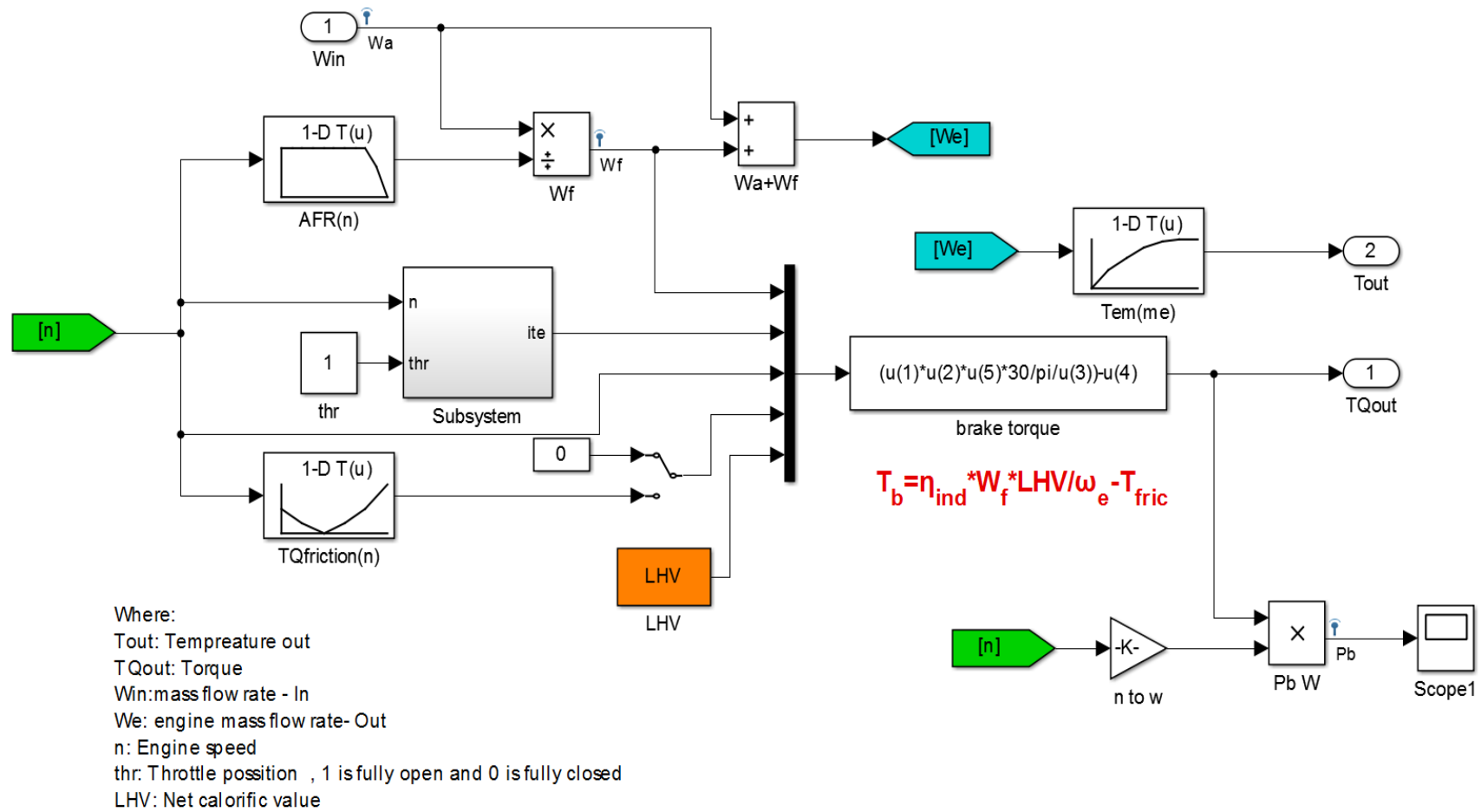


Figure 57: Cylinder flow-charts

4.1.4 Volumetric efficiency modelling

The volumetric efficiency determines the engine's ability to aspirate a volume of air and is of crucial importance at full-load conditions. It is rather difficult to be predicted reliably since many physical complex effects influence it. In this work volumetric efficiency is defined as a LUT based on experimental data versus engine speed and intake manifold pressure p_m .

Once η_{vol} is noted, the air mass flow entering the cylinder can be easily evaluated through the volumetric efficiency definition (n_{rc} is the number of revolution per cycle, which is equal to 2 for 4-stroke engines):

$$\eta_{vol} = LUT(n_{eng}, p_m) \quad [12]$$

$$W_a = \eta_{vol} \rho_m V_d n_{eng} / n_{rc} \quad [13]$$

Figure 58 shows the volumetric efficiency map. The map was created and calibrated based on the 1.0L Ford engine. The volumetric efficiency map is based on experimental measurement and it has been used as the basis for a look-up table in the simulations.

The volumetric efficiency is just a metric, a way to evaluate how good the induction of the cylinders with fresh air is, compared with a reference value. The reference mass is usually the product between the intake density condition and the cylinder displacement. The actual mass drawn in the cylinders is important because it is directly proportional to the torque the engine can deliver. But the actual mass entering the cylinder is difficult to be predicted in simulation models, therefore prediction won't take place in MVEM models, instead mass flow and intake density will be measured during dyno test on the

real engine, and volumetric efficiency map will be created, Figure 59. Using this map enables the simulation to calculate the expected mass flow needed in the cylinder for a given speed and intake condition. The volumetric efficiency table can be found in appendix section, Table 14, Page 204.

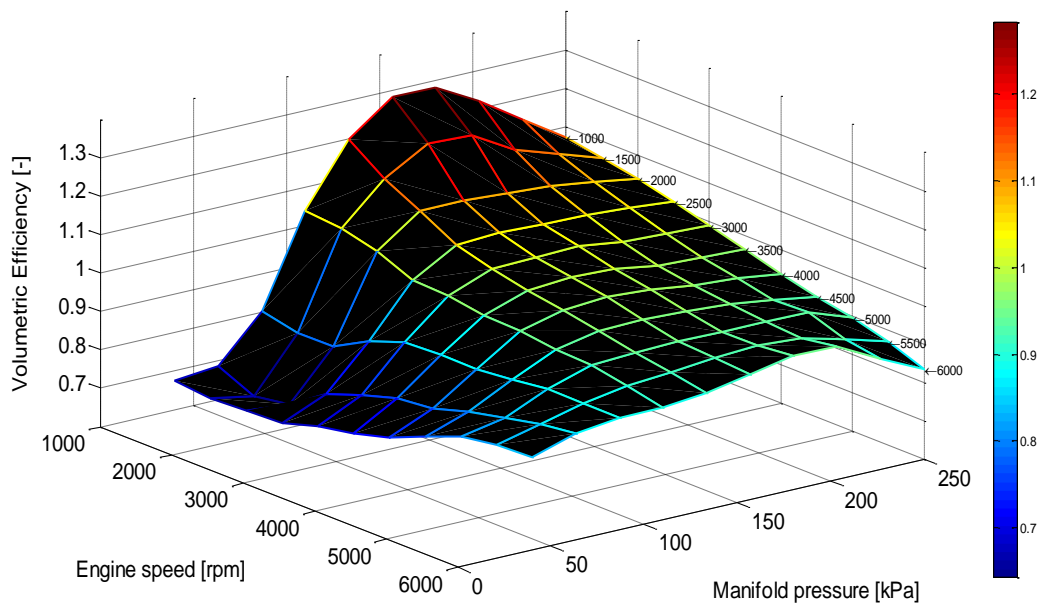


Figure 58: Volumetric efficiency map as a function of manifold pressure and engine speed

4.1.5 Restriction modelling

Restriction blocks, such as throttle body or by-pass valves, define the massflow through the orifice cross section area according to the upstream and downstream states. The pressure difference drives the fluid in a nonlinear way.

For compressible fluids, using the thermodynamic relationships for isentropic expansion, the following equation for the flow can be obtained (bidirectional flow). Since the real flow is never isentropic, a discharge coefficient lower than 1 multiplies the geometrical cross section area, resulting in the effective area A_{eff} , as shown in Figure 59.

$$\begin{cases} PR = \min\left(\frac{p_{out}}{p_{in}}, \frac{p_{in}}{p_{out}}\right) \\ p = \max(p_{in}, p_{out}) \\ T = T_{in} = T_{out} \end{cases} \quad [14]$$

$$W = \text{sign}(p_{in} - p_{out}) A_{eff} \frac{p}{\sqrt{RT}} \psi(PR) \quad [15]$$

where:

$$PR_{cr} = \left(\frac{2}{\gamma+1}\right)^{\frac{\gamma}{\gamma-1}} \quad [16]$$

$$\psi = \begin{cases} \sqrt{\gamma \left(\frac{2}{\gamma+1}\right)^{\frac{\gamma+1}{\gamma-1}}} & , 0 \leq PR < PR_{cr} \\ PR^{\frac{1}{\gamma}} \sqrt{\frac{2\gamma}{\gamma-1} \left(1 - PR^{\frac{\gamma-1}{\gamma}}\right)} & , PR_{cr} \leq PR < PR_{th} \\ a(PR-1)^3 + b(PR-1) & , PR_{th} \leq PR \leq 1 \end{cases} \quad [17]$$

PR is a chosen value close to 1 and:

$$\begin{cases} a = \frac{\psi'|_{th} (PR_{th} - 1) - \psi|_{th}}{2(PR_{th} - 1)^3} \\ b = \psi'|_{th} - 3a(PR_{th} - 1)^2 \end{cases} \quad [18]$$

$$\psi' = \frac{\partial \psi}{\partial PR} \quad [19]$$

The third equation in Ψ definition is added to avoid simulation instability for $PR \approx 1$, since nonlinear function Ψ has an infinite gradient at $p_{out} = p_{in}$.

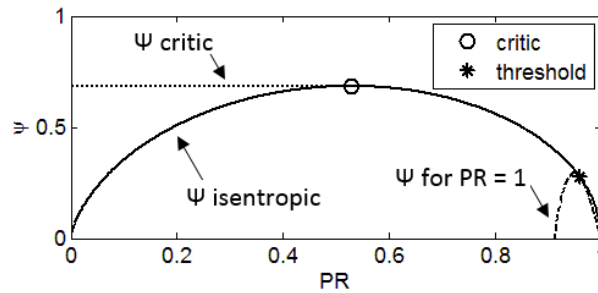


Figure 59: Ψ function for restriction modelling, as a combination of three models

Temperature change through the orifice is neglected.

4.1.6 Adiabatic pipe modelling

All control volumes are modelled with filling and emptying dynamics using two states: pressure and temperature.

Considering n inlet ports and m outlet ports, according to energy and mass conservation and to the ideal gas law, for each pipe of volume V is:

$$\begin{cases} \frac{dp}{dt} = \frac{\gamma R}{V c_p} (I\dot{\Phi}_1 - I\dot{\Phi}_2) \\ \frac{dm}{dt} = W_1 - W_2 \\ T = \frac{pV}{Rm} \end{cases} \quad [20]$$

Where:

$$\begin{cases} W1 = \sum_{j=1}^n W_{in,j} \\ W2 = \sum_{k=1}^m W_{out,k} \end{cases} \quad [21]$$

$$\begin{cases} \dot{H}1 = c_p \sum_{j=1}^n W_{in,j} \cdot T_{in,j} \\ \dot{H}2 = c_p \sum_{k=1}^m W_{out,k} \cdot T_{out,k} \end{cases} \quad [22]$$

Heat exchange through pipe wall is neglected. Therefore, proper initial conditions for volume pressure and mass have to be set.

All the pipes used in the models are simulated based on the mentioned method. The inputs of the sub-system are mass flow rate of the previous block, temperature of the previous block, output temperature of the pipe (as shown in Figure 60) and the mass flow rate of the next block fed in the system. The outputs of the sub-systems are pressure and temperature where the temperature is fed back to the pipe as an inlet temperature 2 (T2).

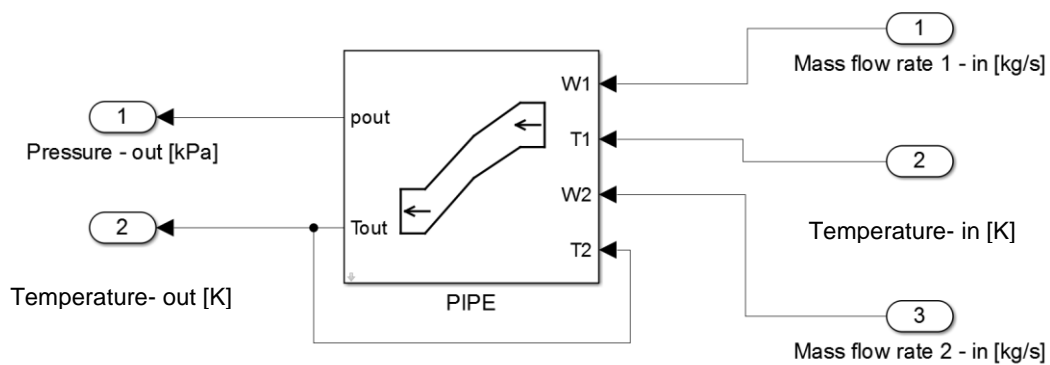


Figure 60: Connecting volumes (adiabatic pipe) block overview

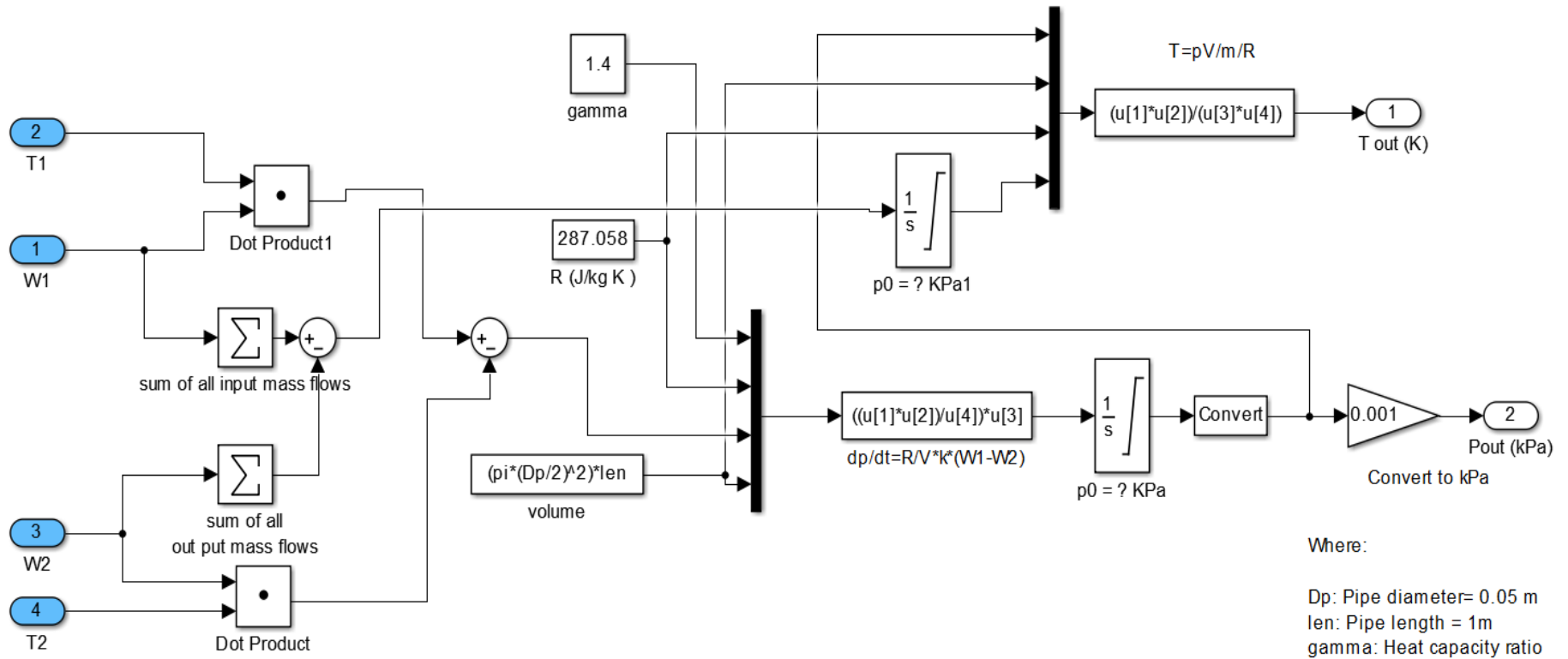


Figure 61: Connecting volumes (adiabatic pipe) flow-chart

4.1.7 Air cooler modelling

Although compressed air increases engine air charge, the thermodynamic transformation happening in the compressor will also increase the gas temperature: this will reduce the density of the air at the outlet (since $\rho = p/R/T$), so less air mass will be available in the cylinders. An air cooler at the outlet of the compressor can overcome this issue.

The air charge cooler block is defined with assumptions of no pressure drop, constant effectiveness and cooler temperature equal to ambient:

$$T_{out} = T_{in} - eff(T_{in} - T_{amb}) \quad [23]$$

Figures 62 and 63 represent intercooler block overview and flowchart respectively.

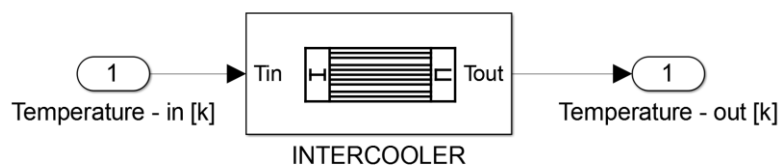


Figure 62 : Intercooler block overview

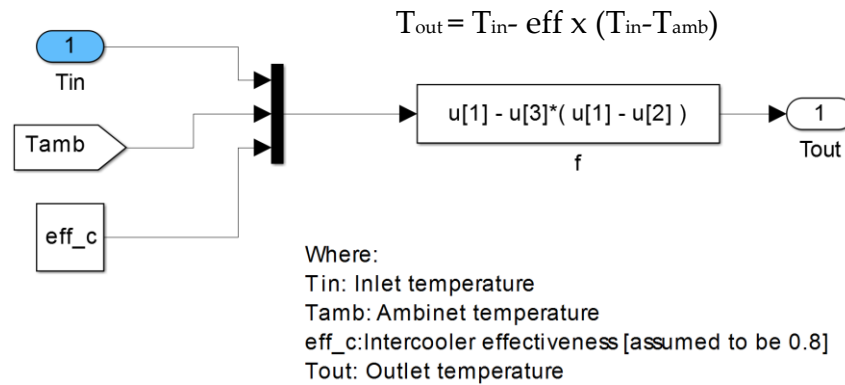


Figure 63 : Intercooler flow-chart

4.1.8 Shaft modelling

Shaft block evaluates its speed through rotational dynamics equation (shaft inertia J has to be set).

Friction torque is proportional to rotational speed and can be considered with a coefficient value different than zero.

$$TQ_{in} - TQ_{out} - b\omega = J \frac{d\omega}{dt} \quad [24]$$

4.1.9 Charging components

In order to improve the specific power of an internal combustion engine, charging elements can help by delivering air charge to the cylinders with higher density: a compressor component is then needed.

The compressor can be driven by an exhaust gas turbine (turbocharger solution), by the engine crank-shaft (mechanical supercharger solution, not included in this work) or by an electric motor (electric supercharger).

Twin-charged solutions refer to a multipart forced induction system. In this work two main parts assessed are: an exhaust-driven turbocharger and an electric-driven supercharger.

These two components mitigate the weaknesses of the other. An electrically driven supercharger offers exceptional response at low-speed as it has relatively small lag (thanks to instantaneous motor torque availability) resulting from its independency of the exhaust gas, while the turbocharger can be used at high-rpm since the high pressure gas is available to drive the turbine. The proper combination of the two can offer a low-lag with high torque at lower engine speeds, and increased power at the higher end.

Other devices are often combined with, such as air cooler, compressor by-pass valve and turbine waste-gate valve.

4.1.9.1 Compressor modelling

The compressor block is a restriction element with energy exchange involved (power from turbine or from electric motor) so massflow through the component is a function of the pressures upstream and downstream and of the rotational speed of the shaft linked to it.

Operating point is calculated with LUTs (built with real machine datasheet) and with the following equations:

$$\left\{ \begin{array}{l} PR = \frac{P_{out}}{P_{in}} \\ n = n_{corr} \sqrt{T_{in}/T_{ref}} \\ W = W_{corr} \frac{\sqrt{T_{ref}/T_{in}}}{P_{ref}/P_{in}} \end{array} \right. \quad [25]$$

$$\begin{cases} W_{corr} = LUT(n_{corr}, PR) \\ \eta_c = LUT(n_{corr}, W_{corr}) \end{cases} \quad [26]$$

$$\begin{cases} T_{out} = T_{in} \left[1 + \frac{1}{\eta_c} \left(PR^{\frac{\gamma-1}{\gamma}} - 1 \right) \right] \\ TQ = W_{c_p} (T_{out} - T_{in}) / (\pi n / 30) \end{cases} \quad [27]$$

Compressor and turbine data are usually provided with “corrected” (or “reduced” for turbine) scaling, in order to account for different intake conditions that affect air density (which can be different from the ones used in the rig).

Both turbo compressor and electric supercharger are modelled in this way.

The TurboClaw mass flow rate and efficiency maps are plotted in Figures 64 and 65 respectively. These two maps were embedded in the simulation as look-up blocks. The inputs of mass flow rate block are pressure ratio and compressor speed and the output is compressor corrected mass flow rate, the corrected mass flow rate which was the output of the mass flow rate block is now the input of the efficiency block as well as compressor speed, see Figure 66. 2-D maps are shown in appendices section, page 205, Figures 142&143.

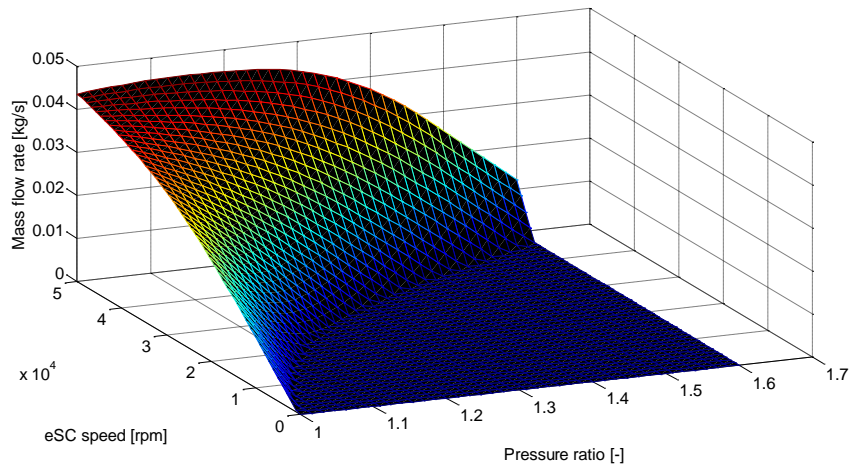


Figure 64: TurboClaw mass flow rate map as a function of compressor speed and pressure ratio

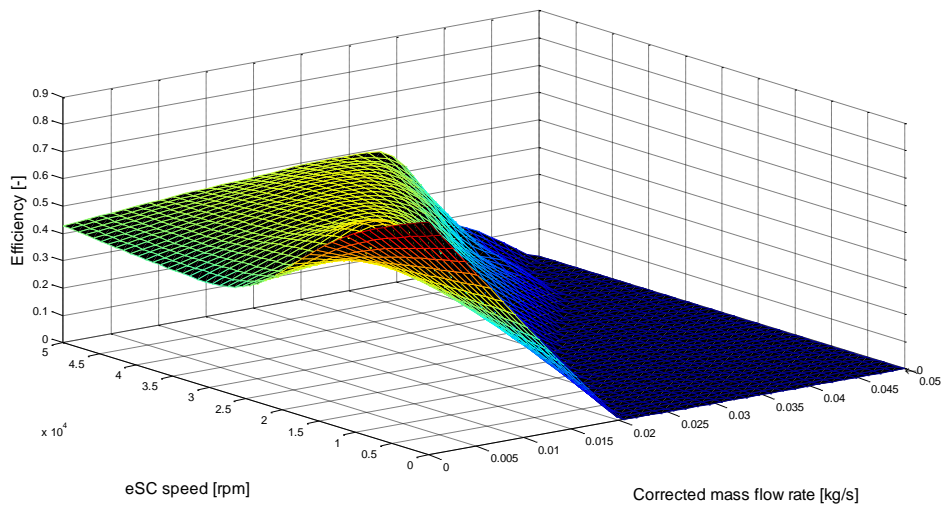


Figure 65 : TurboClaw efficiency map as a function of speed and mass flow rate

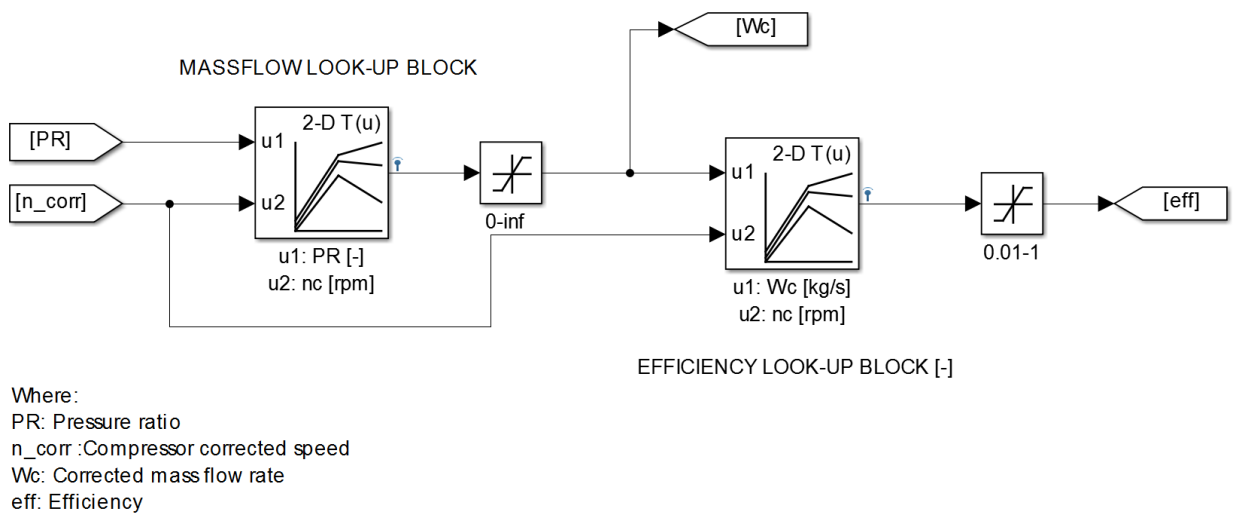


Figure 66 : TurboClaw mass flow rate and efficiency blocks layout

4.1.9.2 Summary of Electric Supercharger Compressor Block

Figure 68 shows an overview of electric supercharger compressor block. The same methodology is also taken towards designing the turbocharger compressor. The main differences between two blocks are the look-up tables; the TurboClaw data was used for eSC unit while the turbo-compressor was chosen based on the TurboClaw performance. Figure 67 displays the eSC compressor flow-charts based on the acknowledged equations in section 3.2.1.

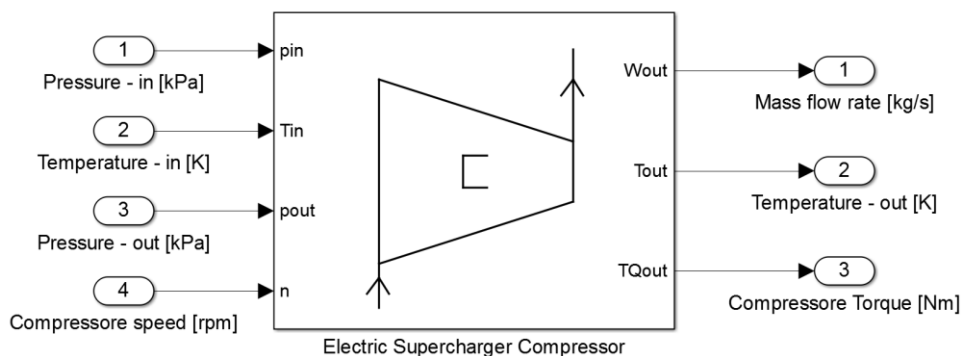


Figure 67: eSC compressor block overview

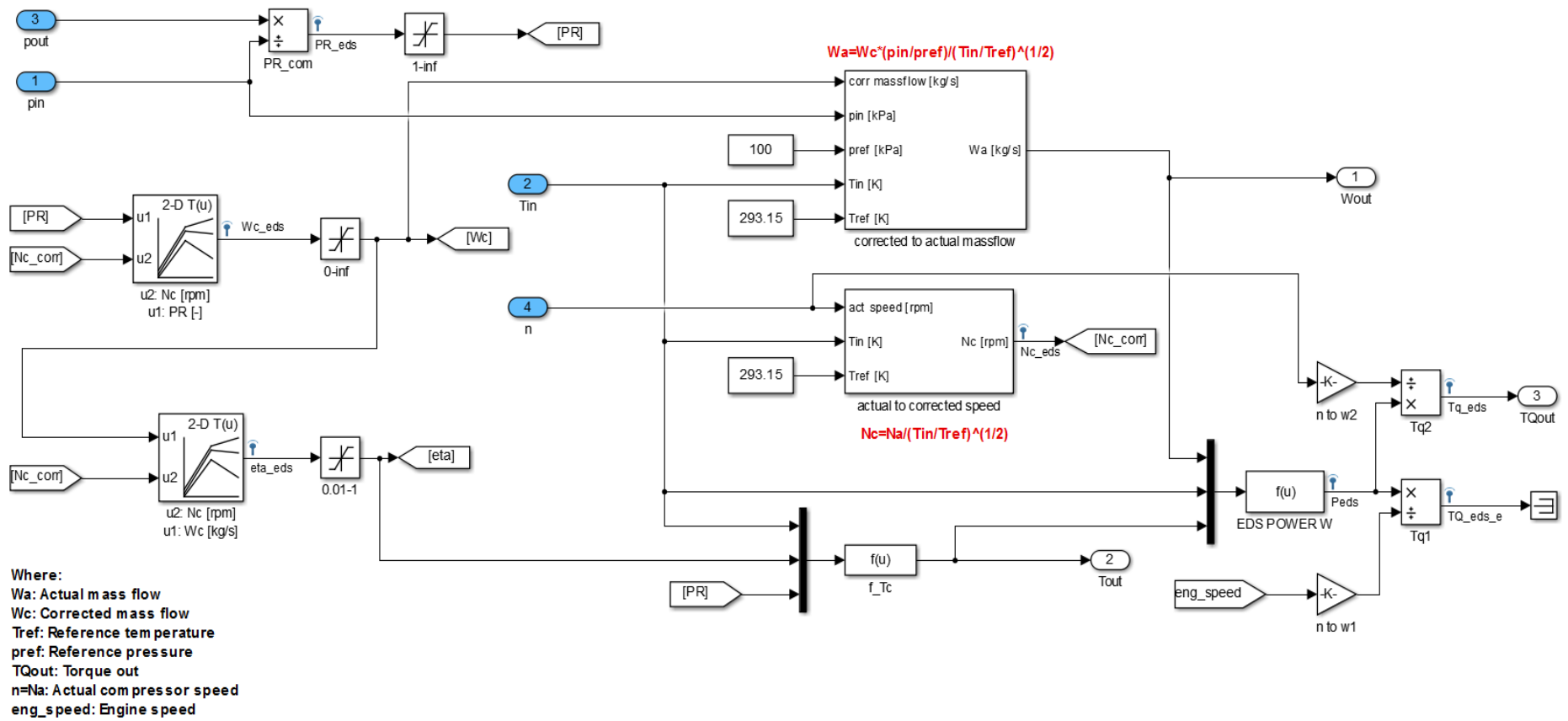


Figure 68 : eSC compressor flow-chart

4.1.9.3 Turbine modelling

As for the compressor block, the turbine operating point is calculated with LUTs (built with real machine datasheet) and with the following equations:

$$\begin{cases} PR = \frac{P_{in}}{P_{out}} \\ n = n_{corr} \sqrt{T_{in}/T_{ref}} \\ W = W_{red} \frac{P_{in}}{\sqrt{T_{in}}} \end{cases} \quad [28]$$

$$\begin{cases} W_{red} = LUT(n_{corr}, PR) \\ \eta_t = LUT(n_{corr}, W_{red}) \end{cases} \quad [29]$$

$$\begin{cases} T_{out} = T_{in} \left[1 + \eta_t \left(PR^{\frac{1-\gamma}{\gamma}} - 1 \right) \right] \\ TQ = Wc_p (T_{in} - T_{out}) / (\pi n / 30) \end{cases} \quad [30]$$

Figures 69 to 72 represent the turbo-compressor and turbine look-up tables in the form of 3D graphs. Figure 73 shows the turbine Simulink block layout.

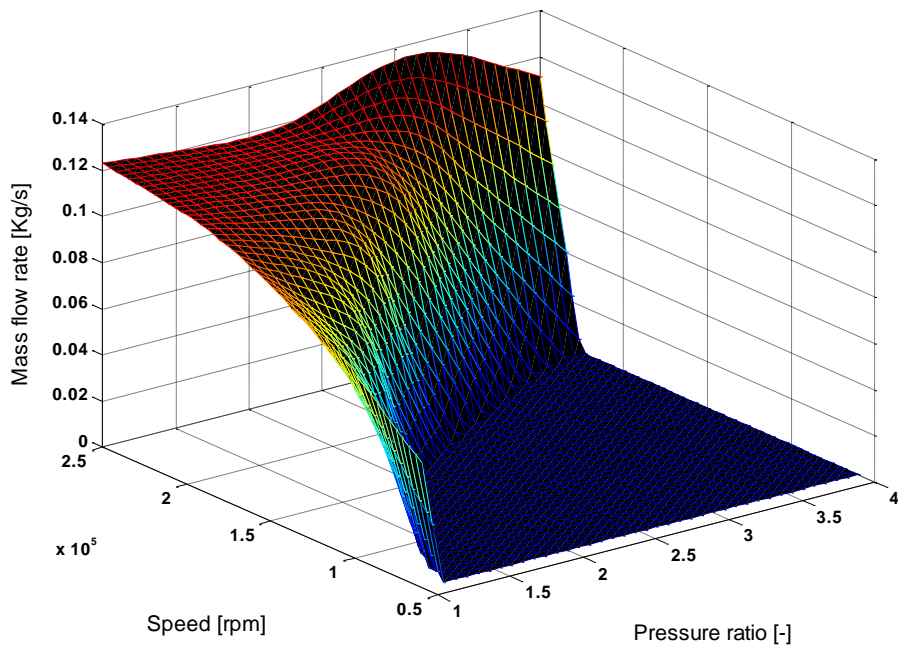


Figure 69 : Turbo-compressor mass flow rate map

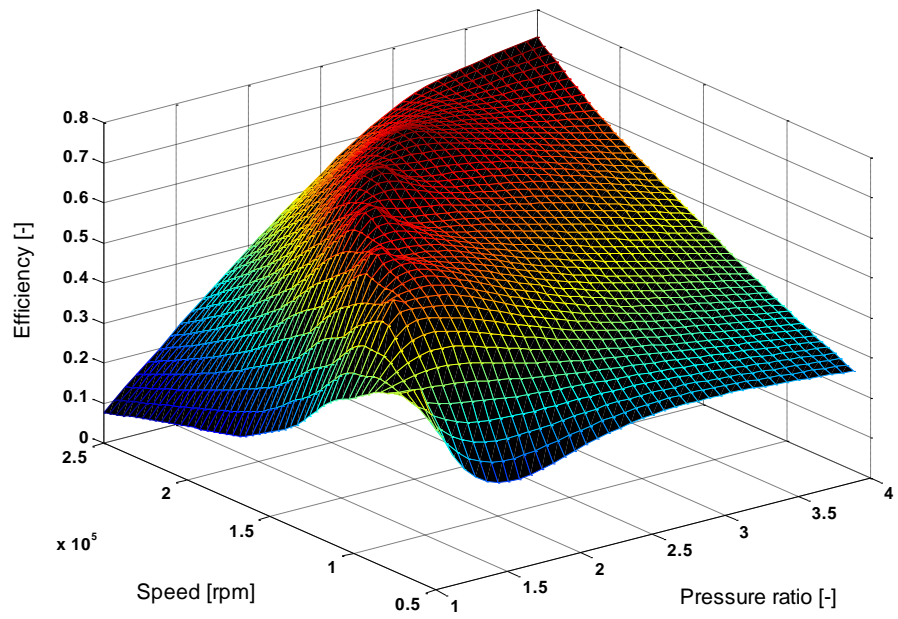


Figure 70 : Turbo-compressor efficiency map

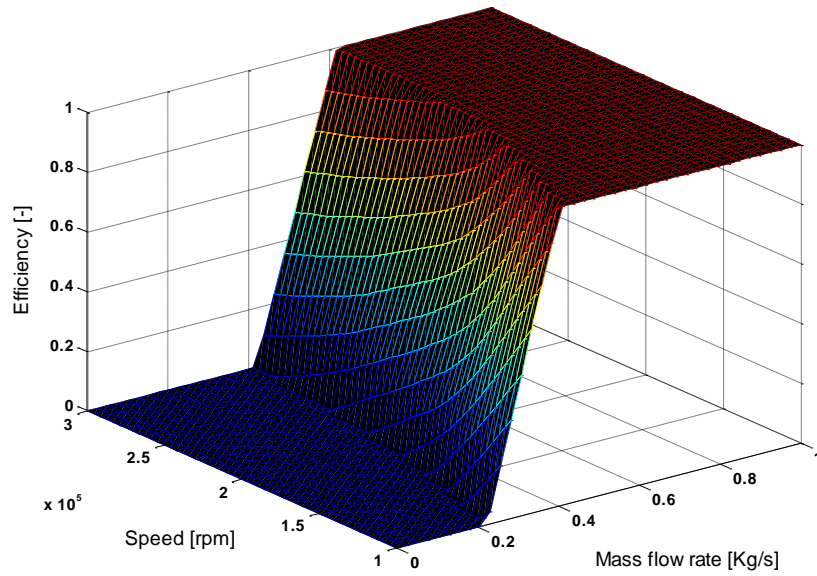


Figure 71 : Turbine efficiency as a function of turbine speed and mass flow rate

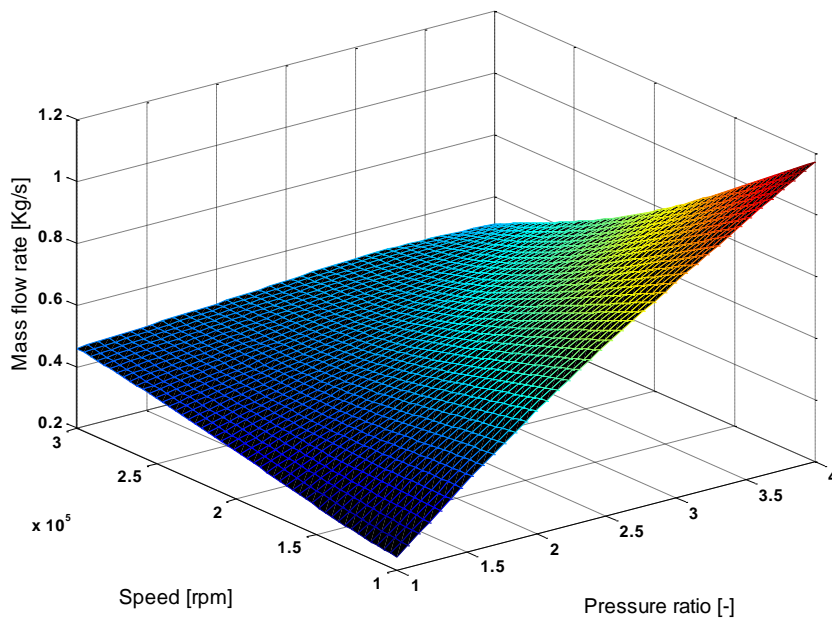


Figure 72 : Turbine mass flow rate as a function of speed and pressure ratio

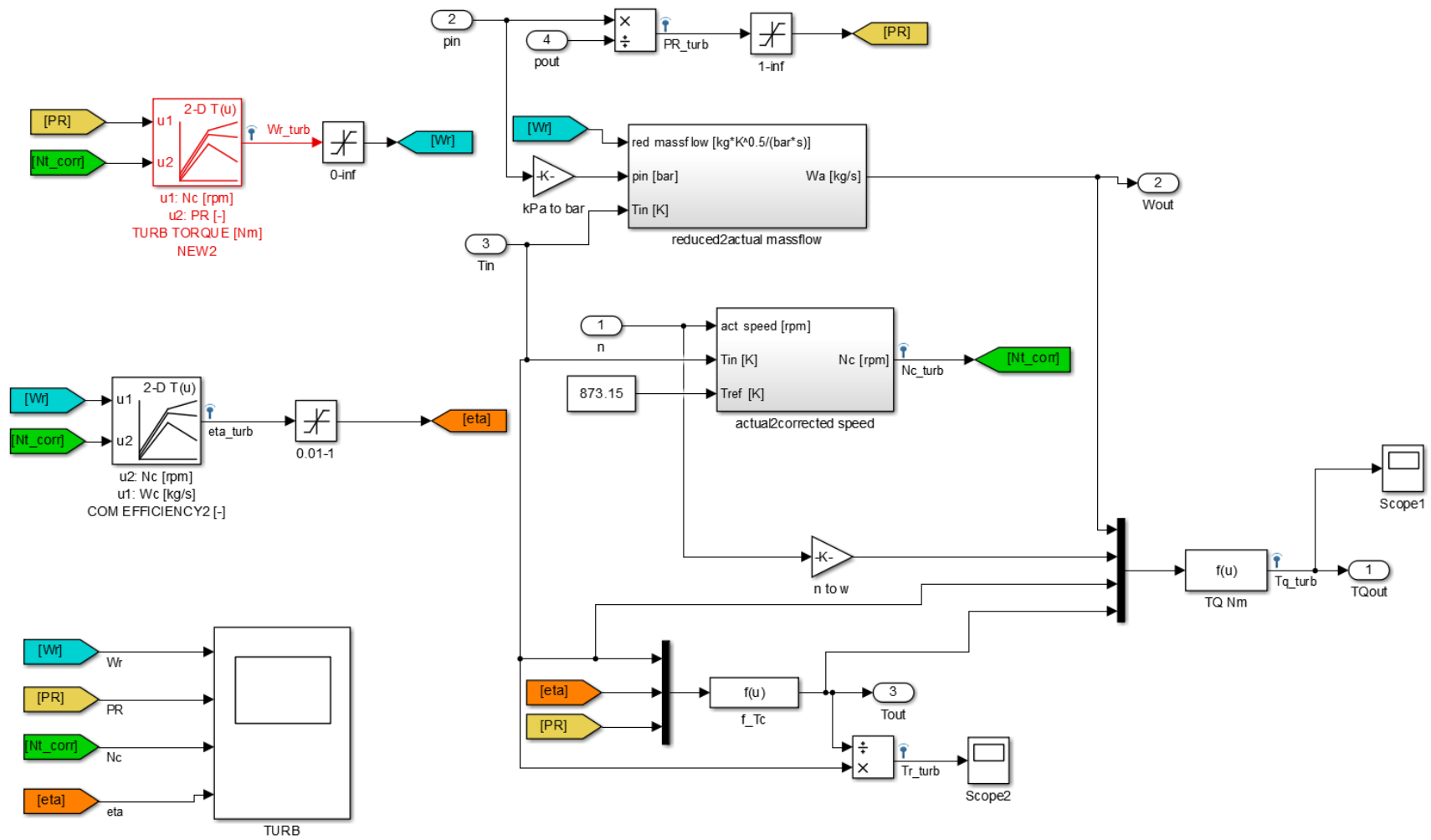


Figure 73 : Turbine Simulink block

4.1.10 Waste-gate controller

A PI controller is used in the model to manage the waste gate massflow. A reference value is set for turbo compressor outlet pressure, as function of engine speed.

When the actual boost pressure goes above the reference value, the waste gate valve is open according to the controller and a certain amount of hot exhaust gas by-passes the turbine. As a consequence less turbine power is available at the turbo-shaft to boost air through the compressor; finally the boost pressure will reduce to meet the reference value (or lower).

4.1.11 eSC Control System

In this section the control system used for eSC system interaction with the engine is described. The control unit is responsible for delivering the desired boost upon request. The main challenge in this section was to design a system which could be used in the vehicle for the future vehicle test.

In real application an eSC controller would define first the motor target speed; then the motor controller would translate this in voltage and so in available torque from to motor to the compressor. This torque needs to overcome the motor/eSC inertia + compressor torque request according to the equation:

$$T_{motor} - T_{sec} = J \times \frac{dw}{dt} \quad [31]$$

In this work, the output of the controller was directly the motor torque (electric latency can be neglected compared to inertia lags) so then a shaft block was used to derive the eSC speed (so the motor/eSC inertia was in account for response estimation). This is important only for the transient simulations. For steady-results it's not important how fast it reaches the boost pressure.

A Proportional–Integral–Derivative (PID) controller is the core of this system which continuously calculates the error value as the difference between set-points (target) and a measured value (feedback - boost pressure). The controller must minimise the error over time; the time taken for the controller to reach its target depends on the application and design. The desired time taken for the eSC to reach its target must be a fraction of a second, 0.5 second or less.

The control unit for this project consists of two core parts; set points look-up block and PID loop. The look-up block is responsible for providing the set point values (boost pressure [kPa]) to the loop based on the throttle position and engine speed. Table 9 gives the look-up block of proposed setpoints. Throttle position values in the range of 0 to 1. 0 means the throttle is fully closed and 1 represents the fully open throttle.

		Engine speed [rpm]											
		1000	1200	1400	1600	1800	2000	2200	2400	2600	2800	3000	3200
Throttle position [%]	0.1	0	0	0	0	0	0	0	0	0	0	0	0
	0.2	0	0	0	0	0	0	0	0	0	0	0	0
	0.3	150	163	168	168	168	168	168	168	168	162	162	160
	0.4	184	204	210	210	210	210	210	210	210	203	203	200
	1	184	204	210	210	210	210	210	210	210	203	230	200

Table 9: Boost pressure set points [kPa] as a function of engine speed and throttle position - Throttle position: 0 and 1 are fully closed, and fully open throttle respectively

The eSC control block flow-chart is shown in Figure 74. The output of the PID block is compressor speed [rpm] but there is a gain of 0.0001 which converts compressor speed [rpm] to a number [0 to 5] depending on the output. The reason is that the ECU chip which will be installed in the vehicle simply accepts 0 to 5 volts as an

input; therefore, this gain converts the output of the PID controller to a value which ECU can receive as input.

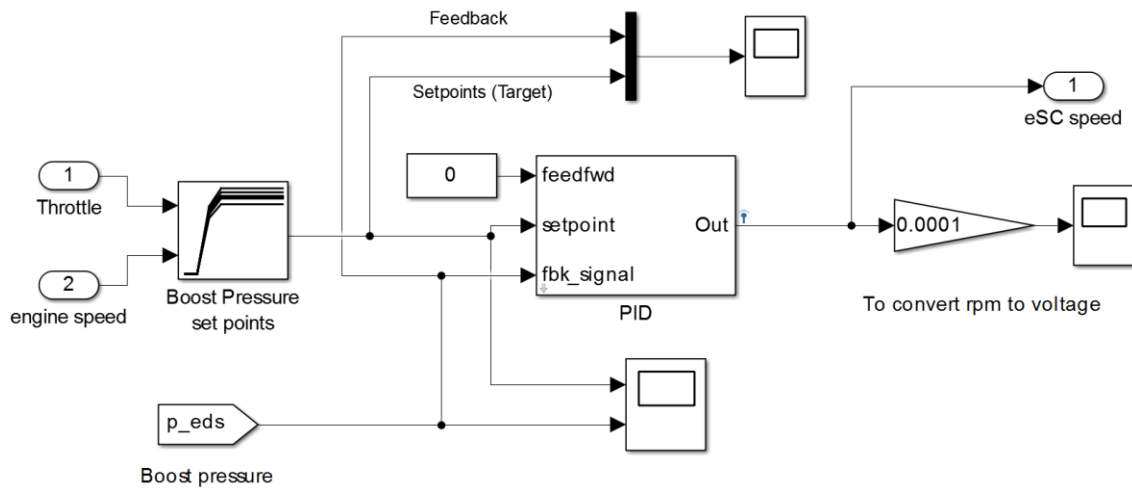


Figure 74: eSC controller flow-chart

Figure 75 shows the accuracy and fast response of the controller. It took the controller only 0.41 of a second to reach the desired boost at an engine speed of 2800 rpm. Note that the controller starts to operate after 10 seconds, these 10 seconds are required for the model to load all the blocks and to stabilize the system.

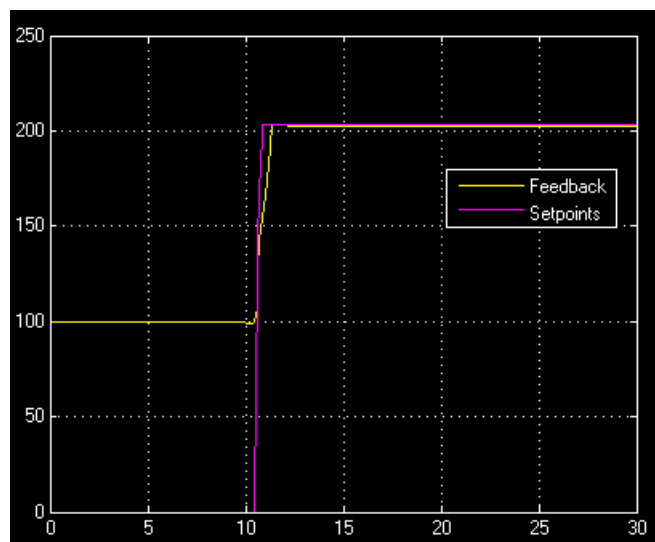


Figure 75: PID controller performance

4.2 Summary

The equations, logics and look-up tables which were used in each Simulink block were described in details in chapter 4. Four different layouts were created based on mentioned logics in order to accomplish the targets of this project; a Naturally Aspirated engine which is the foundation of other layouts, a Turbocharged engine which is simply the NA engine boosted with Turbocharger, and the other two layouts are the Dual-Charged engine, eSC+TC and TC+eSC which the differences between these two were described earlier.

The simulation results and comparison between these models and also the models validation are presented in chapter 5.

CHAPTER 5

5 Simulation results- Mean Value Engine model

The scope of this chapter is to show the use of the MVEM for a downsized (1.0 L) SI turbocharged engine, constructed in MATLAB/Simulink and validated using experimental data, in order to evaluate a rapid assessment of several combinations of turbocharger, electric supercharger and air cooler both in terms of steady-state full load operation and transient tip-in response.

5.1 Naturally Aspirated (NA) Engine Simulation Results

The results data presented in Figure 76 shows the steady-state performance of a 1.0L NA engine based on the simulation results. The engine has the peak; 80 Nm and bottom; 65 Nm torque when engine speeds are 3000 and 1000 rpm respectively. The input cylinder mass flow rate increases linearly as the engine speed increases, as expected. Upon generating satisfactory results from the simulation, the next step is to add necessary components to the NA Engine Block in order to form dual charged engine simulations for further investigation.

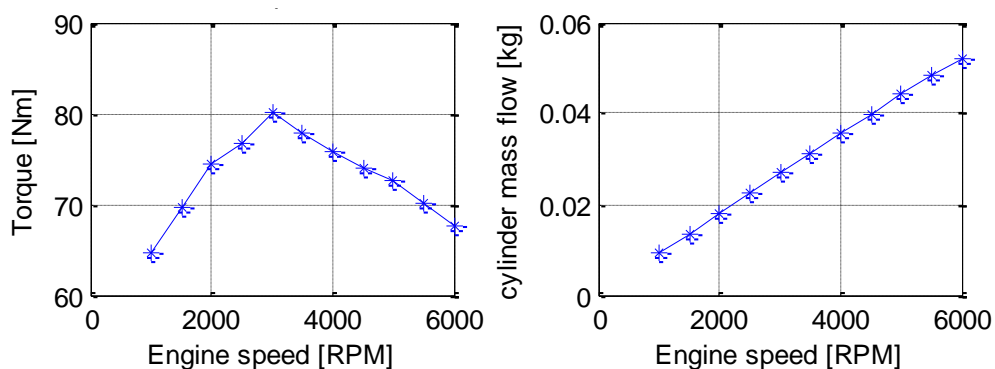


Figure 76: Left: Torque vs engine speed - right: cylinder mass flow rate as a function of engine speed

System validation is an important part of any software based investigation. At first stage, the simulation results for 1.0 L NA engine are being compared to two set of data. Figures 77 and 78 give the results of this comparison. The first sets of data (red dotted line) from LIUZHOU WULING LIUJI POWER company (69) represent a 1.0 L NA engine and the second set of data (blue dashed line) are being derived from a Ford company presentation (70). The original data was for a 1.6 L NA engine; and a direct scale down method was used to convert the 1.6 L engine to a 1.0 L engine in order to make a comparison.

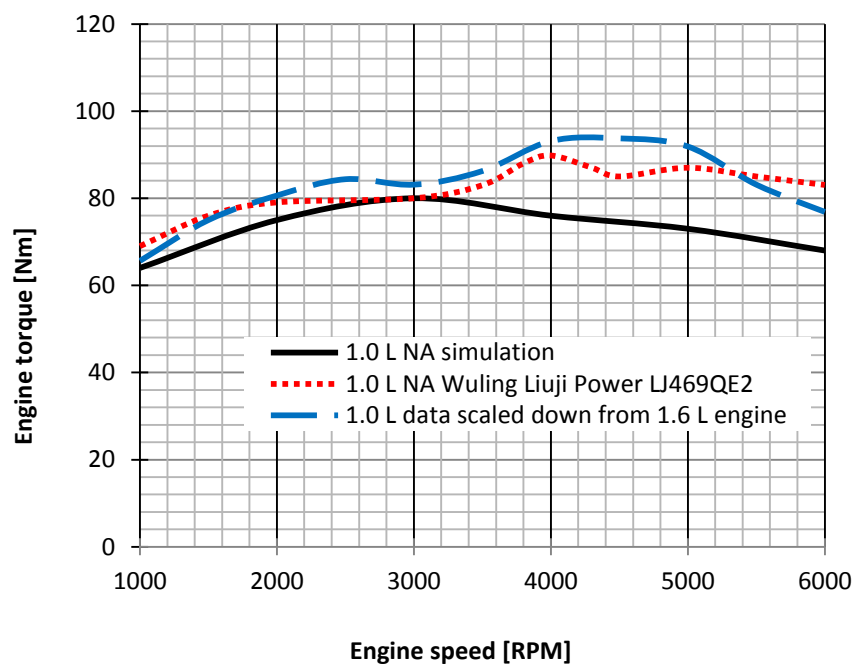


Figure 77 : 1.0 L NA engine validation plot (70), (69)

High-pressure charge-air is required across a broad range of engine speeds, and to meet driveability requirements, this high pressure charge-air needs to be available almost instantly. One of the benefits of electric supercharger is the boost availability at low engine speeds, less than 2000 rpm (51). The only issue preventing instant response is rotor inertia.

Figure 78 shows the comparison between the simulation and the data found in the literature for the engine speeds of 1000-2000 rpm. The comparison shows that the

simulation results are close to the results found in literature up to 3000 rpm; there is approximately 5% difference between the simulation results and other two engines. Many factors could cause this discrepancy such as using variable valve timing or engine tuning which was ignored in simulation modelling due to its complexity for Simulink environment. However the engine efficiency map which was used in turbocharged engine model (TC) which is the basis of the dual charged models is taking into account the effects of variable valve timing and engine tuning.

The difference between simulation results and the other data beyond 3000 rpm could be minimised by adjusting the inputs to the simulation such as; engine thermal efficiency, engine losses and etc.

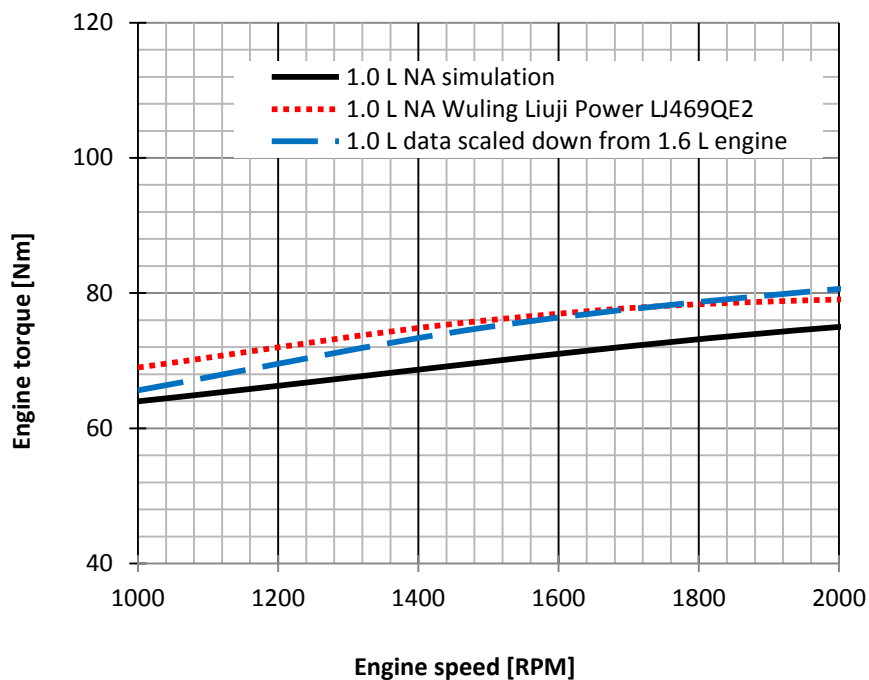


Figure 78: 1.0 L NA engine validation plot- 1000-2000 rpm

5.2 eSC effect on Steady State simulation

The NA model comparison with commercial similar engines was necessary to guarantee a good level of confidence about the physical representation of the MVEM in terms of combustion process and emptying and filling pipes behaviour.

The further step was to define a baseline model for the assessment of the electric supercharger impact: the single turbocharger model (named as TC: Turbocharger + AfterCooler) was chosen for this purpose in order to represent the common use case for electric supercharger application for engine downsizing.

Based on the NA model, a conventional turbocharger, waste-gate and compressor by-pass valves and after-cooler were added.

The TC model has been validated using real engine experimental data (1.0 l, TGDI with air cooler) running WOT steady-state simulations for several engine speeds. Figure 79 shows the matching between the simulation and measured data (71).

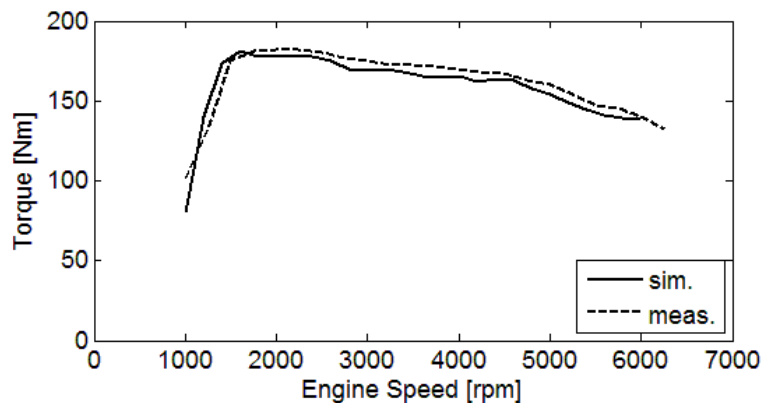


Figure 79 : Simulation vs measured data, eSC+TC (ETC layout)

The desired outlet pressure of the turbocompressor, used in the waste gate controller, has been set equal to experimental values in order to reach the same intake manifold conditions.

The matching is presented section 5.2.2. Therefore the tuned model is used as the reference for the different charging layout assessment with the additional electric supercharger (eSC).

According to the following terminology, they are:

- ETC: low pressure ESC + high pressure Turbocompressor + aftercooler ,
Figure 80
- TEC: low pressure Turbocompressor + high pressure ESC + aftercooler ,
Figure 81

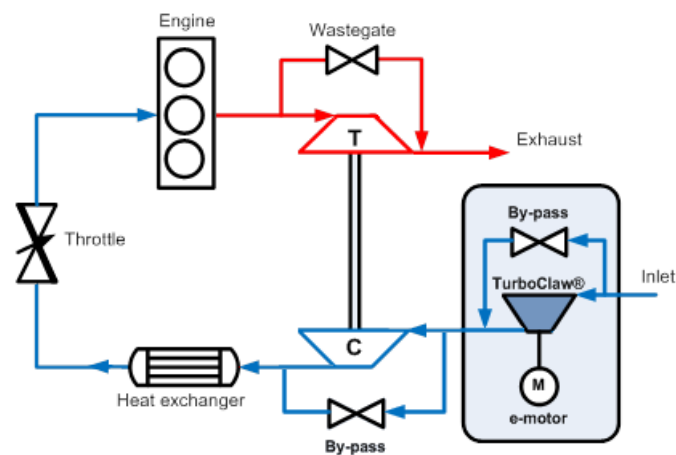


Figure 80: eSC + TC System Layout (ETC)

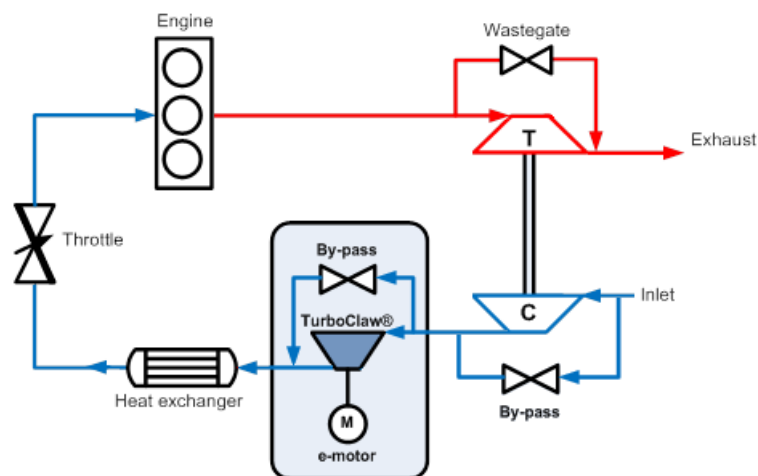


Figure 81: TC + eSC System Layout (TEC)

5.2.1 Boost condition evaluation

Models that combine a turbocharger with the electric supercharger have two degrees of freedom: desired pressure ratios for waste gate and eSC controllers.

In order to define these set-points, a simple model with only the engine block has been simulated with inlet states of pressure and temperature equal to parameterized boost conditions; in this way it is possible to create performance maps as function of low-pressure and high-pressure PRs and to choose the proper values for full model simulation. These set-points limit the amount of boost that the system accepts therefore it is important to choose the correct set-points in order to maximise the boost provided to the engine. The results and effects of these set-points can be seen in Figure 86.

Design of Experiment (DOE) values for TCOM and eSC pressure ratios for this investigation are shown in the Figure 82.

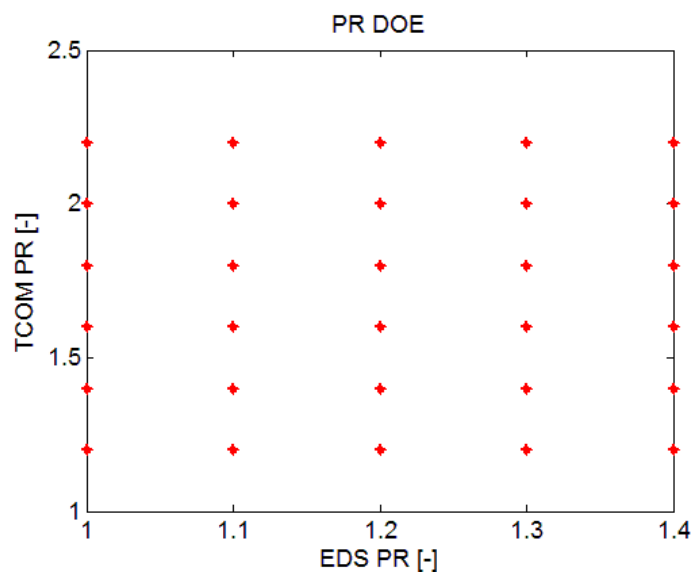


Figure 82 : Compressor PR Design Of Experiment

For each testing point, a unique boost condition can be derived in terms of engine inlet pressure and temperature, according to the following thermodynamic equations:

$$\begin{cases} T_{lp} = T_{amb} \left[1 + \frac{1}{\eta_{c,lp}} \left(PR_{lp}^{\frac{\gamma-1}{\gamma}} - 1 \right) \right] \\ p_{lp} = p_{amb} PR_{lp} \end{cases} \quad [32]$$

$$\begin{cases} T_{hp} = T_{lp} \left[1 + \frac{1}{\eta_{c,hp}} \left(PR_{hp}^{\frac{\gamma-1}{\gamma}} - 1 \right) \right] \\ p_{hp} = p_{lp} PR_{hp} \end{cases} \quad [33]$$

$$\begin{cases} T_b = T_{hp} - \varepsilon_{ac} (T_{hp} - T_{amb}) \\ p_b = p_{hp} \end{cases} \quad [34]$$

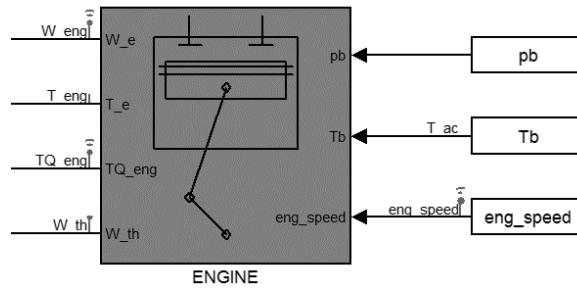


Figure 83 : simplified MVEM for boost condition evaluation

In this way, the simplified engine model is tested in steady-state simulations without the turbocharger for all the speed range and for each boost condition defined by the PRs DOE matrix. As a result, the estimation of engine brake torque and air massflow delivered for each set of boost condition can be collected.

For simplicity, the pressure drop in the pipe and cooler are neglected (usually around 50 mbar for flow in the cooler less than 100 g/s) as well as temperature change in the pipes (72).

Compressor efficiencies and cooler effectiveness are assumed constant; their values and PRs DOE range are shown in the following table.

η_{esc}	η_{tcom}	ε_{ac}
0.4	0.6	0.8

Results based on these simulations are shown in Figures 85 and 86. For each boost condition tested there are two possibilities: in ETC layout the low-pressure quantities of the previous thermodynamic equations refer to the eSC and the high-pressure ones to the TCOM; for the TEC is the opposite. This means that the operating point on the compressor maps has to be plotted accordingly: for example, the turbo-compressor in the TEC layout will take in account that its inlet pressure and temperature are higher than ambient for the calculation of the TCOM corrected massflow.

In particular, for a given engine speed (1200 rpm in this example, Figure 84), all the operating points as results of simplified engine simulation for the set of design of experiment are calculated and shown against the eSC map, TCOM (turbocompressor) map and Engine Brake Torque. Legends show the value of the other pressure ratio, constant over the relative coloured line.

The setpoint pressure ratios for ETC and TEC are chosen by matching the following conditions:

- Respect of TC model pressure and temperature maximum values (240 kPa and 440 K)
- Margin from surge line (and choke);
- Attaining the nominal maximum torque at all the speed range
- Similar overall boost pressure to allow a reasonable comparison between ETC and TEC

Red points in the results, Figures 84 and 85, are over maximum boost pressure and temperature, so unfeasible and to be excluded from the choice. Green points are chosen for the set-points condition at this engine speed. For example in the ETC layout, Figure 84, at 1200 rpm, if one chooses PReds equal to 1.35 and then intersects to PRtcom (green on EDS map) line of 1.4 will yield to around 0.025 kg/s of EDS corrected massflow (basically equal to the actual engine air flow, since the

EDS is at low pressure position with ambient inlet conditions), 0.02 kg/s TCOM corrected massflow and to around 175 Nm of engine brake torque.

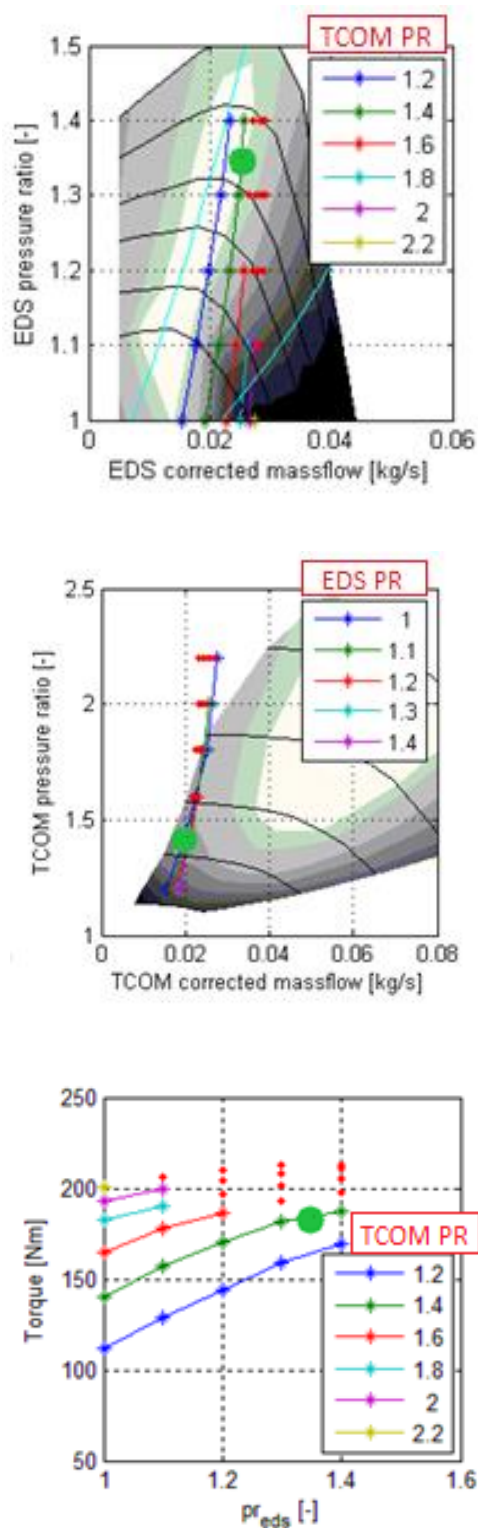


Figure 84 : ETC operating points at 1200 rpm (cyan lines on EDS map approximate the surge and choke limits)

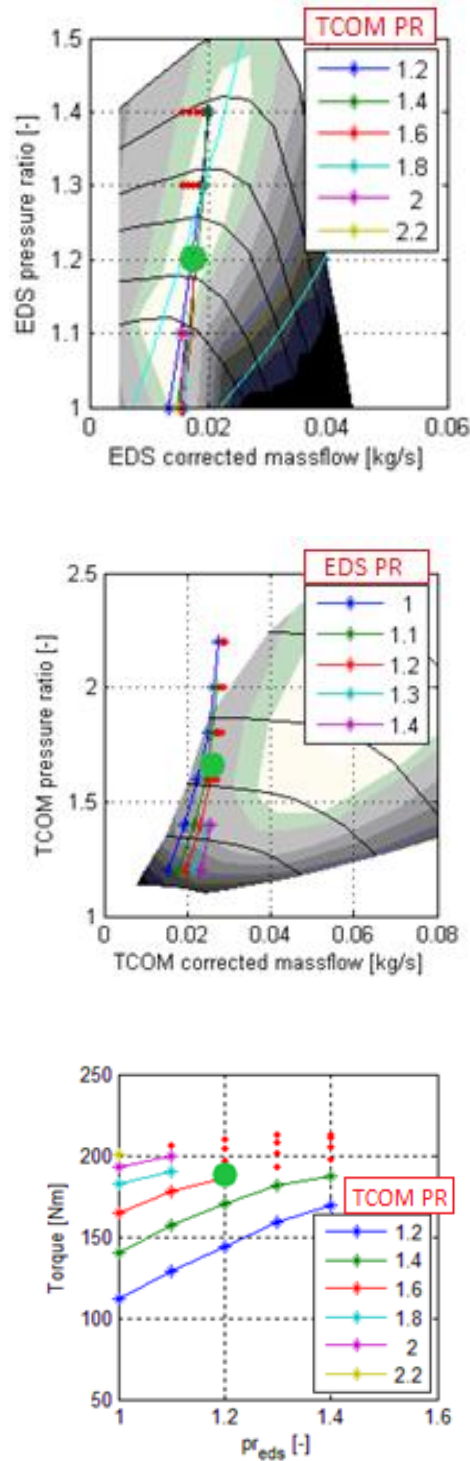


Figure 85 : TEC operating points at 1200 rpm (cyan lines on EDS map approximate the surge and choke limits)

In the TEC layout, Figure 85, at 1200 rpm, if one chooses P_{Reds} equal to 1.2 and then intersects to P_{Rtcom} (green on EDS map) line of 1.4 will yield to around 0.013

kg/s of EDS corrected massflow, 0.025 kg/s TCOM corrected massflow and to around 192 Nm of engine brake torque.

Figure 86 shows the summary of the chosen PRs for eSSC and TCOM that will be used as set point in the wastegate and eSC controllers, as a function of engine speed for ETC and TEC layouts.

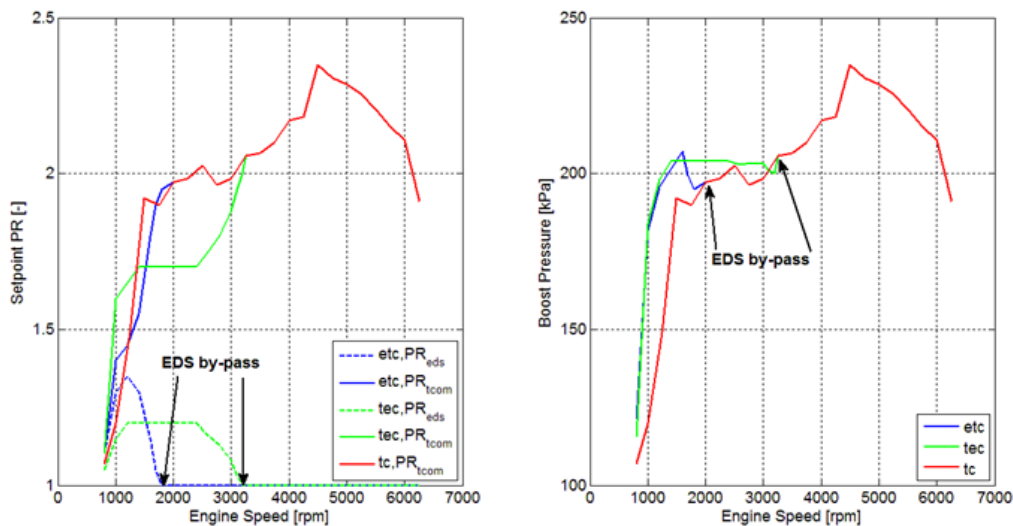


Figure 86 : Chosen final setpoint PRs and resulting overall boost pressure for each engine speed

eSC by-pass is necessary for ETC and TEC model because of choke limit and corrected massflow range; TEC range is anyway higher because eSC is at 2nd stage of compression, so higher inlet pressure reduces the corrected massflow at higher speeds. Therefore, after by-pass, setpoints are set equal to default values (TC model).

5.2.2 Charging layout comparison

The following graphs show the comparison between TC, ETC and TEC models according to desired PRs chosen with previous simple model (boost pressure for ETC and TEC is quite similar so performance comparison is reasonable).

Results are up to 3000 rpm, where eSC becomes ineffective because of its by-pass.

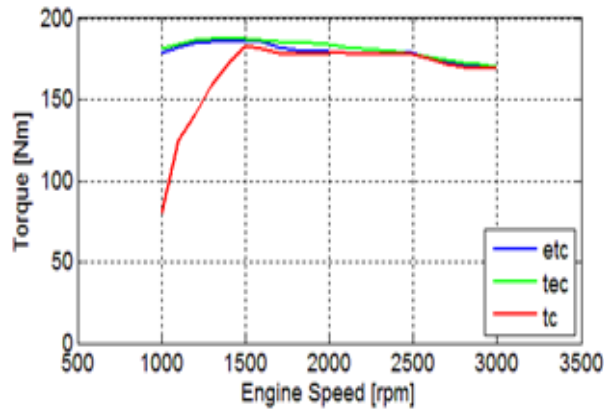


Figure 87 : steady-state WOT results for ETC and TEC models and comparison with TC model- Torque vs Engine speed

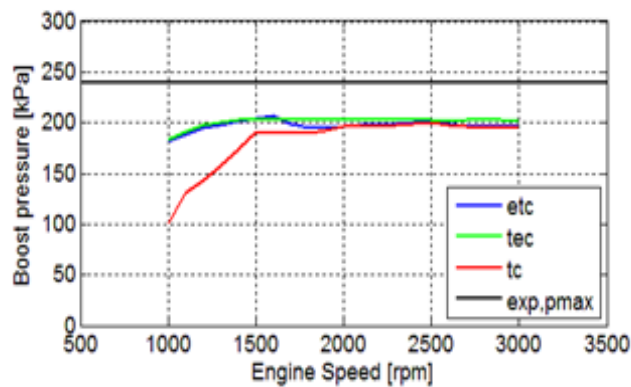


Figure 88 : steady-state WOT results for ETC and TEC models and comparison with TC model- Boost pressure vs Engine speed

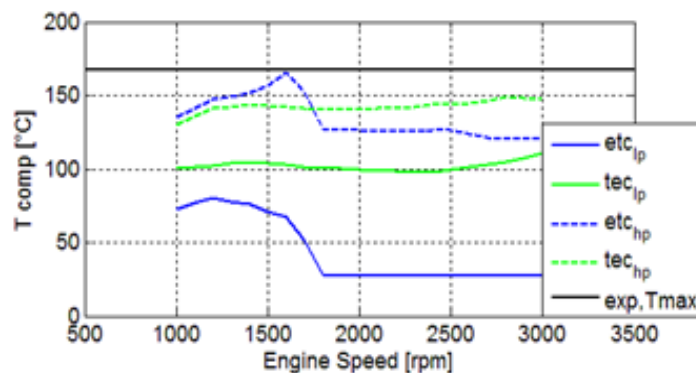


Figure 89 : steady-state WOT results for ETC and TEC models and comparison with TC model- Compressor temperature vs Engine speed

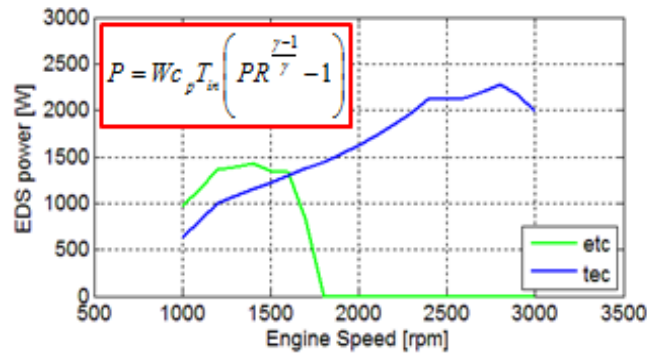


Figure 90 : steady-state WOT results for ETC and TEC models and comparison with TC model- eSC power required be Engine speed

The eSC helps turbine to produce more power and lets the turbocompressor work out of surge at low engine speed; this makes the engine reach the nominal torque even at low speed range.

ETC and TEC produce basically the same torque increase; the real eSC benefit is at low speed where the nominal maximum torque is recovered for all the range.

The thermodynamic power requested by eSC is less than 1.5 kW for ETC and less than 2.5 kW for TEC (that's because power is directly proportional to inlet temperature, higher for TEC model). The effective power request is higher, since electrical and mechanical efficiencies have to be taken in account.

Use of eSC over 2000 rpm for TEC is not a real advantage because it needs more EDS power at high speeds and engine produces basically the same torque of TC model.

Although all the temperatures are lower than the maximum TC model temperature, the eSC compressor for TEC undergoes a greater thermal stress which can drastically reduce the component life.

The Figure 91 shows operating points for different engine speeds on the compressors map. All the points are in the acceptable zone and in respect of the set-points selection.

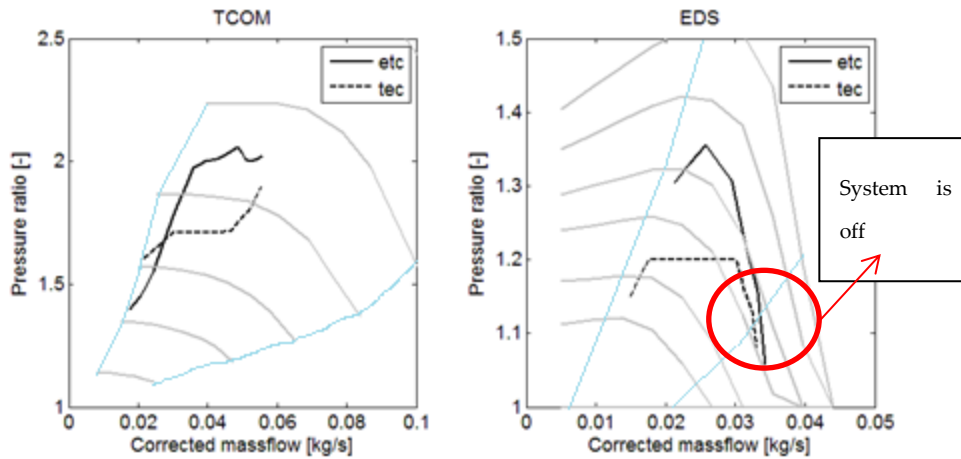


Figure 91 : Operating points on compressors map for steady-state simulation of TEC and ETC

5.3 eSC effect on Transient simulation

The transient responses of ETC and TEC versus only TC model has been simulated using 2 step signals at 10 sec at several fixed engine speed:

- Throttle tip-in to 100%;
- Electric motor torque for EDS from 0 to 0.5 Nm;

Turbocharger inertia is $5E-05 \text{ kg}\cdot\text{m}^2$ and it has been chosen according to the following figure, for wheel diameter equal approximately to 40 mm ,typical turbine size for 1.0L application (73).

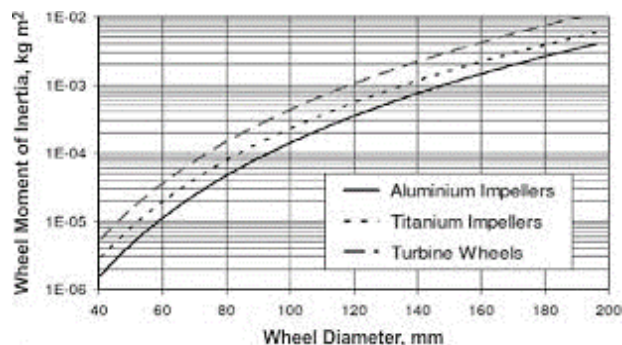


Figure 92 : Common turbocharger inertia values [www.dieselnets.com]

eSC + motor inertia has been set equal to $5E-05 \text{ kg}\cdot\text{m}^2$ as well.

The benefit of eSC can be evaluated considering the saved time to reach the steady-state WOT torque of TC model.

Figure 93 shows comparison between ETC, TEC and TC model for the speed range of eSC operation. More data are presented in appendix section, figures 121-132.

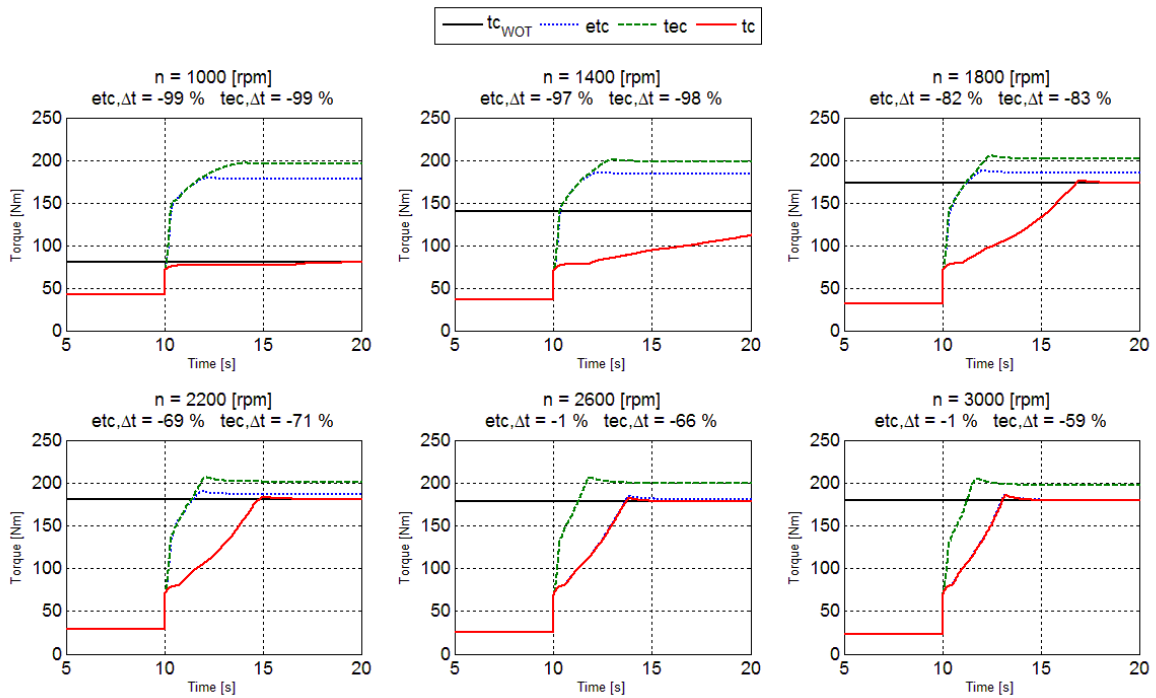


Figure 93: transient torque evolution for TC, ETC and TEC

ETC and TEC models have basically the same trend because it doesn't make any difference if the air is pulled or pushed in terms of boosting speed response. The main difference is that, according to the steady-state results, between 1600 and 1800 rpm eSC has to be bypassed, hence ETC overlaps TC model line.

eSC gives strong support at lower speed up to 1800 rpm (time to TC target reduction of 99% at 1000 rpm and around 70% at 1600 rpm). At higher speeds the TC model increases its speed and gets closer to TEC; finally, over 3000 rpm, eSC for TEC is bypassed.

Following figures show the lines representing the time evolution of the operating points on TCOM and EDS maps for TEC and ETC; all operating points are in the acceptable zone on the maps.

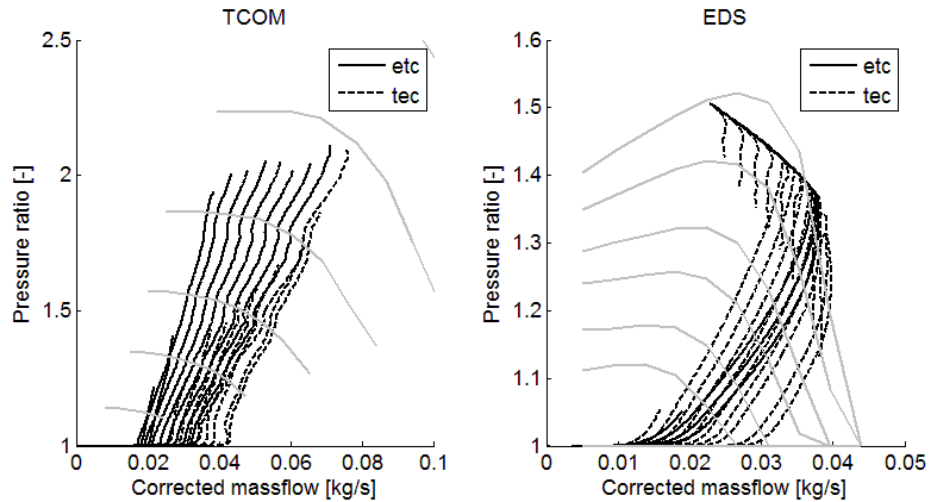


Figure 94: Time evolution of compressors operating point for ETC and TEC

5.4 eSC effect on Vehicle simulation

For transient simulation purpose, the Mean Value Engine Model (MVEM) has been connected to a fixed transmission ratio vehicle model as shown in the following picture. The flow of the torque/force are from the power source (engine) to the vehicle dynamic balance block where they are used to calculate the vehicle velocity. The velocity/speed flow then goes backward up to the engine.

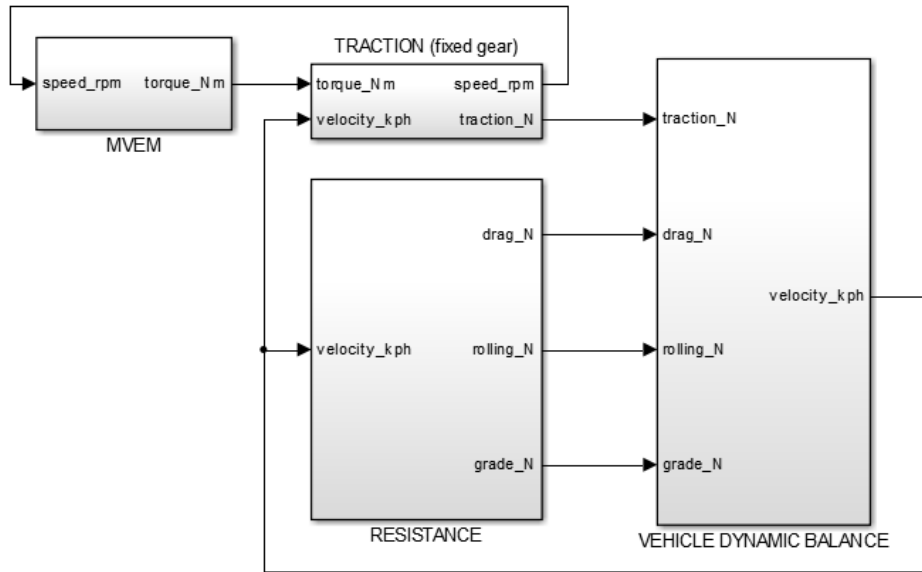


Figure 95: MVEM connected to a fixed gear vehicle

The model has been built according to the following equations, based on longitudinal dynamics between traction force, resistances (air, rolling and grade) and vehicle inertia:

$$F_{tract} - F_{air} - F_{roll} - F_{grade} = M_v \frac{dv_v}{dt} \quad [35]$$

$$\begin{cases} F_{air} = \frac{1}{2} \rho_{air} C_d A_{frontal} v_v^2 \\ F_{roll} = C_r M_v g \cos \mathcal{G} \\ F_{grade} = M_v g \sin \mathcal{G} \end{cases} \quad [36]$$

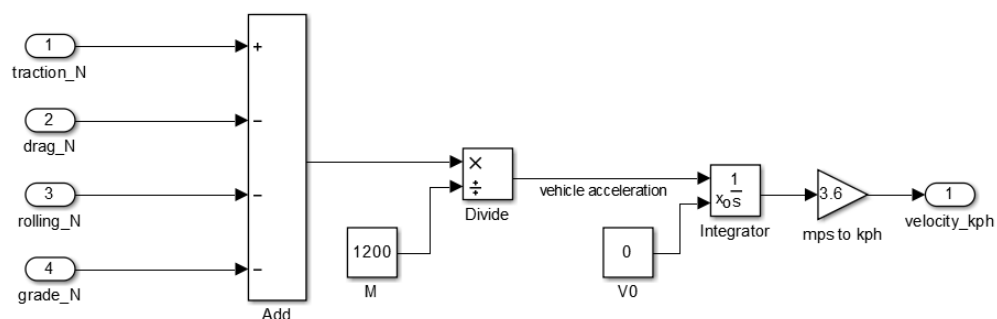


Figure 96: vehicle dynamic balance block

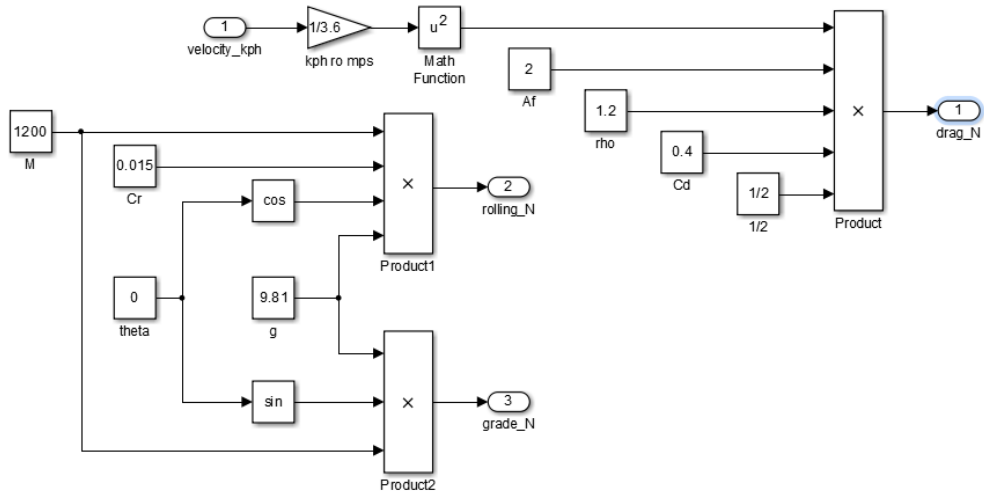


Figure 97: block for resistances calculation

The power from the engine is converted to traction available at the wheel to accelerate the vehicle through the transmission: this is modelled using a fixed transmission ratio (which take in account the gearbox ratio and the final drive ratio), the overall transmission efficiency and the wheel radius:

$$\begin{cases} n_{eng} = \frac{60}{2\pi R_w} v_v i \\ F_{tract} = \frac{\eta_{fric}}{R_w} TQ_{eng} i \end{cases} \quad [37]$$

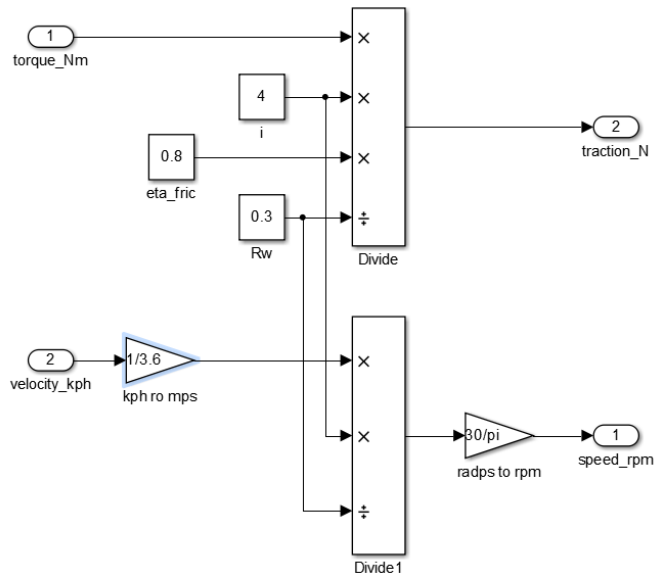


Figure 98: block for traction calculation

In order to simulate the transient response under tip-in manoeuvre, the following assumptions have been used:

- Throttle tip-in after constant vehicle speed;
- Electric motor torque for eSC from 0 to 0.5 Nm;
- Boost pressure limit of 200 kPa (acting on the waste gate controller).

η_{fric}	i	R_w	M_v	A_{frontal}	ρ_{air}	C_d	C_r	ϑ
0.8	4	0.3 [m]	1200 [kg]	2 [m ²]	1.2 [kg/m ³]	0.4	0.015	0 [deg]

Following figures show results comparison for all the layouts.

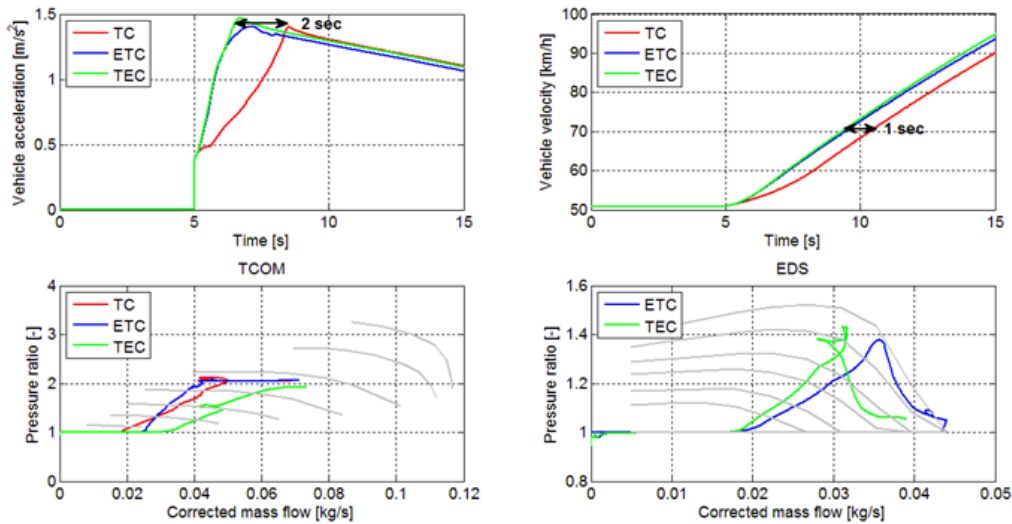


Figure 99: tip-in vehicle simulation results for TC, ETC and TEC models

The acceleration comparison shows how the use of an electric supercharger helps the vehicle reaching the acceleration peak 2 seconds earlier. This peak amplitude ($\sim 1.4 \text{ m/s}^2$) is similar for all the layouts (the same velocity slope) but the faster response with eSC yields to a constant delay in the velocity profile of about 1 sec.

Another remark is that vehicle response is basically the same for ETC and TEC layouts. This again confirms that eSC position is insignificant for transient operation.

Finally, the traces of the operating points on the TCOM and eSC map during the tip-in show them working in the good area.

5.5 Summary about MVEM simulation

The original TC model showed full load torque limits below 2000 rpm; in this range compressor surge limits the air mass flow, hence torque. Turbo lag also limits transient response at low speeds.

Steady – State simulations showed:

- eSC can completely recovers the WOT torque deficit at low speeds and its position is not relevant to reach the nominal engine torque

- TEC can extend the range of use from 1700 rpm to 3200 rpm but with increase of electric power request (ETC and TEC max power required are 1.5kW and 2.3 kW respectively as shown in Figure 91).
- eSC wheel in TEC is more stressed at higher temperatures, so it needs better thermal characteristics and hence more expensive

Transient simulations showed:

- Transient reduction of turbo lag during acceleration for 2 seconds as shown in Figure 99.
- ETC and TEC models have basically the same trend.
- Vehicle dynamic during tip-in manoeuvre improved without any significant influence of the eSC position as shown in figure 99.

CHAPTER 6

6 Hardware in the Loop (HiL) Test

The HiL test consists of a real-time simulation in which portions of controllers or plants to be controlled are replaced with real components then connected through sensors and actuators to the rest of the virtual system. In this way one can test how the controller responds, in real time, to realistic virtual stimuli or also use HIL to determine if the plant model is valid.

In this work a real electric supercharger was integrated in the virtual loop (rest of the MVEM) that needs to run in real-time in order to be synchronised to the hardware.

This test was designed to enable the user to produce new set of results by testing different compressors for the future, but the most significant part of this section is to design a Proportional–Integral (PI) controller for the transient response. The transient response indicates the novelty of the electric motor and TurboClaw performance. The response time of the system should be a fraction of seconds in order to mitigate turbo lags. A test set up was designed by Dynamic Boosting Systems Ltd (DBS) engineers for this purpose considering various testing requirements. The test set up has previously been used to perform the compressor performance and the produced map was embedded in the simulations. The compressor used for the HIL testing is 85 mm x 5.4 mm (diameter x blade height) running with DBS Brushless DC Motor (BLDC) motor.

The engine control system is based on dSPACE AutoBox architecture. The engine control system is a large Simulink model, which is compiled using Real Time Workshop. The generated code is then executed in real time on the AutoBox rig.

6.1 Test Rig

This section describes the test rig components used for HIL test. Figure 101 demonstrates the connections between the HiL hardware and the test rig. The rig consists of eSC system, pressure and temperature sensors, mass flow meter and a fast valve which acts as a throttle valve used to equate the desired mass flow rate with the simulated engine mass flow model.

Figure 102 shows the test cell assembled at City University for trial. The purpose of this trial was to develop dSPACE unit knowledge and learn how to control the system via dSPACE. This trial was successfully completed and a good level of understanding of the software was obtained. The test cell was moved to DBS for an advanced assembly and also to acquire professional assistance from DBS engineers on the project.

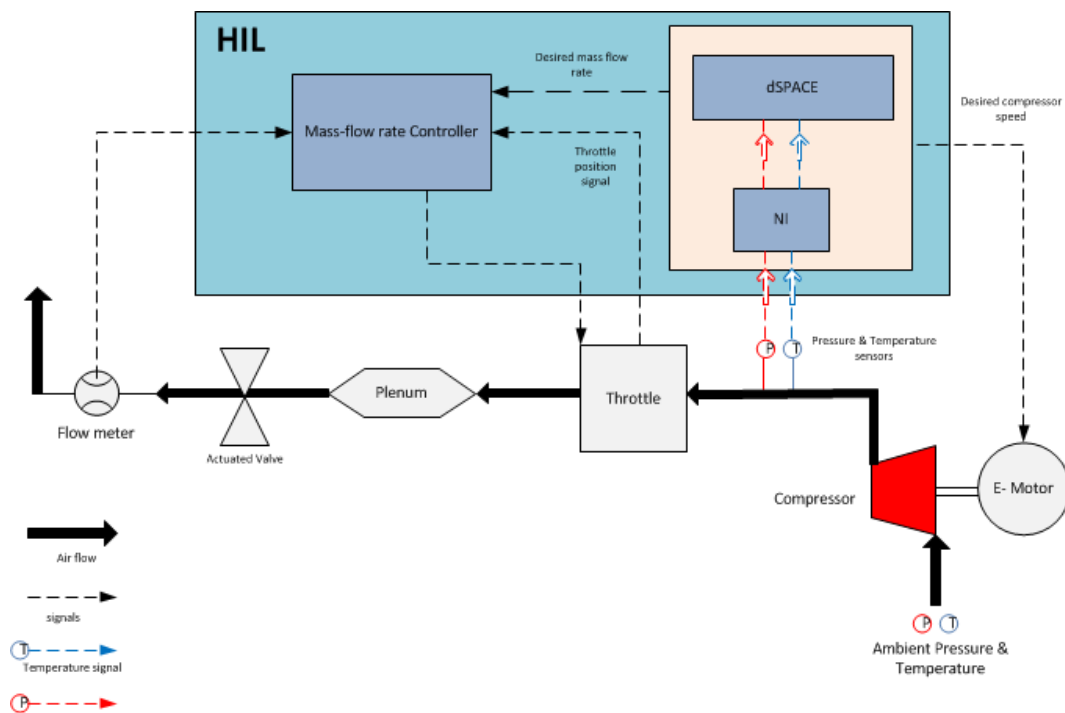


Figure 100: Test rig layout



Figure 101: Phase 1 -Test cell

The major focus of this part of the project is to set up a test rig in order to obtain a performance matrix as a function of different impeller sizes and different engine sizes. Upon completion the test rig and control system, different compressors with optimised moment of inertia and different engine sizes (800 cc to 1400 cc) could be tested and, with the results, a performance matrix could be formed. See Table 10. The mentioned matrix enables the design engineer to select the appropriate compressor size based on the engine size and performance. The first HiL simulation was carried out with an eSC system having a 2 kW motor and a compressor with an 85 mm rotor diameter and 5.46 mm height.

The test was done at a constant engine speed. Compressor speed was adjusted manually until reaching the target mass flow rate at each point in order to get the maximum torque generated by the engine with the eSC.

		Different engine sizes			
		Engine X	Engine Y	Engine Z	Engine W
Different impeller sizes	Compressor 1	Performance 1	Performance 2	Performance 3	Performance 4
	Compressor 2	Performance 5	Performance 6	Performance 7	Performance 8
	Compressor 3	Performance 9	Performance 10	Performance 11	Performance 12
	Compressor 4	Performance 13	Performance 14	Performance 15	Performance 16

Table 10: Desired HiL test outcome- Performance matrix

6.2 National Instrument Modules³

The test rig monitoring and data acquisition system consists of several National Instrument (NI) modules. This section describes all the modulus used for HiL testing and their specifications and a summary are given in Table 11.

6.2.1 NI 9205

The NI 9205 module is used for analog inputs .The NI 9205 features 32 single-ended or 16 differential analog inputs, 16-bit resolution, and a maximum sampling rate of 250 kS/s. Each channel has programmable input ranges of ± 200 mV, ± 1 , ± 5 , and ± 10 V. To protect against signal transients, the NI 9205 includes up to 60 V of overvoltage protection between input channels and common (COM). In addition, the NI 9205 also includes a channel-to-earth-ground double isolation barrier for safety, noise immunity, and high common-mode voltage range. It is rated for 1,000 Vrms transient overvoltage protection.

³ All the information about the NI modules are from the national instrument webpage (www.sine.ni.com)

6.2.2 NI 9264

The NI 9264 module is used for analog outputs. This module voltage range is -10 to 10 volts, with an accuracy of 0.01025 V. Each channel can update at up to 25 kS/s since each channel has its own digital-to-analog converter. The spring-terminal version of the NI 9264 uses a 36-position connector for the 16 channels of output, each of which has a ground connection. The D-SUB version of the NI 9264 module was designed to accommodate standard 37-pin D-SUB components.

6.2.3 NI 9211

The NI 9211 thermocouple input module for use with NI CompactDAQ and CompactRIO chassis includes a 24-bit delta-sigma analog-to-digital converter, anti-aliasing filters, open-thermocouple detection, and cold-junction compensation for high-accuracy thermocouple measurements. The NI 9211 features NIST-traceable calibration and a channel-to-earth ground double isolation barrier for safety, noise immunity, and high common-mode voltage range.

6.2.4 NI 9217

The NI 9217 resistance temperature detector (RTD) analog input module features 4 channels and 24 bits of resolution for PT100 RTD measurements. The NI 9217 can be configured for two different sampling rate modes. With the high-sampling-rate mode, sample rate is 400 S/s (100 S/s per channel). Using the high-resolution mode, sample rate is 5 S/s (1.25 S/s per channel) with built-in 50/60 Hz noise rejection.

6.2.5 NI 9215

The NI 9215 is used to control the fast valve. This module includes four simultaneously sampled analog input channels and successive approximation register (SAR) 16-bit analog-to-digital converters (ADCs). The NI 9215 contains NIST-traceable calibration, a channel-to-earth ground double isolation barrier for safety and noise immunity, and high common-mode voltage range. Its voltage range is from -10 V to 10 V with an accuracy of 0.003456 V.

6.2.6 NI 9234

The NI 9234 is a 4-channel C Series dynamic signal acquisition module for making high-accuracy audio frequency measurements from integrated electronic piezoelectric (IEPE) and non-IEPE sensors with NI CompactDAQ or CompactRIO systems. The NI 9234 delivers 102 dB of dynamic range and incorporates software-selectable AC/DC coupling and IEPE signal conditioning for accelerometers and microphones. The four input channels simultaneously digitize signals at rates up to 51.2 kHz per channel with built-in anti-aliasing filters that automatically adjust to your sampling rate. The NI 9234 voltage range is from -5 V to 5 V. This module was used to monitor compressor vibration for the safety aspects of the test. Monitoring vibration helps to prevent any failure in the system and furthermore indicates if the motor is balanced in order to run at high speeds.

6.3 Flowmeter (ABB TRIO-WIRL Flowmeter)

The VT4000 Vortex and ST4000 Swirlmeters are supplied with an integrally mounted microprocessor-based signal converter using state-of-the-art Digital Signal Processor (DSP) technology for superior flow and vibration noise immunity.







This combination of flowmeter and electronics allows maximum flexibility for on-site configuration and maintenance.

The flowmeter used in this project is the Swirlmeter (ST 400), Figure 102. The volumetric flowrate of steam, gases and liquids can be measured over wide flow ranges independent of the fluid properties with this newest member to the Swirlmeter line. Special features of this Swirlmeter are:

- Accuracy: $\leq \pm 0.5\%$ of rate
- Minimal piping
- Wide flow range (Max 200 m³/h)
- Suitable for liquids with viscosities up to 30 cst (1centi-Stoke = 1 mm² /s)
- Measuring medium temperature (-55° C to 280° C)



Figure 102: ABB Flowmeter

NI 9205	NI 9264	NI 9211	NI 9217	NI 9215	NI 9234
					
<p>32-Ch ± 200 mV to ± 10 V, 16-Bit, 250 kS/s Analog Input Module</p> <p>32 single-ended or 16 differential analog inputs</p> <p>16-bit resolution; 250 kS/s aggregate sampling rate</p> <p>± 200 mV, ± 1, ± 5, and ± 10 V</p>	<p>± 10 V, Analog Output, 25 kS/s/ch, 16 Ch</p> <p>16 channels, 25 kS/s per channel simultaneous analog output</p> <p>± 10 V output range, 16-bit resolution</p> <p>NIST-traceable calibration</p>	<p>± 80 mV Thermocouple Input, 14 S/s, 4 Ch Module</p> <p>4-channel thermocouple input, 14 S/s</p> <p>± 80 mV analog inputs, 24-bit resolution; 50/60 Hz noise rejection</p> <p>Support for J, K, T, E, N, B, R, and S thermocouple types</p>	<p>PT100 RTD Analog Input, 100 S/s/ch, 4 Ch Module</p> <p>4 channels, 400 S/s (100 S/s per channel) RTD analog input</p> <p>PT100 RTD, 24-bit resolution, 50/60 Hz noise rejection</p> <p>Support for 3- and 4-wire RTDs with built-in excitation and automatic</p>	<p>± 10 V, Simultaneous Analog Input, 100 kS/s, 4 Ch Module</p> <p>4 differential channels, 100 kS/s per channel sample rate</p> <p>± 10 V measurement range, 16-bit resolution</p> <p>250 Vrms channel-earth, CAT II (screw terminal), or 60 VDC channel-earth,</p>	<p>± 5 V, IEPE and AC/DC Analog Input, 51.2 kS/s/ch, 4 Ch Module</p> <p>51.2 kS/s per channel maximum sampling rate; ± 5 V input</p> <p>24-bit resolution; 102 dB dynamic range; anti-aliasing filters</p> <p>Software-selectable AC/DC coupling; AC-</p>

programmable input ranges	250 Vrms isolation (spring terminal) or 60 VDC isolation (D-SUB)	250 Vrms, CAT II bank isolation	detection	CAT I (BNC) isolation	coupled (0.5 Hz)
Hot-swappable operation; overvoltage protection; isolation; NIST-traceable calibration	Spring-terminal or D-SUB connectivity	10-position screw-terminal connectivity	250 Vrms, CAT II bank isolation	10-position screw-terminal or BNC connectors available	Software-selectable IEPE signal conditioning (0 or 2 mA)
-40 to 70 °C operating range	-40 °C to 70 °C operating range	-40 °C to 70 °C operating range, 5 g vibration, 50 g shock	Screw-terminal connectivity		Smart TEDS sensor compatibility
			-40 °C to 70 °C operating range, 5 g vibration, 50 g shock		-40 °C to 70 °C operating range, 5 g vibration, 50 g shock

Table 11: NI modules summary

6.4 Pressure Sensors

Two pressure sensors were used to measure the ambient and output pressure of the compressor. The PTX 1400 is used to measure the ambient pressure. The accuracy of this sensor is $\pm 0.15\%$ with the temperature operating range of -20 to $+80^\circ\text{C}$ and a maximum pressure reading of 10 bar. The specifications of PTX 1400 can be found in table 12.

The Omegadyne PXM 219 sensor is used to measure the TurboClaw output pressure. The PXM 219 accuracy is 0.25% full scale including linearity, hysteresis and repeatability. This sensor has a broad temperature-compensated Range and an extensive operating range of -20 to 80°C and -54 to 121°C respectively with a response time of 2 ms.



Figure 103: PTX 1400 Pressure sensor

Accuracy	$\pm 0.15\%$
Analogue Output	4 \rightarrow 20 mA
Maximum Operating Temperature	$+80^\circ\text{C}$
Maximum Pressure Reading	10bar
Media Measured	Fluid
Minimum Operating Temperature	-20°C

Table 12: PTX 1400 specifications



Figure 104: Omegadyne PXM 219 Pressure sensor

Accuracy	±0.25 %
Analogue Output	4 → 20 mA
Maximum Operating Temperature	+121°C
Media Measured	Fluid
Minimum Operating Temperature	-20°C
Minimum Pressure Reading	0bar

Table 13: Omegadyne PXM 219 specifications

6.5 Temperature sensors

The Resistance temperature detectors (RTDs) are sensors used to measure outlet TurboClaw and ambient temperature for the HIL test. The same type of RTD, (pt100 -3mm diameter x 100 mm long), was used to measure both ambient and outlet compressor temperature. The sensor operating range is from -75°C to +350°C. The thermocouples used for the safety aspect in the HIL test are K TYPE THERMOCOUPLES with a temperature range of -200°C to +1250°C. The K TYPE has 0.75% above 0°C and 1.5% below 0°C limits of error.



Figure 105: PT100 RTD

The Figures 106-108 show the test cell installation at DBS for the purpose of HIL testing. As explained earlier in chapter 5, the ETC layout was chosen as the final configuration; therefore the test cell was designed according to ETC specifications.

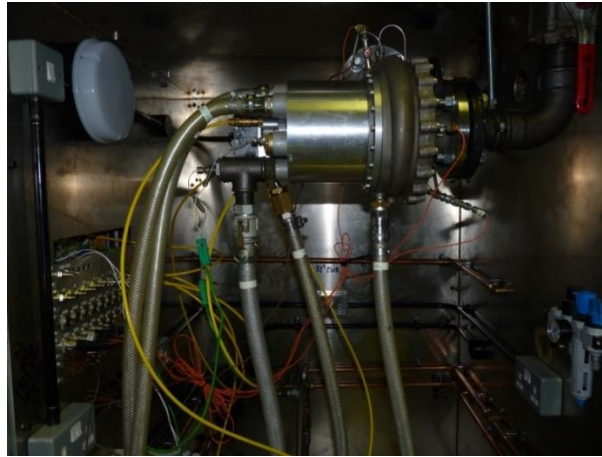


Figure 106: Test Cell- TurboClaw installation

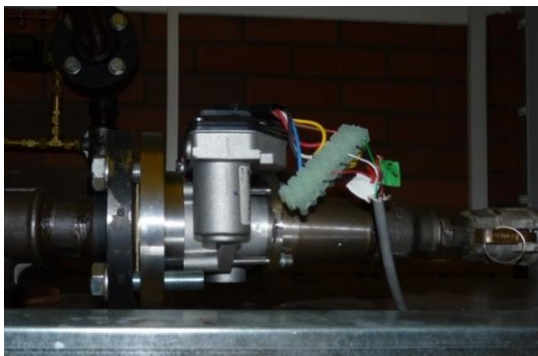


Figure 107: Left: Fast valve, Right: dSPACE unit

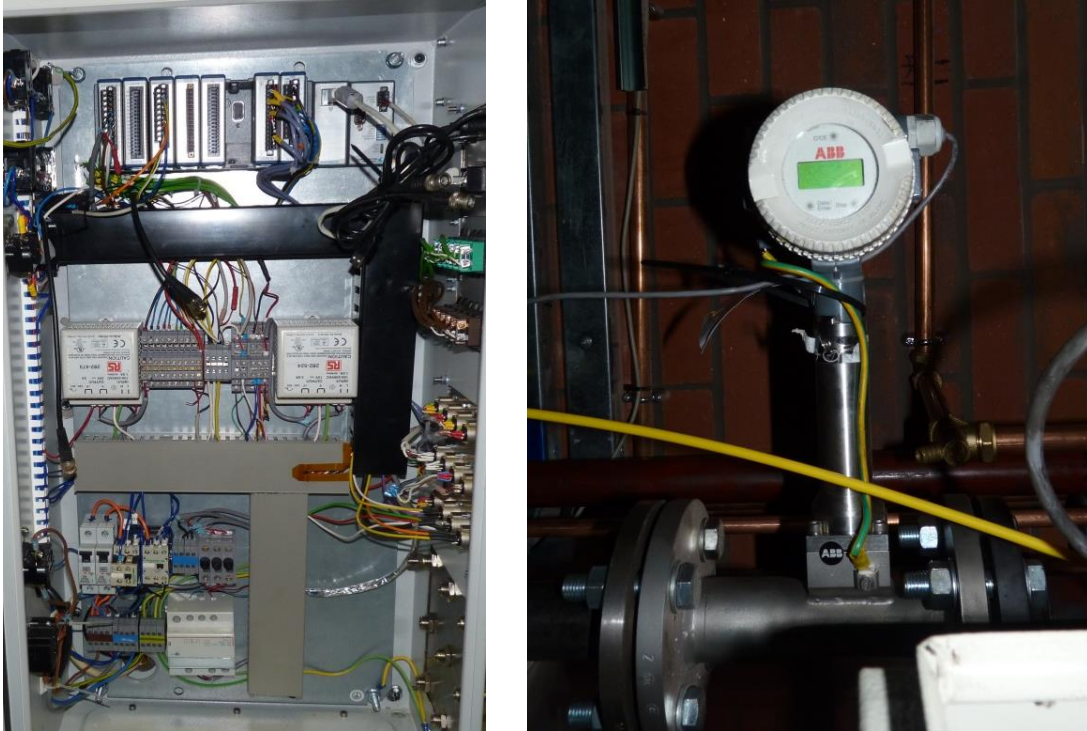


Figure 108: Left: ABB Flow meter, Right: NI units

6.6 The steady state HiL test results

There are different possible strategies to perform the HiL testing, such as matching the compressor speed between HiL and Simulation, pressures, mass flow rates and etc. The TurboClaw performance map implemented in the simulations is based on torque sensor data and everything above 40kRPM and below 15kRPM is extrapolated (The performance test will be repeated in the near future for the full range speed). The strategy used in this section to perform the HiL testing was to match the TurboClaw mass flow rate with the simulation by manually tuning the eSC speed. The graphs presented in this section are based on the mentioned approach.

The charging layout for this test is the ETC (low-pressure eSC + high-pressure Turbo-Compressor + Air Cooler).

Figure 109 shows the comparison between HIL test and Simulation results.

The electric motor used in HIL test was not balanced enough in order to run the compressor at speeds higher than 40 kRPM therefore it was not possible to reach some simulation condition when speed was higher than this limit.

As shown in Figure 109, the TurboClaw outlet mass flow rates in the two environments (HIL and Simulations) are presenting the identical performance up to 1400 RPM and beyond this point the HIL results are slightly different. The figures 110 and 111 represent the comparison between the torque and compressor speed vs engine speed for HIL and simulation.

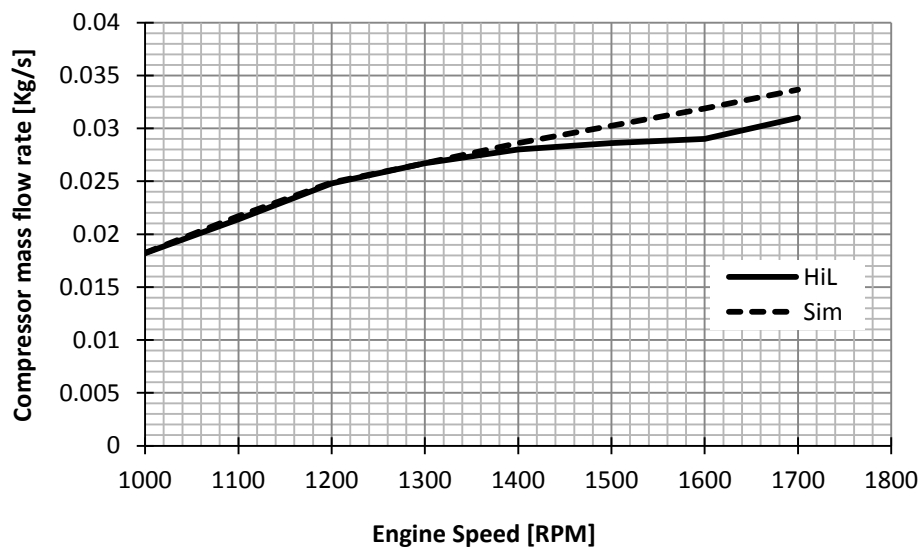


Figure 109: TurboClaw mass flow rate vs engine speed for eSC+TC layout

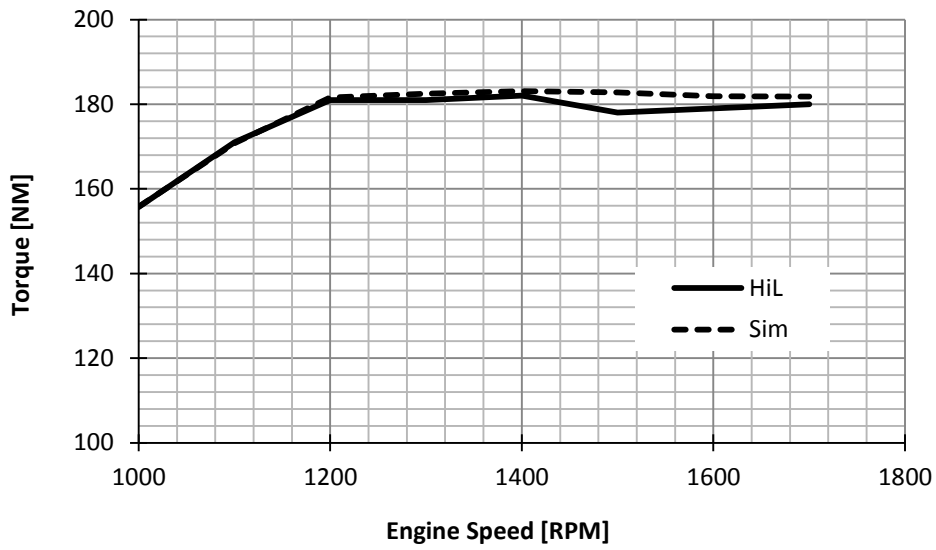


Figure 110: Torque vs engine speed for eSC+TC layout

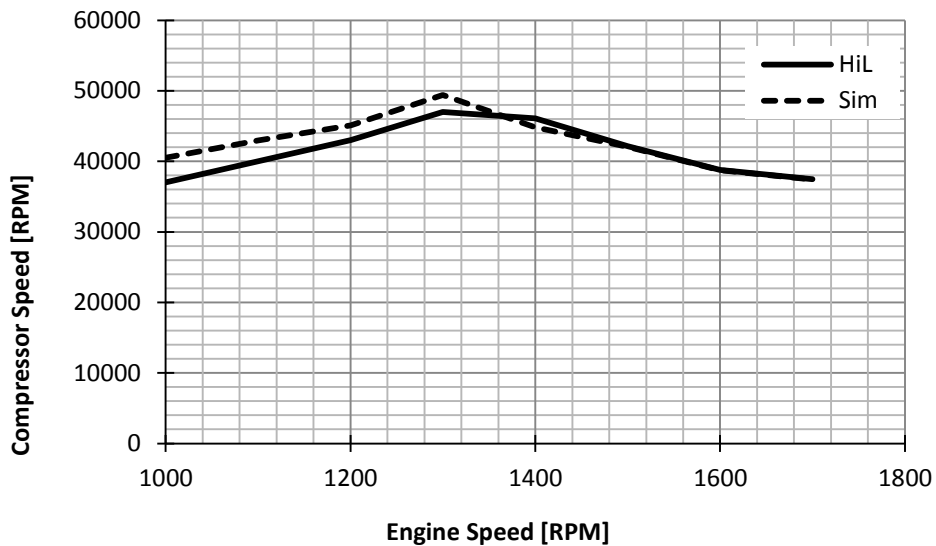


Figure 111: Compressor speed (eSC) vs engine speed for eSC+TC layout

The full compressor pressure ratio and temperature curves obtained from experiment (HiL) for a 1.0 L eSC+TC engine are shown in Figure 112 and 113 for comparison with simulation results. The conclusion from these graph is that the system reaches the desired mass flow rate at a lower temperature and pressure in

the HiL environment compared to simulation up to 1600 rpm, but as it was discussed previously the system could not reach the target (mass flow rate) due to unbalanced electric motor, therefore this difference in pressure and temperature could be justified since the HiL is providing lower mass flow rate beyond 1400 rpm. Based on the ideal gas law ($PV = nRT$ where the letters denote pressure, volume, amount (in moles), ideal gas constant, and temperature of the gas, respectively), pressure and temperature are directly related to each other and to the gas volume, and the gas volume is directly related to the compressor speed in this case, therefore running the compressor at lower speeds results in having lower outlet temperature and pressures. However; further investigation needs to be done to understand the reason behind the difference in pressure and temperature for engine speeds of 1000 to 1400 rpm.

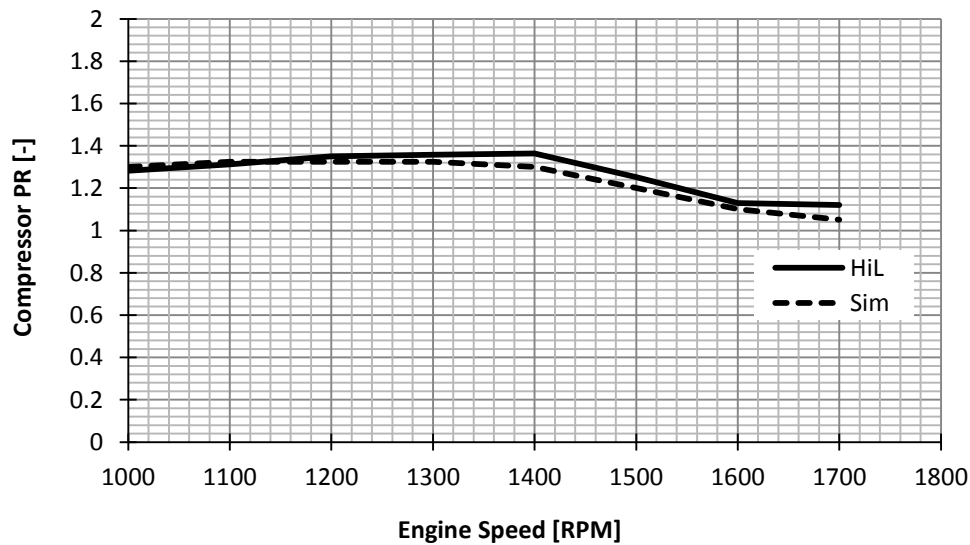


Figure 112: TurboClaw pressure ratio vs engine speed for eSC+TC layout

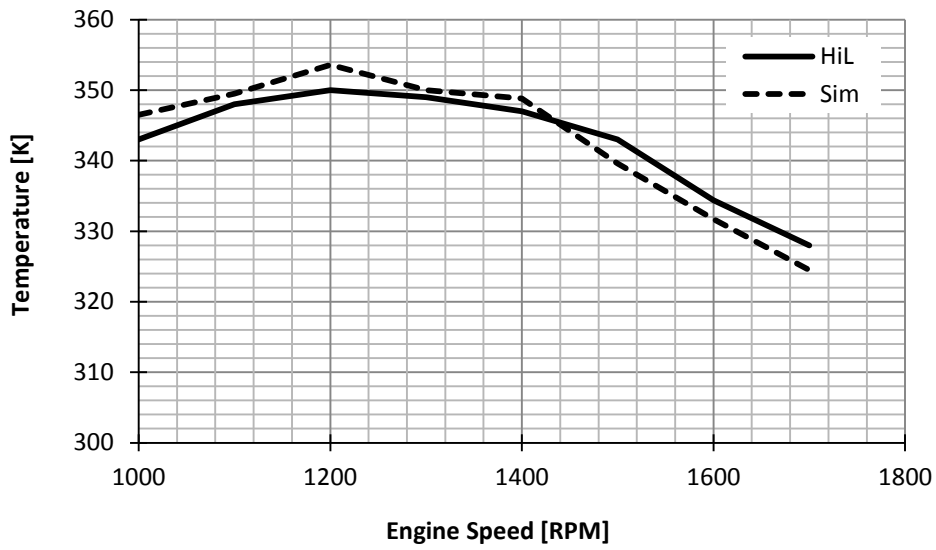


Figure 113: TurboClaw temperature vs engine speed for eSC+TC layout

Similarly, the same behaviour was observed for the speeds above 1400 rpm for the turbine and turbo compressor; obeying the simulation patterns up to 1400 rpm and significant decrease for the rest of the points. Figure 114 shows the HiL and simulations behaviours of the inlet turbine temperature vs engine speed.

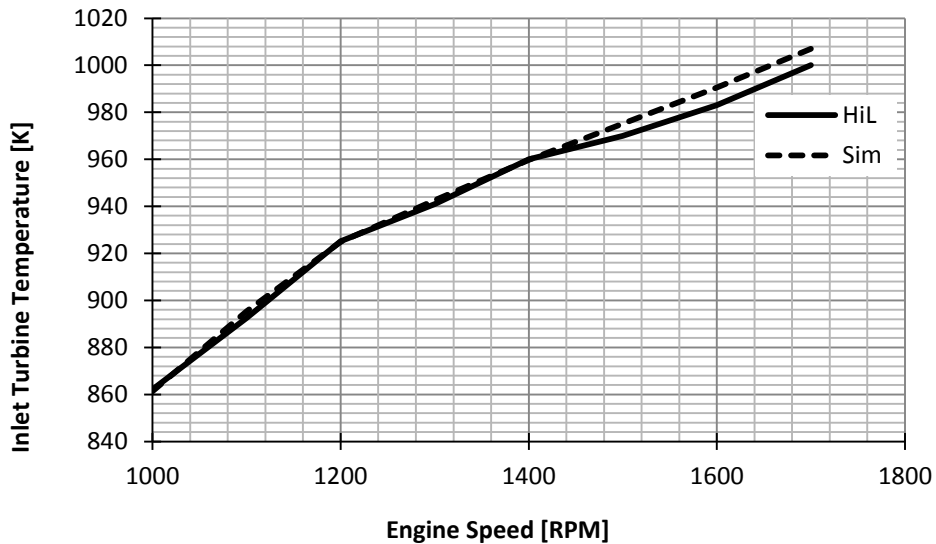


Figure 114: Inlet turbine temperature vs engine speed for eSC+TC layout

There are two main scenarios from the results:

- Before 1400 RPM - same massflow, lower HIL compressor speed, lower HIL pressure ratio
- After 1400 RPM – lower HIL massflow, same HIL compressor speed, higher HIL pressure ratio

The mismatch in the results that yields to these two scenarios is related to the way the compressor was controlled during the HIL test. Figure115 shows the concept.

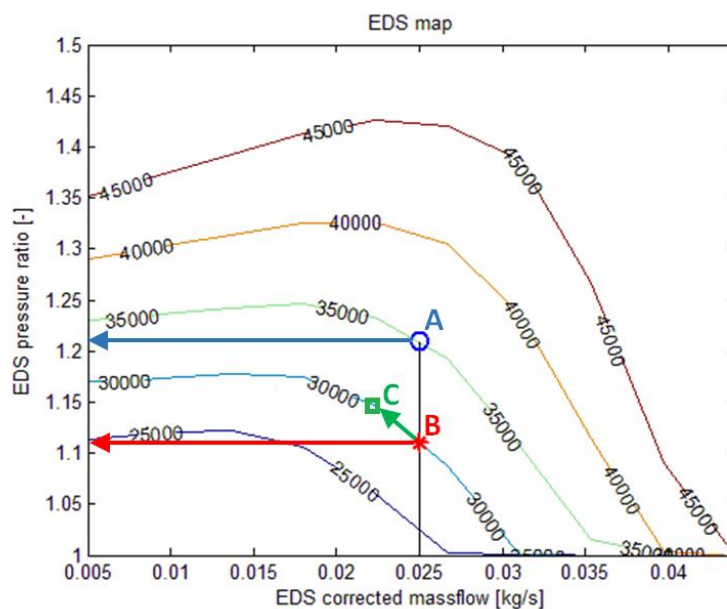


Figure 115: example of operation points on compressor map

Giving a desired massflow (0.025 kg/s in the example), by manually tuning the compressor speed to reach the target one can find several points, such as A and B which will satisfy the desired massflow but at different speed and pressure ratio. In particular, for the scenario before 1400 RPM, B would represent the HIL operation point and A the Simulation point.

The reason is that the operator was only controlling the compressor speed without taking into account the pressure setpoints which was explained in chapter 5, Figure 82. As a result, the desired mass flow rate was achieved at a lower pressure ratio and speed. The scenario above 1400 RPM would be represented by point C, since it sits on the same speed-line, but at lower massflow and so higher pressure ratio. A more robust controller which tries to match not only the massflow but also output pressure could be more efficient to meet the simulation results.

In addition, potential mismatch with simulation results can be affected to how the EDS data are used in simulation: the compressor is virtually represented by look-up tables to output the massflow and efficiency based on experimental data. In particular the massflow lookup table is inverted (with some lack of accuracy due to non-monotonic trend of speed-lines); efficiency table can generally mismatches from reality test under different condition and this can cause a difference in the outlet temperature.

In conclusion, considering the simple approach used to control the compressor operation point, the overall comparison between HIL test and simulation results is quite good and acceptable.

6.7 Dyno Test Results

This section represents the installation of the eSC system on the vehicle and also the dyno test results. It is expected to get the same results as the simulations which was carried out in early phases of this project since the engine data used in simulations are taken from the same vehicle.

The eSc system consists of the 85x150 mm TurboClaw compressor, a permanent magnet brushless dc motor (BLDC), 60 kRPM at 24 Volts DC. 1.2 kW continuous.

The installation and the initial tests were performed by Torque Developments International (TDI). TDI is one of the UK's service providers to the motorsport and high performance automotive industries. TDI was established in around 1984 as a specialist automotive engineering operation to fulfil a demand for a high level of technical and practical expertise within the racing and high performance road car sectors. Figures 116 - 119 show the vehicle selected for the dyno test and installation.



Figure 116: Selected vehicle for the dyno test



Figure 117: Dyno test room

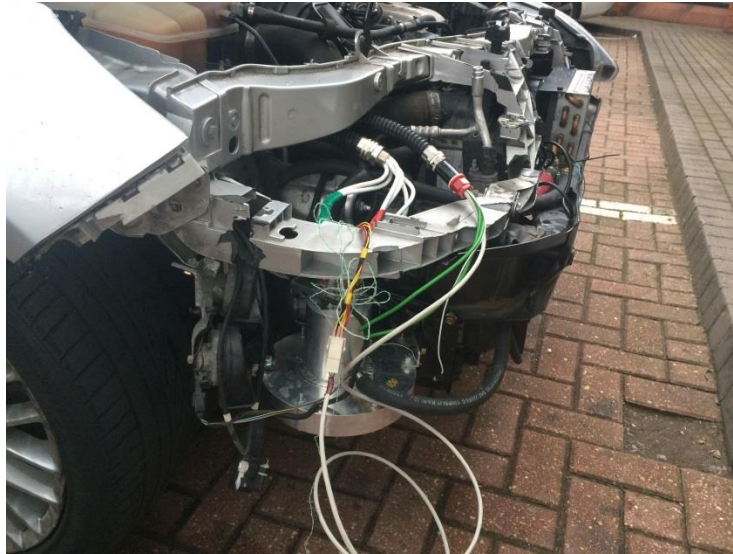


Figure 118: eSC mounted on the vehicle

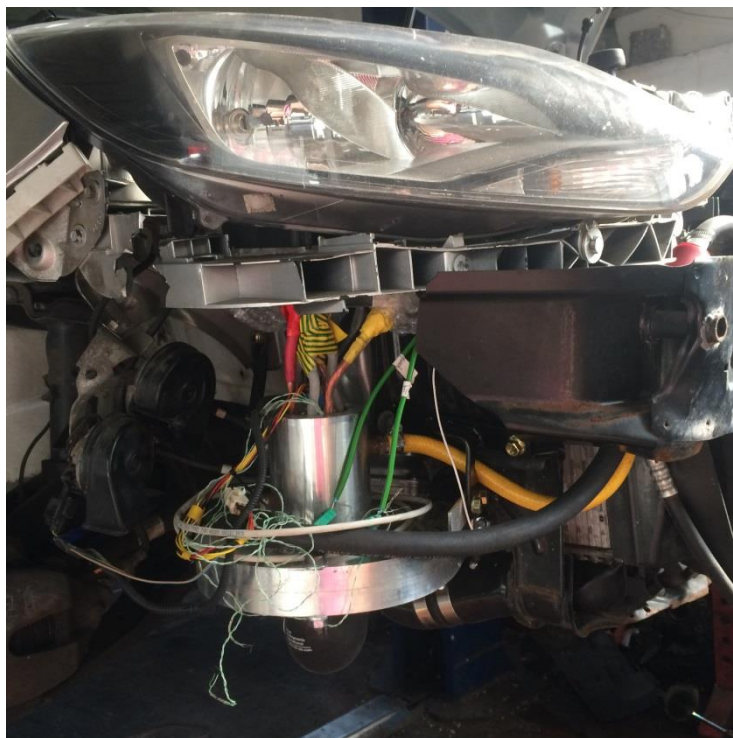


Figure 119: eSC mounted on the vehicle-2

Figure 122 shows the dyno test results vs simulations for the ETC layout. The dotted lines represent the simulation results and the continuous ones represent

dyno results. The dyno results are not as expected; they do not match the simulations and are not within the acceptance region. The reason is that the Engine Control Unit (ECU) is not accepting the extra boost.

6.8 Summary

The ECU is throttling the flow to either a fixed manifold pressure or torque. Although it seems this was only happening (at a constant torque value) above 2kRPM because the torque curve is so clearly capped. This is happening (with a variable torque or P manifold vs rpm) below 2kRPM, as there is no difference in pressure after the throttle with or without the eSC. The solution to this problem is to remove this limitation from the ECU and repeat the test. Unfortunately this was realised too late into this part of the work and also due to financial limitations the test could not be repeated.

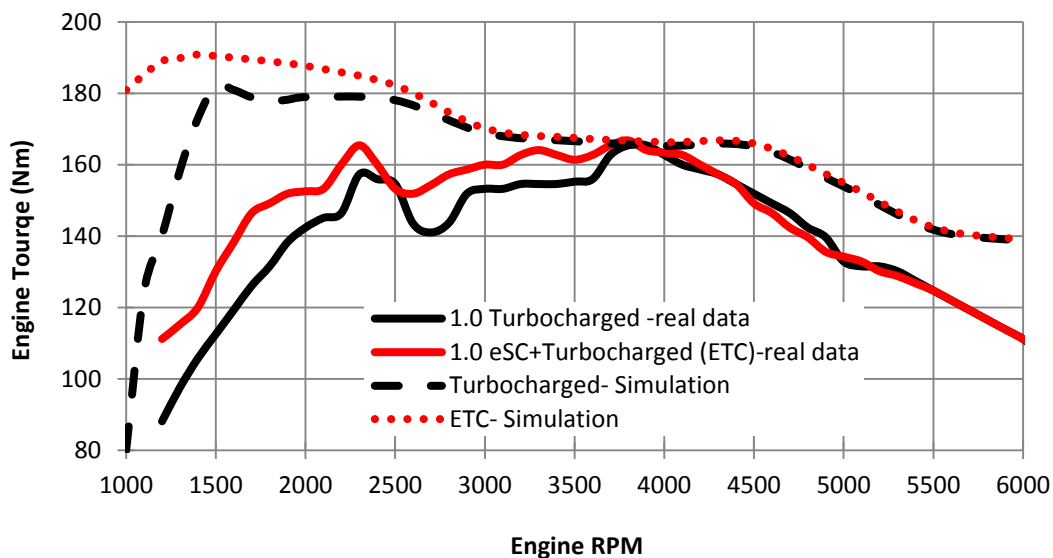


Figure 120: 1.0 L Turbocharged engine with and without eSC

Chapter 7

7 Conclusion

Engine downsizing is an attractive solution to reduce fuel consumption and CO₂ emissions (when coupled with superchargers and turbochargers to provide high torque when needed).

Mean value engine simulation modelling using the Simulink environment is a powerful tool to enable rapid assessment of different boost architectures involving turbocharger and electric supercharger combinations. It also provides simple integration into further HIL tests.

Three models were created in order to rapid assess different charging layout involving electric supercharger: TC model (only turbocharged engine, used as baseline), ETC model (low pressure electric supercharger + high pressure turbo-compressor) and TEC model (turbo-compressor low pressure + high pressure electric supercharger). The TC model showed full load torque is limited below 2000 rpm; in this range compressor surge limits air mass filling and hence torque. Turbo lag also limits transient response at low speeds.

Steady state simulation with additional eSC showed how an electrically driven supercharger helps the turbine to produce more energy and lets the turbo-compressor work outside of surge at low engine speeds. ETC and TEC layouts produce similar torque output; the real eSC benefit is seen at low speed, with more than 50% torque increase below 1100 rpm. The electric supercharger stops being usable for the ETC model when it begins to choke and it must be bypassed; eSC for the TEC layout can be used up to 3200 rpm, since the inlet boost pressure coming from the turbo-compressor moves the corrected massflow to smaller values, so far from choke limit. Use of eSC over 2000 rpm (for TEC) is not a real

advantage because it needs more eSC power at high speeds and the engine produces basically the same torque as in the TC case. The eSC wheel in TEC would also undergo higher stress due to the higher temperatures.

Transient simulations show how eSC gives strong support at lower engine speeds up to 1600 rpm (time to TC target reduction between 90% and 30% in the range 1000-3000 RPM); ETC and TEC models show basically a similar trend. Over 1600 rpm eSC overlaps the TC model because the eSC is bypassed; at these speeds the TC model increases its response and gets closer to TEC; finally, over 3000 rpm, eSC for TEC is bypassed. Vehicle tip-in simulations have shown a good acceleration improvement (acceleration peak reached 2 seconds earlier) without any significant influence of the eSC position.

It was finally concluded that the characteristics of the TurboClaw compressor can best be utilized to provide boost at the lower RPM ranges of a <1.4L gasoline engine, with the higher RPM operation being boosted by a conventional turbocharger. A test cell has been specially designed for the required testing of the eSC compressor and its control hardware along with all required instrumentation. "Hardware-in-the-Loop" environment allows testing of eSC system to validate initial performance predicted by simulations and to assess different compressor and engine sizes to determine the best combination.

Early HIL results show a good matching with simulation operation points. Some lack of accuracy at engine speed above 1400 RPM was accepted in order to preserve the eSC controller simplicity. The next step would be to implement a more robust controller which could precisely match the target eSC operation point. The following step in developing eSC technology is testing the system along with a turbocharged in a vehicle selected from the performance matrix.

At the moment five different screw compressors are simulated and the results prove that screw compressors are not suitable for small engines since they have very poor efficiency at the low mass flow rate required rates (in the order of 40-80 m³/hr) . SCORPATH correctly simulated a screw compressor based on its geometry, hence direct scaled down method was used to simulate smaller compressors. The firm conclusion drawn from this study is TurboClaw has significantly better performance so focus should continue on this machine for eSC research.

7.1 Future work

- Number of features could be added to the models in order to produce more precise data such as EGR and the knock model which is used to determine ignition timing and control the combustion phasing in those simulations.
- A better control system could be designed for the HIL purpose. As explained previously the discrepancy in data was caused by the control system as a simple approach was used in order to reach the target in HIL test.
- The vehicle ECU needs to be programmed for the dyno test. The simulation results are not matching the dyno test results as shown on Figure 120, and this is happening due to rejecting the boost by ECU.
- The ETC could be installed on different vehicles in order to produce a performance matrix. Therefore it is important to test different sizes of compressors on different engines.

8 References

1. *Overview of boosting options for future downsized engines.* **Ricardo, M, Apostolos, P and Yang, M.** 2, 2011, Science China Technological Sciences, Vol. 54.
2. **Europa.** ec.europa.eu. [Online] 02 December 2016. [Cited: 02 December 2016.] http://ec.europa.eu/clima/policies/transport/vehicles/cars_en#top-page.
3. **Grove, Jeremy.** *Vehicle Licensing Statistics:Quarter 4 (Oct - Dec) 2015.* London : Department for Transport, 2016.
4. *Overview of boosting options for future downsized engines.* **Martinez-Botas, Ricardo, Apostolos, rPesiridis and Yang, MingYang.** 2, 2011, Science China Technological Sciences, Vol. 54, pp. 318-331.
5. **European Comission, Fact Sheet.** www.europa.eu. [Online] 2016. [Cited: 2016 December 05.] http://europa.eu/rapid/press-release_MEMO-16-2499_en.htm.
6. **Zhou, Angie.** *Analysis of the Volkswagen Scandal - Possible solutions for Recovery.* San Diego : School of Global Policy and Strategy, 2016.
7. **Kollewe, Julia.** www.theguardian.com. [Online] 2015. [Cited: 05 December 2016.] <https://www.theguardian.com/business/2015/dec/10/volkswagen-emissions-scandal-timeline-events>.
8. **Kubota, Yoko.** www.wsj.com. [Online] 2016. [Cited: 05 November 2016.] <http://www.wsj.com/articles/mitsubishi-fuel-economy-scandal-may-affect-more-vehicles-1462967737>.
9. **Riley, Charles and Kobayashi, Chie.** www.money.cnn.com. [Online] 2016. [Cited: 2016 June 2016.] <http://money.cnn.com/2016/05/11/news/companies/mitsubishi-fuel-economy-tests/>.

10. **Mitsubishi Motors.** [www.bbc.co.uk](http://www.bbc.co.uk/news/business-36099044). [Online] 2016. [Cited: 05 December 2016.] <http://www.bbc.co.uk/news/business-36099044>.
11. *The Prospects for Hybrid Electric Vehicles, 2005-2020: Results of a Delphi Study.* **Henry, K. Ng, Anant, D. Vyas and Danilo, Santini.** 2942, 1999, SAE Technical paper, Vol. 2, p. 14.
12. *A New 3 Cylinder 1.2l Advanced Downsizing Technology Demonstrator Engine.* **Hancock, Dave, et al., et al.** 2008, SAE Technical paper, Vol. 01, p. 16.
13. **Edenhofer, O., et al., et al.** www.epa.gov. [Online] 2016. [Cited: 5 December 2016.] <https://www.epa.gov/ghgemissions/global-greenhouse-gas-emissions-data>.
14. **wltpfacts.eu, WLTP Facts,.** WLTP Facts. [Online] 2017. [Cited: 25 11 2017.] http://wltpfacts.eu/wp-content/uploads/2017/04/WLTP_Leaflet_FA_web.pdf.
15. **Mock, Peter, et al., et al.** *The WLTP: How a new test procedure for cars will affect fuel consumption values in the EU.* s.l.: The International Council on Clean Transportation, 2014.
16. **Calais.** www.calaisturbo.org. [Online] 2016. [Cited: 1 December 2016.] <http://www.calaisturbo.org/history-of-the-supercharger.php>.
17. **Reifarth, Simon.** *EGR-Systems for Diesel Engines.* Stockholm : Royal Institute of Technology , Department of Machine Design, 2010.
18. **Heywood, John B.** *Internal Combustion Engine Fundamentals.* Unoted states of America : McGraw-Hill, 1988.
19. **Zhen, Xudong, et al., et al.** *The engine knock analysis – An overview.* Tianjin : Tianjin University,, 2011.

20. **Reif, Konrad.** Fundamentals of Automotive and Engine Technology. *Combustion knock*. Wiesbaden : Springer Vieweg, 2014, pp. 66-69.
21. **Kasseris, Emmanuel P.** *Knock Limits in Spark Ignited Direct Injected Engines Using Gasoline/Ethanol Blends*. MASSACHUSETTS : MASSACHUSETTS INSTITUTE OF TECHNOLOGY, 2011.
22. **Honeywell.** www.honeywell.com. [Online] 2016. [Cited: 6 December 2016.] <http://www51.honeywell.com/honeywell/news-events/case-studies-n3n4/turbochargers.html?c=36>.
23. **Pandey, Raghvendra Kumar.** www.slideshare.net. [Online] 10 Nov 2013. [Cited: 10 Apr 2017.] <https://www.slideshare.net/raghvmech/fuel-injection-system>.
24. *Comparison of a Supercharger vs. a Turbocharger in a Small Displacement Gasoline Engine Application.* **Singer, David A.** 1985, SAE International Congress and Exposition, p. 16.
25. *Engine Downsizing- an Analysis Prespective- MAHLE Powertrain.* **Stephenson, Mark.** s.l. : MAHLE Powertrain, 2009.
26. **Chis, Alexandru Radu.** www.autoevolution.com. [Online] 2010. [Cited: 06 December 2016.] <http://www.autoevolution.com/news/hondas-vtec-system-explained-20338.html>.
27. **Andersson, Per.** *Air Charge Estimation in Turbocharged Spark Ignition Engines*. Linköping, Sweden : Linköping University,, 2005.
28. *Turbine adapted maps for turbocharger engine matching.* **Tancrez, M, et al., et al.** 2011, Experimental Thermal and Fluid Science, Vol. 35, pp. 146-153.

29. *Supercharging performance of a gasoline engine with a supercharger.* **Lee, Chang Sik, et al., et al.** 5, 1997, KSME International Journal, Vol. 11, pp. 556-564.
30. **Hiereth, Hermann and Prenninger, Peter.** Mechanical supercharging. *Charging the Internal Combustion Engine. Powertrain.* Vienna : Springer, 2007, pp. 51-59.
31. **Volkswagen.com.** www.volkswagen.co.uk. [Online] 2015. [Cited: 07 December 2016.] <http://www.volkswagen.co.uk/technology/petrol/tsi>.
32. *Electrically Driven Supercharger using TurboClaw Compressor For Engine Downsizing.* **Pullen, Keith, et al., et al.** 2012, IMechE.
33. **Zhao, F, La, M.-C. and Harrington, D.L.** *Automotive Spark -ignited direct-injection gasoline engines.* USA : Elsevier Science Lt, 2001.
34. *Development of a Three-Phase Sequential Turbocharging System with Two Unequal-Size Turbochargers.* **Qian, Yuehua, Zhang, Zhe and Deng, Kangyao.** 951096, 2012, International Journal of Rotating Machinery, Vol. 2012, p. 8.
35. *A Sequential Turbocharging Method for Highly-Rated Truck Diesel Engines.* **Borila, Y. G.** 860074, 1986, SAE International, Vols. 95-86, p. 12.
36. **Kusztelan, Alex, et al., et al.** Investigating the Effects on the Low Speed Response of a Pressure Charged IC Engine Through the Application of a Twin-Entry Turbine Housing. [ed.] Dordrecht. *IAENG Transactions on Engineering Technologies.* 213 : Springer, 2013, p. 201.
37. **Wan, Mark.** www.autozine.org. [Online] 2005. [Cited: 07 December 2016.] http://www.autozine.org/technical_school/engine/tech_engine_3.htm.

38. **Ehsani, Mehrdad, Gao, Yimin and Emadi, Ali.** Modern Electric,Hybrid Electric and Fuel Cell Vehicles. [ed.] Taylor & Francis Group. *Fundamentals, Theory , and design.* New york : Taylor & Francis Group, 2010, pp. 14-16.
39. **Wakefield, E H.** *HISTORY OF THE ELECTRIC AUTOMOBILE - HYBRID ELECTRIC VEHICLES.* Warrendale : Society of Automotive Engineers, 1998.
40. **Toyota-global.** www.toyota-global.com. [Online] 2016. [Cited: 09 December 2016.] http://www.toyota-global.com/innovation/environmental_technology/hybrid/.
41. **Ihlemann, Arndt and Nitz, Norbert.** www.schaeffler.com. [Online] 2014. [Cited: 13 December 2016.] http://www.schaeffler.com/remotemedien/media/_shared_media/08_media_library/01_publications/schaeffler_2/symposia_1/downloads_11/schaeffler_kolloquium_2014_11_en.pdf.
42. *Cylinder Deactivation with Mechanically Fully Variable Valve Train.* **Flierl, R., et al., et al.** 2, s.l. : SAE Int, 2012, SAE Int, Vol. 5, pp. 207-215.
43. **MAHLE Powertrain Ltd.** www.aeristech.co.uk. [Online] 2014. [Cited: 06 Jan 2017.] http://aeristech.co.uk/wp-content/uploads/case_study__esupercharger_for_rex_engine_v22.pdf.
44. **Tsourapas, Vasilios and Benjey, Robert P.** Eaton's Electrically Assisted TVS Supercharger with Variable Speed, Mild-Hybrid and Engine Start/Stop Functionalities. *www.tib.eu.* [Online] 2013. [Cited: 06 Jan 2017.] https://www.tib.eu/en/search/id/tema%3ATEMA20150202000/Eaton-s-Electrically-Assisted-TVS-Supercharger/?tx_tibsearch_search%5Bsearchspace%5D=tn.

45. *Observations on and potential trends for mechanically supercharging a downsized passenger car engine: a review.* **Hu, B., et al., et al.** 4, 2017, Journal of Automobile Engineering, Vol. 231, pp. 435-456.
46. *TVS^oR V-Series Supercharger Development for Single and Compound Boosted Engines.* **Froehlich, M and Stewart, N.,** 2013-01-0919, 2013, SAE paper.
47. **CPOWER**. www.cpowert.com. [Online] Apr 2014. [Cited: 09 Jan 2017.] [http://www.cpowert.com/assets/CPT%20COBRA_4pp_APR2014_4print%20\(2\)-1.pdf](http://www.cpowert.com/assets/CPT%20COBRA_4pp_APR2014_4print%20(2)-1.pdf).
48. **Sayers, A.T.** *Hydraulic and Compressible Flow Turbomachines.* s.l. : McGraw Hill, 1990.
49. **King, Jason, et al., et al.** *HyBoost: An Intelligently Electrified Optimised Downsized Gasoline Engine Concept.* London : Institution of Mechanical engineering, 2012.
50. *10 th International conference on turbochargers and turbocharging.* **Paul, King, et al., et al.** London : Woodhead Publishing, 2012. IMechE. pp. 3-15.
51. **Bassett, M., et al., et al.** www.aeristech.co.uk. [Online] 2015. [Cited: 09 Jan 2017.] <http://www.aeristech.co.uk/wp-content/uploads/E-supercharging-for-downsized-engine-SIA-V121.pdf>.
52. **Aeristech Ltd.** www.aeristech.co.uk. [Online] 2015. [Cited: 09 August 2017.] <http://www.aeristech.co.uk/electric-supercharger/>.
53. **Bassett, M, et al., et al.** www.aeristech.co.uk. *E-supercharging for Heavily Downsized Gasoline Engines.* [Online] 2015. [Cited: 27 Jan 2017.] <http://www.aeristech.co.uk/wp-content/uploads/E-supercharging-for-downsized-engine-SIA-V121.pdf>.

54. **Thornton, Warren E.** *A Low specific Speed, Multistage, Turbo-Compressor for Microturbine Fuelling*. London : Imperial College London, 2005.
55. *Design of Radial Turbomachines*. **Whitfield, A, and Baines, N.C.** 1990, Longman Scientific and Technical, pp. ISBN 0-582-49501-6.
56. **Watson, N and Janota, M.S.** *Turbocharging the internal combustion engine*. first. London : the Macmillan press ltd, 1982.
57. *The effects of Reynolds Number on the Efficiency of Centrifugal*. **Casey, M V.** 1985, Journal of Engineering for Gas Turbines and Power, pp. Vol 107 541-548.
58. *Performance Measurements of a Low Specific Speed TurboClaw Compressor*. **Parra, J, et al., et al.** 2015, 9th International Conference on Compressors and their Systems.
59. *Experimental Investigation of the TurboClaw Low Specific Speed Turbocompressor*. **Pullen, K. R., Etemad, S. and Cattell, R.** 2012, THE AMERICAN SOCIETY OF MECHANICAL ENGINEERS (ASME), pp. 735-742.
60. **DBS.** dynamicboost.com. [Online] 2017. [Cited: 20 Jan 2017.] <http://dynamicboost.com/about-turboclaw>.
61. *REAL-TIME ENGINE MODELLING FOR ENGINE DOWNSIZING USING AN ELECTRIC SUPERCHARGER*. **Parra, Juan, et al., et al.** s.l. : IEEE XPLORE, 2011. Vehicle Power and Propulsion Conference (VPPC), 2011 IEEE.
62. **Vine, Andrew.** *The Aerodynamic Design and Evaluation of a Low Specific*. London : Imperial College London, Department of Mechanical Engineering, PhD thesis, 2005.
63. *Low specific speed turbocompressors*. **Vine, A J, et al., et al.** 2005, Institution of Mechanical Engineers, p. 9.

64. *Geometry of Screw Compressor Rotors and their tools*. **Stosic, Nikola, et al., et al.** 2011, Journal of Zhejiang University-SCIENCE A (Applied Physics & Engineering), p. 316.
65. **Bruce, Trent.** *Screw Compressors: Misconception or Reality a Discussion of the Application and Operation of Oil Flooded Rotary Screw Compressors and a Comparison to the Conventional Reciprocating Machines*. Calgary, Alberta, Canada : Semantic Scholar, 2012.
66. **Andersson, Per.** *Air Charge Estimation in turbocharged spark Ignition Engines*. Sweden : Linkoping University, Department of electrical engineering, 2005.
67. **Pettersson, F.** *Simulation of a Turbo Charged Spark Ignited Engine-PhD thesis*. Sweden : linkopings university ,Vehicular Systems Dept. of Electrical Engineering, 2000.
68. **Guzzella, L and Onder, C. H.** *Introduction to modeling and control of internal combustion engine systems*. Berlin : Springer, 2004.
69. **Teacher, Xiao.** www.cqgjqp.com. [Online] 2013. [Cited: 21 Sep 2017.] <http://www.cqgjqp.com/company/productlist2.aspx?p=120139>.
70. **Wiesner, Sven.** www.slideshare.net. [Online] 2012 Mar 2012. [Cited: 03 Feb 2017.] <http://www.slideshare.net/svenwiesner/ord-focus-1-l-ecoboost-presentation>.
71. **Mohan, Pradeep.** www.riotengine.in. [Online] 2013. [Cited: 21 Sep 2017.] <http://www.riotengine.in/2013/05/12/ford-ecosport-1-0-litre-ecoboost-review-first-drive/>.
72. **Apikol.** www.myaudis4.com. [Online] 2017. [Cited: 23 Aug 2017.] <http://www.myaudis4.com/apikol-ic-flow-test/>.

73. **Garrett.** www.turbobygarrett.com. [Online] V4 2017. [Cited: 23 Aug 2017.] https://www.turbobygarrett.com/turbobygarrett/sites/default/files/turboTech/Garrett_Catalog_V4.pdf.
74. *Electrically Driven Supercharger using TurboClaw Compressor For Engine Downsizing.* **K R Pullen, S Etemad, W Thornton, J Villegas.** 2012, IMechE.
75. **F. Zhao, M.-C. Lai, D.L. Harrington.** *Automotive Spark -ignited direct-injection gasoline engines.* USA : Elsevier Science Lt.
76. **UCSUSA.org.** www.ucsusa.org. [Online] [Cited: 12 December 2016.] <http://www.ucsusa.org/clean-vehicles/electric-vehicles/how-do-hydrogen-fuel-cells-work#.WE6227KLTRY>.
77. **mathworks.com.** www.mathworks.com. [Online] 2017. [Cited: 26 Jan 2017.] <https://www.mathworks.com/products/simulink.html>.
78. **Wieltsch, Martin.** *PROJECT TSB EDS TURBOCLAW™ - AVL Powertrain UK Internal report.* s.l. : AVL, 2010.
79. *HyBoost: an intelligent electrified optimised downsized gasoline engine concept.* **King, J., et al., et al.** London : Institution of MECHANICAL ENGINEERS-IMEche, 2012. 10th International conference on Turbochargers and Turbocharging. pp. 3-14.
80. *HyBoost – An intelligently electrified optimised downsized gasoline engine concept.* **King, J, et al., et al.** s.l. : SAE, 2013. SAE China and Fiesta.
81. **Bohacz, Ray T.** www.zhome.com/. [Online] 2014. [Cited: 5 December 2016.] <http://zhome.com/ZCMnL/PICS/detonation/detonation.html>.

82. www.gemeasurement.com. [Online] 2017. [Cited: 2017 Feb 13.] <https://www.gemeasurement.com/sensors-probes-transducers/depth-level/ptx-1290-series-wastewater-submersible-pressure-transmitter>.
83. www.omega.com. [Online] 2017. [Cited: 2017 Feb 13.] <http://www.omega.com/pptst/PXM42-I.html>.
84. **Sperling, Daniel**. *Future Drive*. Washington DC : Island Press, 1995.
85. **Ogburn, Michael James**. *Systems Integration, Modeling, and Validation of a Fuel Cell Hybrid Electric Vehicle*. Blacksburg, Virginia : Virginia Polytechnic Institute and State University , 2000.
86. *Rotor-stator interactions in an axial turbine, a comparison of transient and steady state frozen rotor simulations*. **Brost, V., Ruprecht, A. and Maihöfer, M.** 2003, TIB, Vol. 11, pp. 1-9.
87. *Study of Multiphase Flow at the Suction of Screw Compressor*. **Arjeneh, Mohammad, et al., et al.** London : Centre for Positive Displacement Compressor Technology, City University London, 2014.
88. **Charles Riley, Chie Kobayashi**. [www.money.cnn.com](http://money.cnn.com). [Online] 2016. [Cited: 2016 June 2016.] <http://money.cnn.com/2016/05/11/news/companies/mitsubishi-fuel-economy-tests/>.
89. *Performance Measurements of a Low Specific Speed TurboClaw Compressor*. **J Parra, R Cattell, S Etemad, K R Pullen.** 2015, 9th International Conference on Compressors and their Systems.
90. *Geometry of Screw Compressor Rotors and their tools*. **STOSIC, Nikola, et al., et al.** 2011, Journal of Zhejiang University-SCIENCE A (Applied Physics & Engineering), p. 316.

91. **Ihlemann, Arndt and Nitz, Norbert.** www.schaeffler.com. [Online] 2014.
[Cited: 13 December 2016.]
http://www.schaeffler.com/remotemedien/media/_shared_media/08_media_library/01_publications/schaeffler_2/symposia_1/downloads_11/schaeffler_kolloquium_2014_11_en.pdf.
92. *Turbine adapted maps for turbocharger engine matching.* **Tancrez, M., et al., et al.**
1, 2011, Experimental Thermal and Fluid Science, Vol. 35, pp. 146-153.

9 Appendices

9.1 Detailed transient response

Steady state simulation was carried out successfully for different configurations. The TC engine results were used in this section as the torque target at fixed engine speed. Then the time taken to reach the target for each configuration was calculated and compared to other cases. The eSC +TC (ETC) configuration is bypassed at 1800 rpm, while this value is 3200 rpm for the TC+eSC (TEC) configuration. As expected, the TC engine struggles to reach the target within a reasonable timeframe due to insufficient amount of exhaust gas. Each figure contains the torque vs time at fixed engine speed; also the time taken to reach the target for different cases is written on the graphs.

Transient simulations are based on the 2 step signals at step time of 10 seconds. It means the simulation has 10 seconds to initialize all the blocks and then it requires the full power from the eSC system (0 to full speed). The peak electric motor output torque assumed to be 1 Nm and the turbocharger inertia set to be $5e-05$ kg m². These values vary in the real applications based on the electric motor and turbocharger criteria. Figures 123 to 134 show the complete version of this study which was presented earlier in chapter 5.

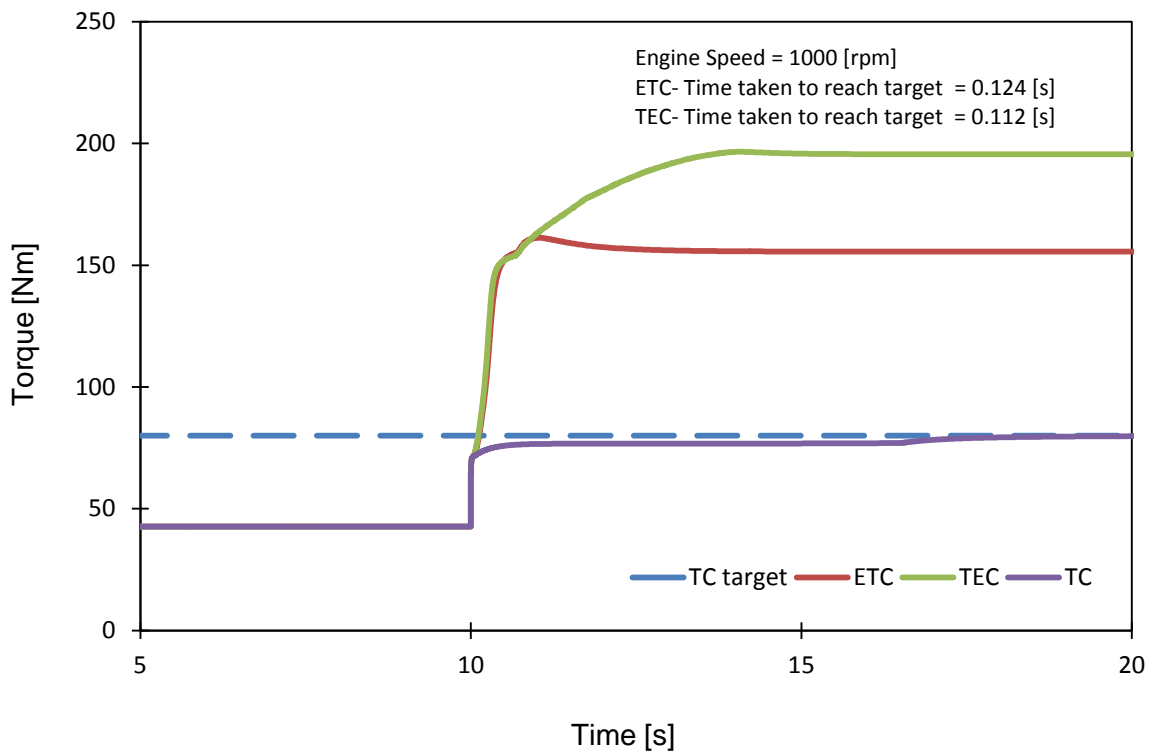


Figure 121: Torque vs time- transient response

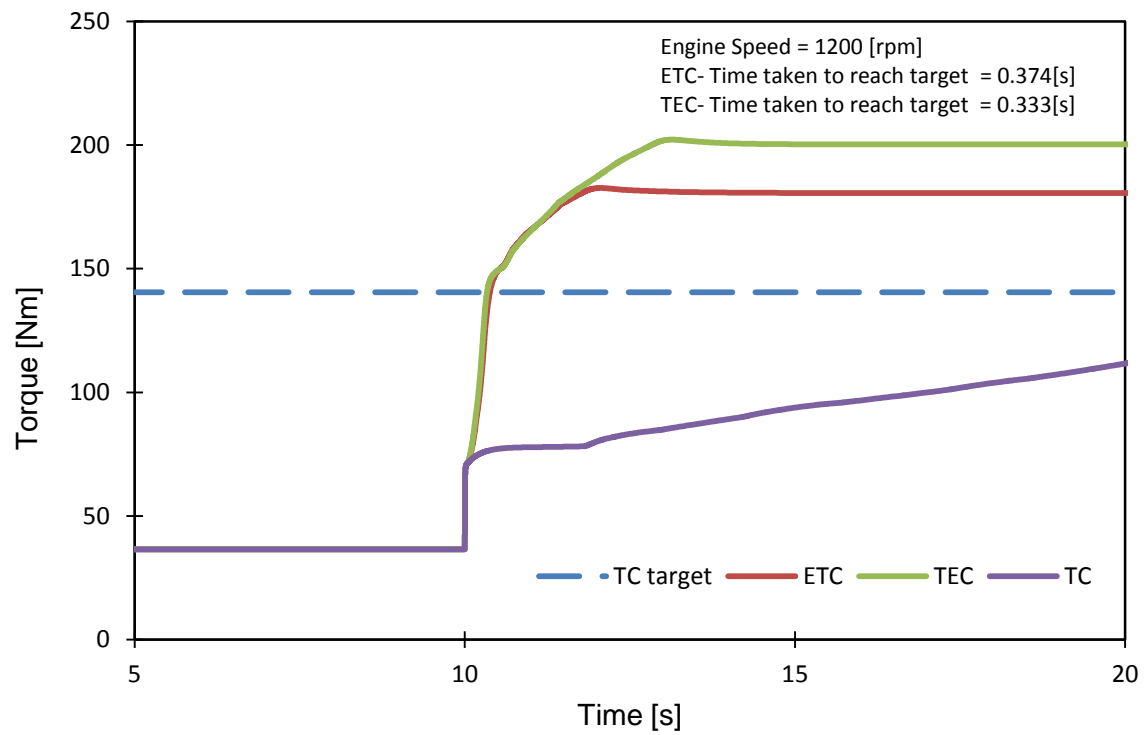


Figure 122: Torque vs time- transient response

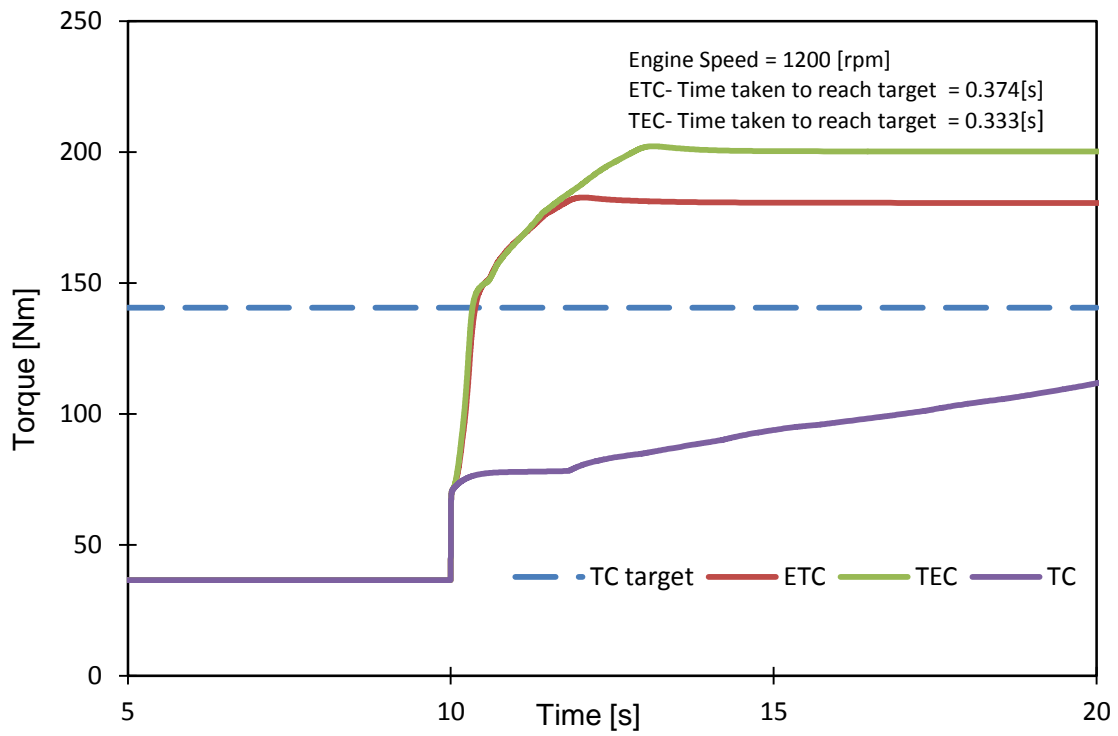


Figure 123: Torque vs time- transient response

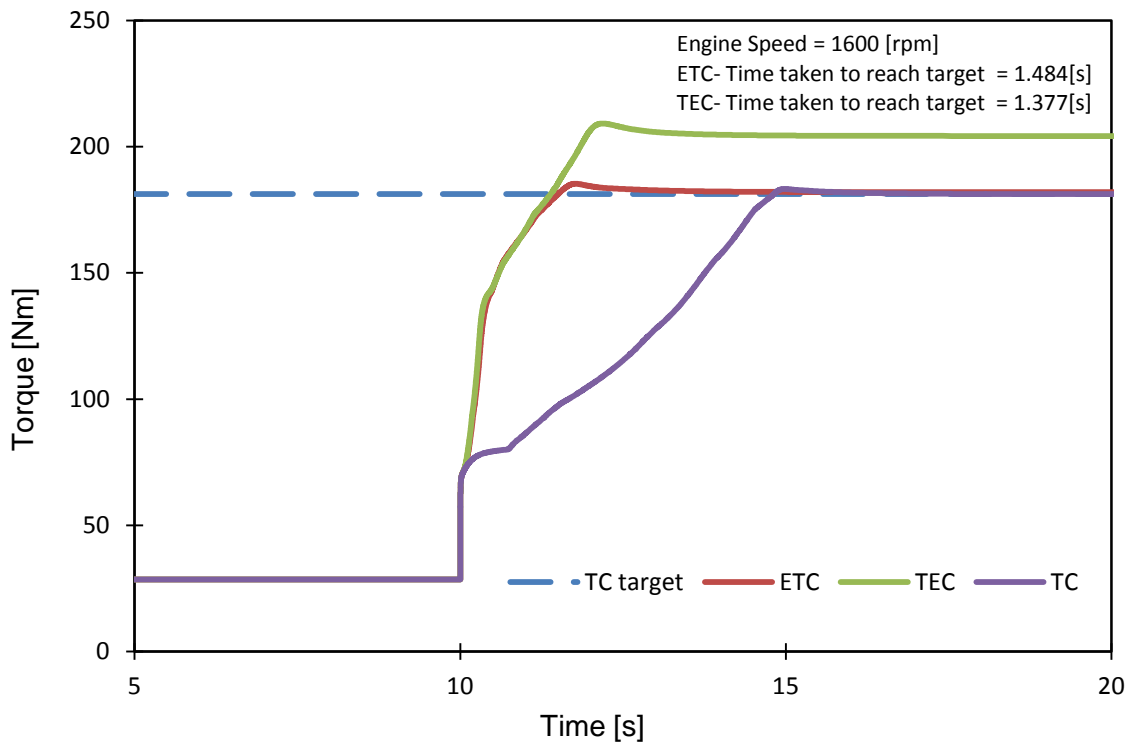


Figure 124: Torque vs time- transient response

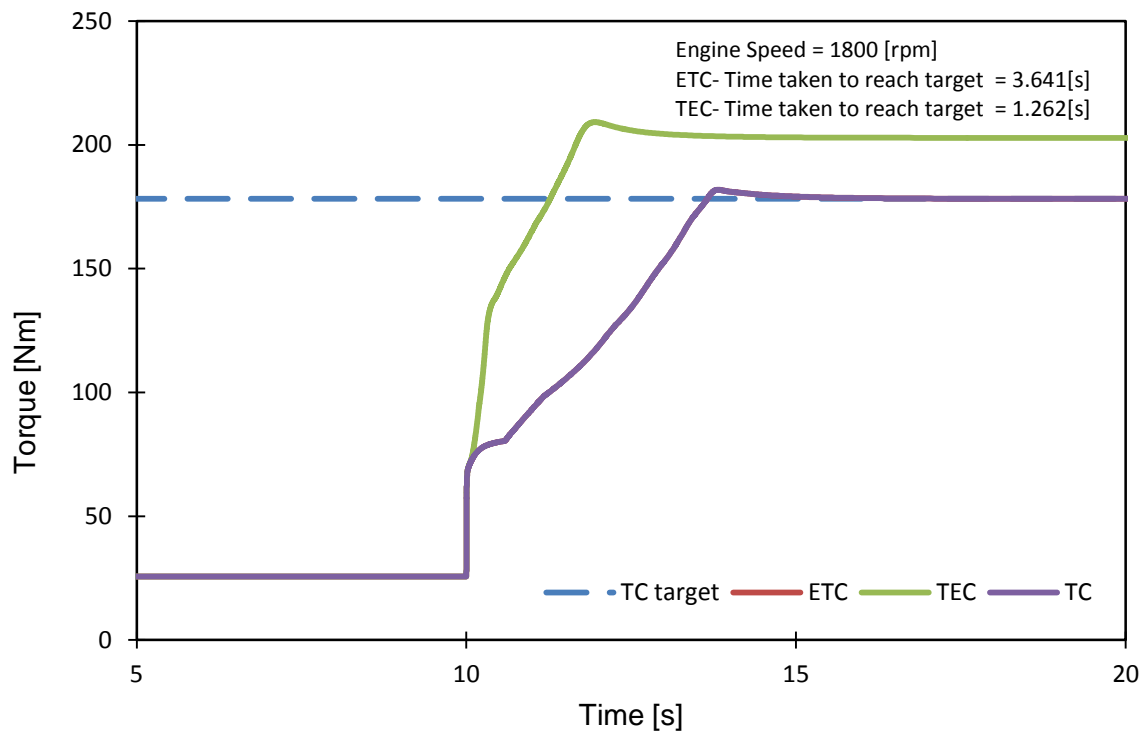


Figure 125: Torque vs time- transient response

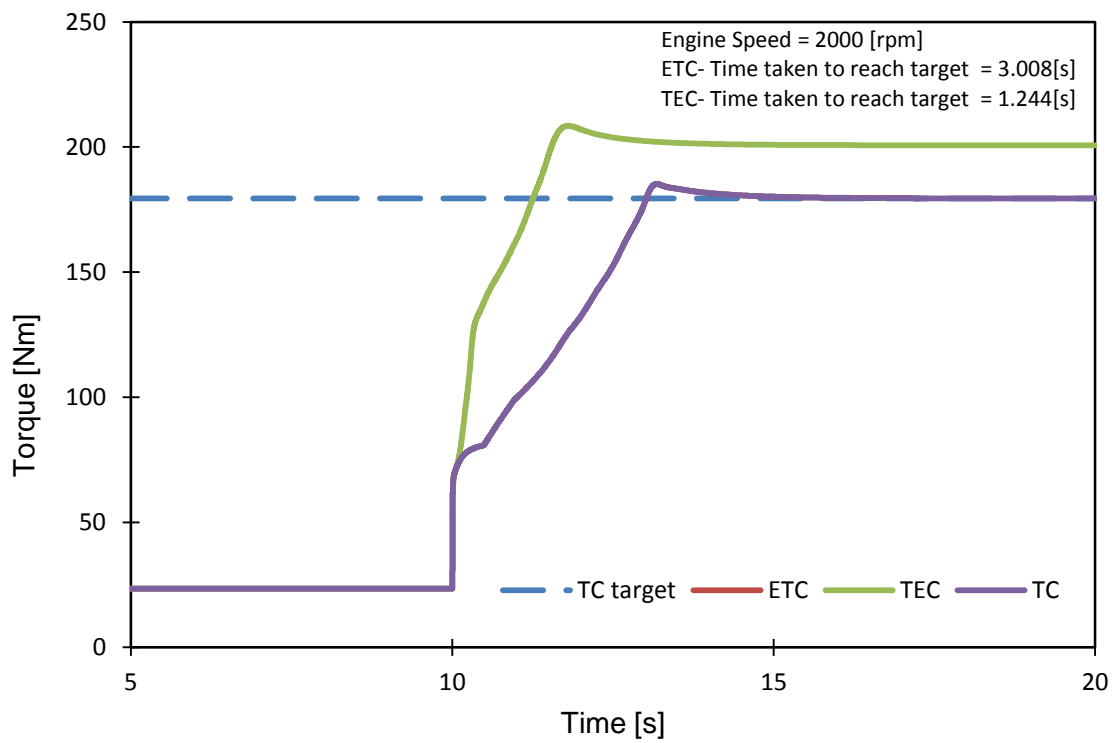


Figure 126: Torque vs time- transient response

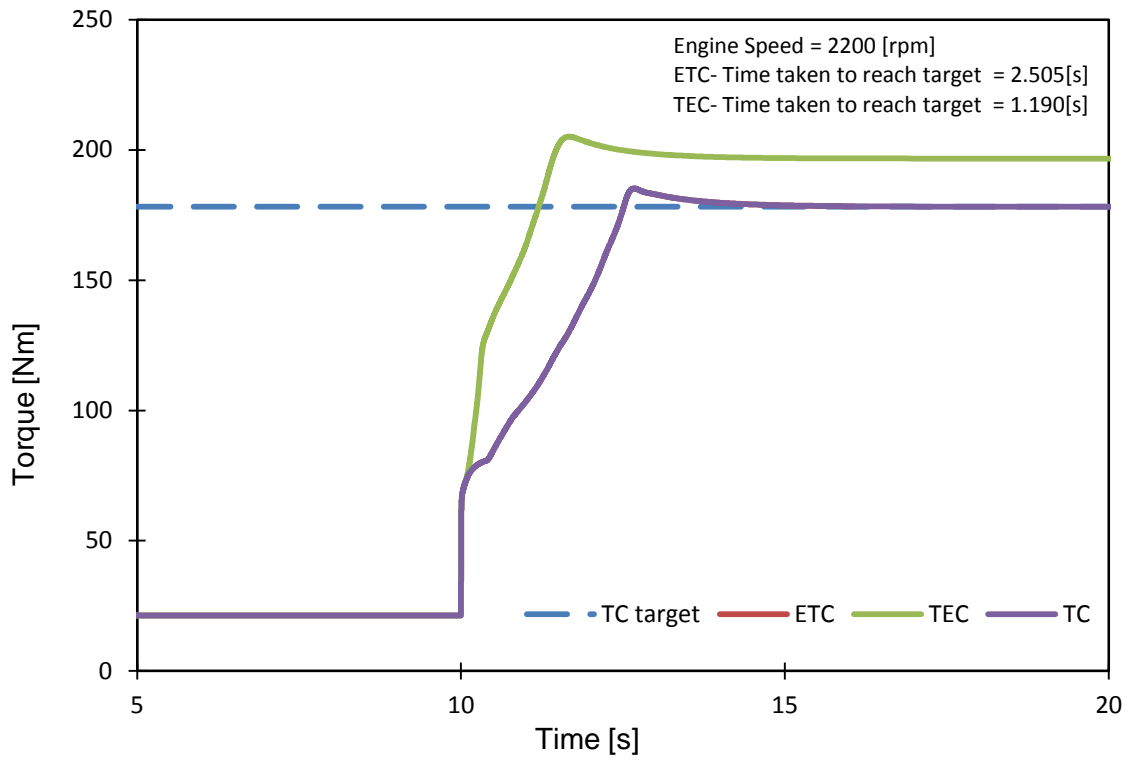


Figure 127: Torque vs time- transient response

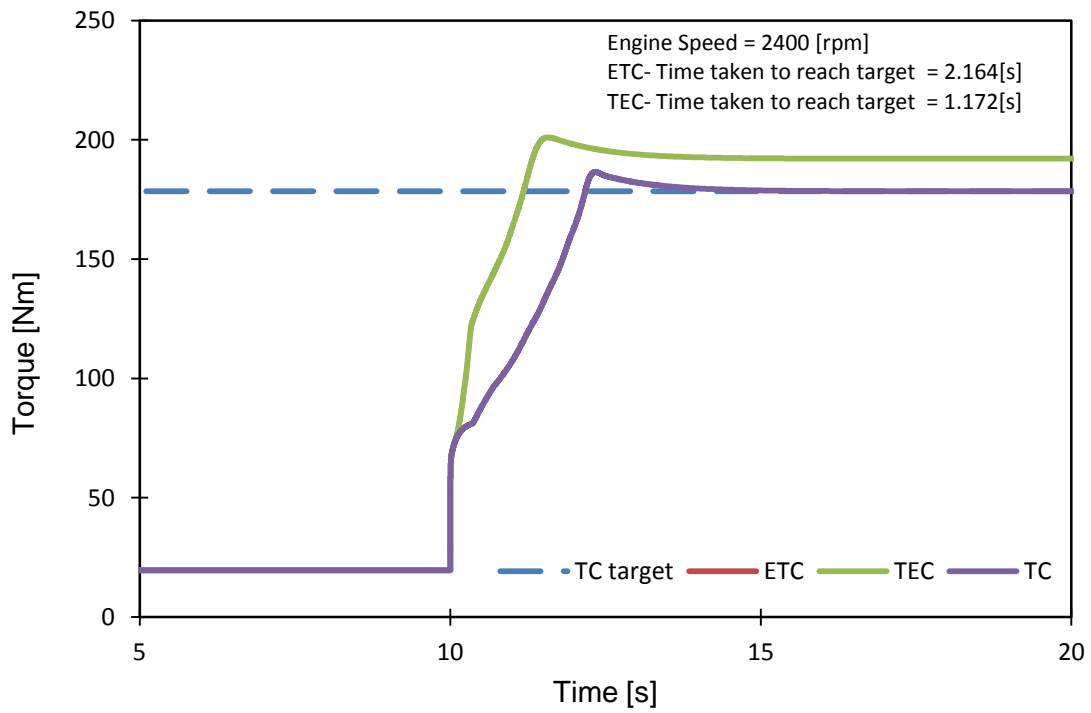


Figure 128: Torque vs time- transient response

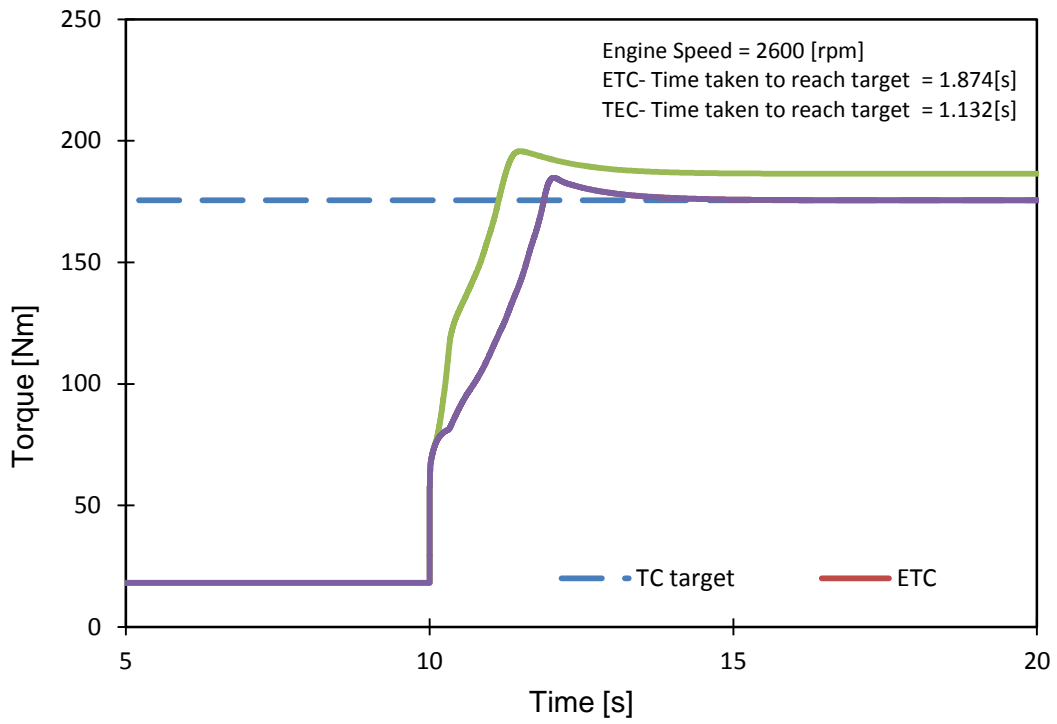


Figure 129: Torque vs time- transient response

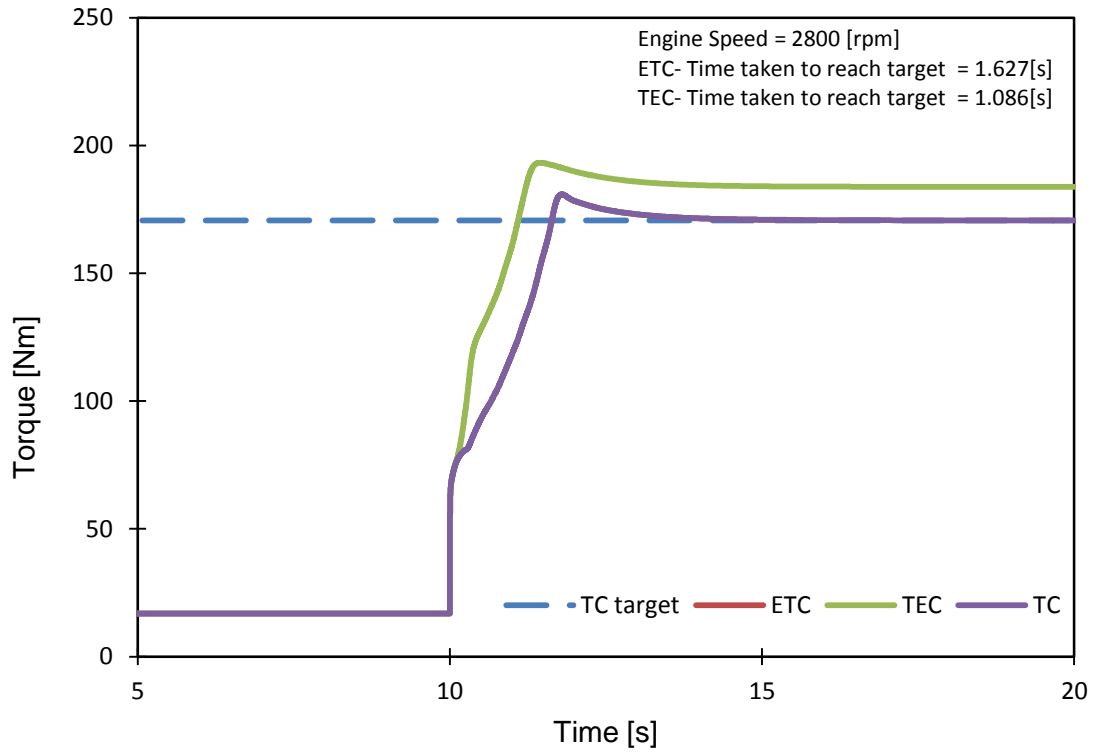


Figure 130: Torque vs time- transient response

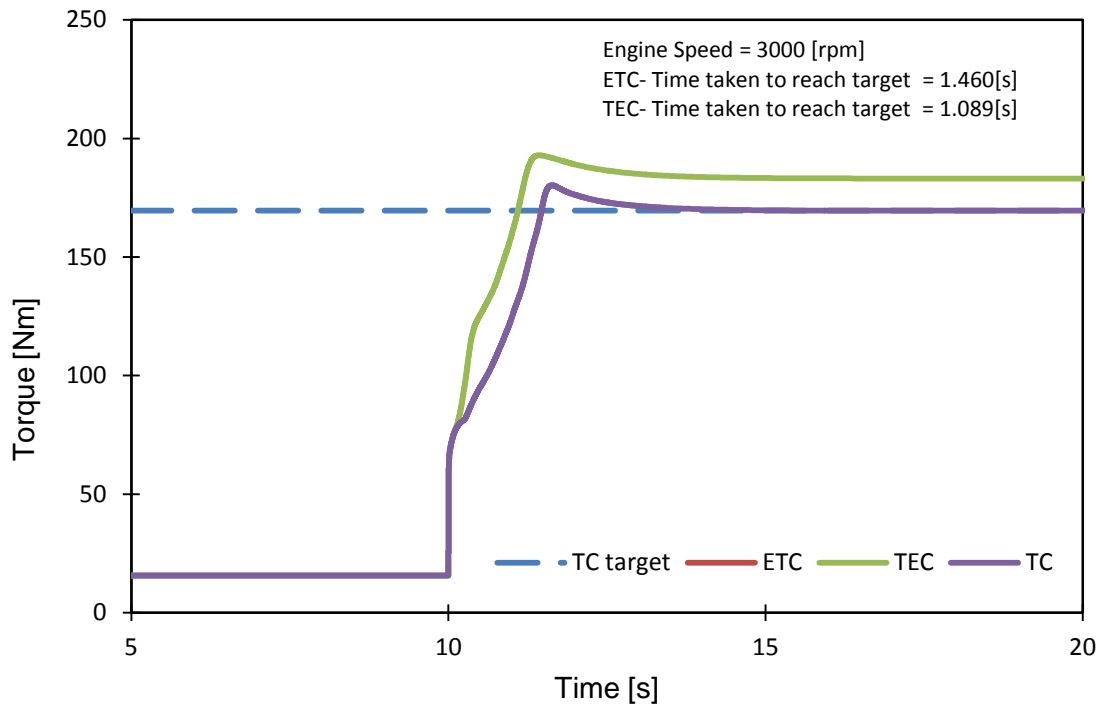


Figure 131: Torque vs time- transient response

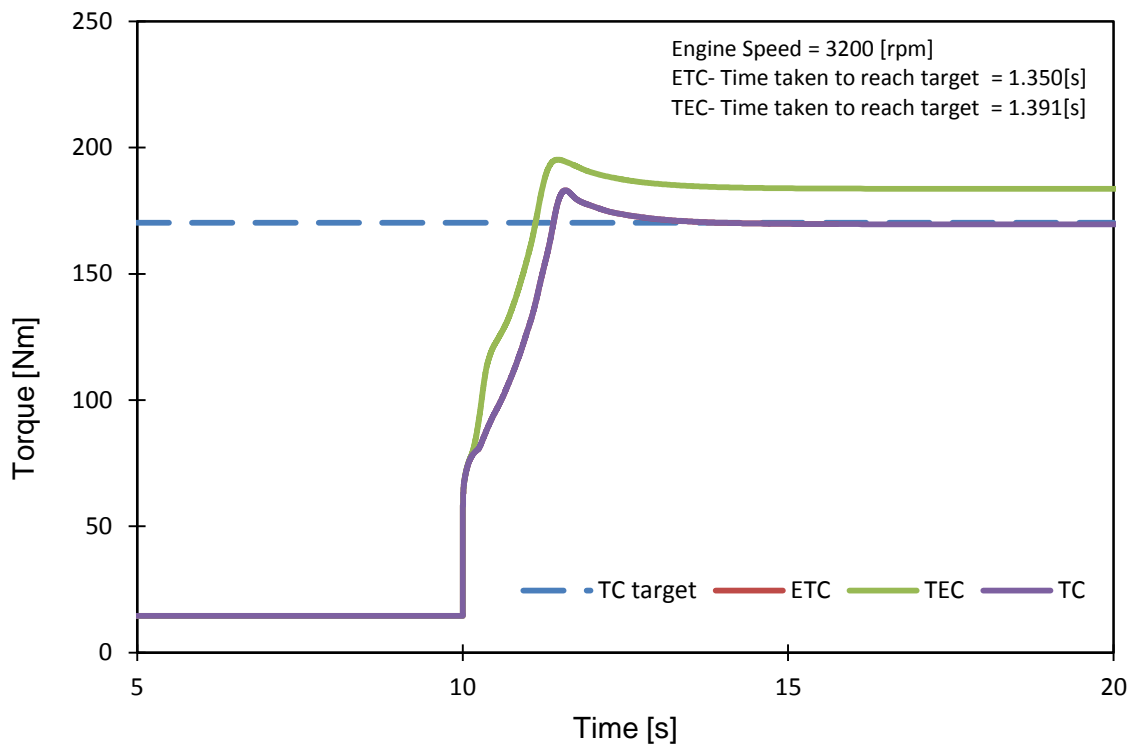


Figure 132: Torque vs time- transient response

9.2 Matlab M-File transcript to control the simulations

This section represents the codes used in M-file environment to control the simulations in Simulink environment. Most of the parameters used in this code are the constant ones. For instance the after-cooler efficiency set to be 80 percent for all the models and it is represented as “eff_ac=0.8” in the file.

The main advantage of choosing this method is that any user can amend and control the simulations according to their needs. All the Look-Up tables also can be controlled from this file. The benefit of this file is that any compressor, turbo-compressor and engine map can be embedded in to this file therefore the new results will be produced based on the new maps/data.

```
%%%%%%%%%%%%%%%%%%%%%%%%%%%%%%%%%%%%%%%%%%%%%%%%%%%%%%%%%%%%%%%%%%%%%%%%
%%
% 1. Choose layout model
% 2. Set engine speed
% 3. Choose air cooler layout by changing effectiveness value
% 4. Set all other general parameters
% 5. Open the relavite Simulink model (for TC layout, both are usable
% 6. Set Elec. Motor Torque switch for steady-state or transient
response
% 7. Run the model
%%%%%%%%%%%%%%%%%%%%%%%%%%%%%%%%%%%%%%%%%%%%%%%%%%%%%%%%%%%%%%%%%%%%%%%%
%%

clear all
close all
clc

load Engine_data
load EDS_gridfit_eta

load TC1_tcom
load TC2_turb
% load new-turboclaw
% load 75369 %1
% load 75321 %2
% load 75321-v2 %2 in the gridfitt we went up to 50 000 rpm
% load 75321-speed-upto-70000rpm % in the gridfitt we went up to 70 000
rpm

% load 20160408_EDSmassflow_75321
% load 20160408_EDSeff_75321
%%%%%%%%%%%%%%%%%%%%%%%%%%%%%%%%%%%%%%%%%%%%%%%%%%%%%%%%%%%%%%%%%%%%%%%%
%%
layout=0; % (0 for TEC; 1 for ETC; 2 for TC)
% eng_speed=1600;
```

```

eff_ic=0.0; % intercooler effectiveness (0 for bypass IC)
eff_ac=0.8; % aftercooler effectiveness (0 for bypass AC)
%%%%%%%%%%%%%%%%%%%%%%%%%%%%%%%%%%%%%%%%%%%%%%%%%%%%%%%%%%%%%%%%%%%%%%%%
%%%
Aeff=pi/4*0.05^2;

tsim=20;
pamb=100;
Tamb=300;

Jtc=5E-05;
ntc0=1000;

Jeds=5E-05;
neds0=10000;

Vd=1e-3; % Displacement Volume

%% COMPRESSORS SETPOINTS
switch layout
    case 0 % TEC p setpoint LUTs
        tc_switch=1; % (0 to bypass the EDS compressor)

%%%%%%%%%%%%%%%%%%%%%%%%%%%%%%%%%%%%%%%%%%%%%%%%%%%%%%%%%%%%%%%%%%%%%%%%
%%%NEW SETPOINT%%%%%%%%%%%%%%%%%%%%%%%%%%%%%%%%%%%%%%%%%%%%%%%%%%%%%%%%%%%%%%%%%%%%%%%%

n_lut=[800,1000,1200,1400,1600,1800,2000,2200,2400,2600,2800,3000,3100,3
200,3250:250:6250];

pr_eds_lut=[1.05,1.15,1.20,1.20,1.20,1.20,1.20,1.20,1.20,1.20,1.20,1.13,1.08,
1.03,1,ones(1,13)];

pr_tcom_lut=[1.10,1.60,1.70,1.75,1.75,1.75,1.75,1.75,1.75,1.75,1.80,1.88
,1.95,2,2.056485356 2.066945607 2.09832636 2.171548117 2.182008368
2.349372385 2.307531381 2.286610879 2.255230126 2.20292887 2.150627615
2.108786611 1.910041841];

    p_eds_setpoint_lut=pr_tcom_lut.*pr_eds_lut.*pamb;
    p_tcom_setpoint_lut=pr_tcom_lut.*pamb;

    n_lut_min=[750 1000 1250 1500 3400 6000];
    pr_eds_lut_min=[1.005 1.005 1.02 1.02 1.00 1.00];
    pr_tcom_lut_min=[1.05 1.05 1.05 1.05 1.05 1.05];

    p_eds_setpoint_lut_min=pr_tcom_lut_min.*pr_eds_lut_min.*pamb;
    p_tcom_setpoint_lut_min=pr_eds_lut_min.*pamb;

    case 1 % ETC p setpoint LUTs
        tc_switch=1; % (0 to bypass the EDS compressor)

%%%%%%%%%%%%%%%%%%%%%%%%%%%%%%%%%%%%%%%%%%%%%%%%%%%%%%%%%%%%%%%%%%%%%%%%
%%%NEW SETPOINT%%%%%%%%%%%%%%%%%%%%%%%%%%%%%%%%%%%%%%%%%%%%%%%%%%%%%%%%%%%%%%%%%%%%%%%%

n_lut=[800,1000,1200,1400,1600,1700,1800,2000:250:6250];
pr_eds_lut=[1.10,1.30,1.35,1.30,1.10,1.05,1,ones(1,18)];
pr_tcom_lut=[1.10,1.20,1.40,1.50,1.8,1.9,1.95,1.972803347
1.983263598 2.025104603 1.962343096 1.983263598 2.056485356 2.066945607

```

```

2.09832636 2.171548117 2.182008368 2.349372385 2.307531381 2.286610879
2.255230126 2.20292887 2.150627615 2.108786611 1.910041841];

```

```

p_eds_setpoint_lut=pr_eds_lut.*pamb;
p_tcom_setpoint_lut=pr_tcom_lut.*pr_eds_lut.*pamb;

```

```

n_lut_min=[750 1000 1250 1500 1750 6000];
pr_eds_lut_min=[1.005 1.005 1.02 1.02 1.00 1.00];
pr_tcom_lut_min=[1.05 1.05 1.05 1.05 1.05 1.05];

```

```

p_eds_setpoint_lut_min=pr_eds_lut_min.*pamb;
p_tcom_setpoint_lut_min=pr_tcom_lut_min.*pr_eds_lut_min.*pamb;

```

```

case 2 % only TC
tc_switch=0;

```

```

n_lut=[800 1000:250:6250];
pr_eds_lut=ones(1,numel(n_lut));
pr_tcom_lut=[1.07 1.19874477 1.491631799 1.920502092
1.89958159 1.972803347 1.983263598 2.025104603 1.962343096 1.983263598
2.056485356 2.066945607 2.09832636 2.171548117 2.182008368 2.349372385
2.307531381 2.286610879 2.255230126 2.20292887 2.150627615 2.108786611
1.910041841];

```

```

p_eds_setpoint_lut=pr_eds_lut.*pamb;
p_tcom_setpoint_lut=pr_tcom_lut.*pr_eds_lut.*pamb;

```

```

n_lut_min=[750 1000 1250 1500 1750 6000];
pr_eds_lut_min=ones(1,numel(n_lut_min));
pr_tcom_lut_min=[1.05 1.05 1.05 1.05 1.05 1.05];

```

```

p_eds_setpoint_lut_min=pr_eds_lut_min.*pamb;
p_tcom_setpoint_lut_min=pr_tcom_lut_min.*pr_eds_lut_min.*pamb;

```

```

end

```

```

%%
%%

```

```

sp=[3,3];
enginespeed_doe=[1000:200:2000];

```

```

for i=1:numel(enginespeed_doe)
eng_speed=enginespeed_doe(i);
sim ETC_v3%TEC_v3_throttle_b
A{i}=export_logsout(logsout);
TQ(i)=A{i}.TQ_eng(end); %Engine toruqe
PReds(i)=A{i}.PR_eds(end); %eSC pressure ratio
Wcorreds(i)=A{i}.Wc_eds(end); %eSC mass flow rate
Weng(i)=A{i}.W_eng(end); %Engine mass flow rate -[out]
eSCcorrectedspeed(i)=A{i}.Nc_eds(end); %eSC speed
eSCactualspeed(i)=A{i}.n_eds(end); %eSC speed-[actual]
Wactualeds(i)=A{i}.W_eds(end); %eSC mass flow -[actual]
% Pengine_in(i)=A{i}.Pin_engine(end); %eSC mass flow [actual]

```

```

spn=1;
% subplot(sp(1),sp(2),spn);spn=spn+1;
plot(A{i}.time,A{i}.TQ_eng),hold on
title('torque')
grid on
PREDS=A{i}.PR_eds; %eSC pressure ratio
WEDS=A{i}.Wc_eds; %eSC mass flow rate
NEDS=A{i}.Nc_eds;

end
%% plot
spn=1;
figure,
subplot(sp(1),sp(2),spn);spn=spn+1;
plot(enginespeed_doe,TQ,'-*'),hold on
title('Engine Torque')
xlabel ('Engine speed [rpm]')
ylabel ('Torque [Nm]')
grid on

spn=2;
subplot(sp(1),sp(2),spn);spn=spn+1;
plot(enginespeed_doe,Weng,'-*'),hold on
title('Engine mass flow rate-[out]')
xlabel ('Engine speed [rpm]')
ylabel ('mass flow rate [kg/s] ')
grid on

spn=3;
subplot(sp(1),sp(2),spn);spn=spn+1;
plot(enginespeed_doe,eSCactualspeed,'-*'),hold on
title('eSC speed [actual]')
xlabel ('Engine speed [rpm]')
ylabel ('eSC speed [rpm] ')
grid on

spn=4;
subplot(sp(1),sp(2),spn);spn=spn+1;
plot(enginespeed_doe,Wactualeds,'-*'),hold on
title('eSC mass flow rate [actual]')
xlabel ('Engine speed [rpm]')
ylabel ('eSC mass flow rate [kg/s] ')
grid on

spn=5;
subplot(sp(1),sp(2),spn);spn=spn+1;
% plot(enginespeed_doe,Pengine_in,'-*'),hold on
title('Engine input pressure')
xlabel ('Engine speed [rpm]')
ylabel ('Pressure ratio [-] ')
grid on

```

```

spn=6;
subplot(sp(1),sp(2),spn);spn=spn+1;
plot(enginespeed_doe,eSCcorrectedspeed,'-*'),hold on
title('eSC speed- [corected]')
xlabel ('Engine speed [rpm]')
ylabel ('eSC speed [rpm] ')
grid on

spn=7;
subplot(sp(1),sp(2),spn);spn=spn+1;
plot(enginespeed_doe,Wcorreds,'-*'),hold on
title('eSC mass flow rate corrected')
xlabel ('Engine speed [rpm]')
ylabel ('eSC mass flow rate [kg/s] ')
grid on

%%%%%%%%%%%%%%%%%%%%%%%%%%%%%%%%%%%%%%%%%%%%%%%%%%%%%%%%%%%%%%%%%%%%%%%%
load COM_exp
% load EDS_gridfit_eta
load new_surge_line
load reshaped_eds_data
% load Engine_data
% load EDS_gridfit_eta
% load TC1_tcom
% load TC2_turb

% latest compressor map from warren
figure,
%
contourf(eds_massflow,eds_pressure_ratio,eds_efficiency,'linestyle','none');
contourf(masscomp_exp,PRcomp_exp,Comp_eff_val,'linestyle','none');
% colormap autumn

hold on
plot(Wcorreds,PReds , 'b-*', 'linewidth',2), % shows the pr vs mass flow
(blue line)
title('PR VS Wcorr')

hold on
plot(w_e_ch,pr_e_ch , 'black', 'linewidth',2 , 'marker', 'none'), % chocke
line

hold on
% plot(new_surge_line_mass,new_surge_line_PR , 'black', 'linewidth',2), %
surge line
plot(w_e_su,pr_e_su , 'black-*', 'linewidth',2, 'marker', 'none'),

hold on
% plot(eds_massflow,eds_pressure_ratio, 'black'); % speed lines
plot(masscomp_exp,PRcomp_exp, 'black'); % speed lines

```



```

clear all
close all
clc
data=xlsread('new75321gridfit','eff');
x=data(51:end,1);
y=data(51:end,2);
z=data(51:end,3);
% x=x(z>0.015);
% y=y(z>0.015);
% z=z(z>0.015);
% x=x(y>1);
% z=z(y>1);
% y=y(y>1);

% X=60000:10000:250000;
% Y=1:0.2:4;
X=linspace(0,60000,35);
Y=linspace(0,0.02,35);

% Y is the variable
Z=gridfit(x,y,z,X,Y,'smooth',5);

Z(Z<0)=0;
Z(Z>1)=1; %this is for efficiency only

% [r,c]=size(Z);
% for i=1:r
%     for j=1:c
%         if Z(i,j)<0
%             Z(i,j)=0;
%         end
%     end
% end

figure,
mesh(X,Y,Z),colormap cool
hold on
plot3(x,y,z,'r*')

figure,
plot(Y,Z,y,z,'r*'),

e2_e=Z;e2_e_N=X;e2_e_w=Y;
save('20160408_EDSeff_75321','e2_e','e2_e_N','e2_e_w')

```

```

function sim_output = export_logstdout(logsout)
sim_output = struct;
recursivelyExpandInBase(logsout);

function recursivelyExpandInBase(log)
class = log.class;
try
    switch class
    case
        {'Simulink.ModelDataLogs', 'Simulink.SubsysDataLogs'}
            %fprintf('%s : found a subsys\n', logName);
            logNames = {log.whos.name};
            for iName = 1:length(logNames)
                logName = logNames{iName};
                logName = strrep(logName, '(', '');
                logName = strrep(logName, ')', '');
                newLog = log.(logName);
                %fprintf('recursing into Level %s\n', logName);
                recursivelyExpandInBase(newLog);
            end
        case 'Simulink.TsArray'
            members = log.Members;
            for member = members
                name = member.name;
                newLog = log.(name);
                %fprintf('recursing into Member %s\n', name);
                recursivelyExpandInBase(newLog)
            end
        case 'Simulink.Timeseries'
            logName = log.Name;
            logName = strrep(logName, '(', '');
            logName = strrep(logName, ')', '');
            dataVariableName = logName;
            dataVariableName = strrep(dataVariableName, '<', '');
            dataVariableName = strrep(dataVariableName, '>', '');
            dataVariableName = strrep(dataVariableName, ' ', '');
            dataVariableName = strrep(dataVariableName, '-', '');
            dataVariableName = strrep(dataVariableName, '&', '');
            dataVariableName =
                strrep(dataVariableName, '', '_dot');
            data = log.Data;
            data = squeeze(data);
            if size(data,2) > size(data,1) % not sure I need
                this
                    data = data';
            end
            %fprintf('Assigning %s\n', dataVariableName);
            % decimatedData = data(1:step:end,:);
            % assignin('base', dataVariableName, decimatedData
        );
            sim_output.(dataVariableName) = data;
        otherwise
            % Don't have any truck with other stuff.
    end
catch exception
    exception.message
end

```

```
end
end
```

```
%%%%%%%%%%%%%%%%%%%%%%%%%%%%%%%%%%%%%%%%%%%%%%%%%%%%%%%%%%%%%%%%%%%%%%%%%
```

```
clear all
close all
clc
data=xlsread('new75321gridfit','m');
x=data(51:end,1);
y=data(51:end,2);
z=data(51:end,3);
% x=x(z>0.015);
% y=y(z>0.015);
% z=z(z>0.015);
% x=x(y>1);
% z=z(y>1);
% y=y(y>1);

% X=60000:10000:250000;
% Y=1:0.2:4;
X=linspace(0,60000,35);
Y=linspace(1,1.7,35);

% Y is the variable
Z=gridfit(x,y,z,X,Y,'smooth',5);
Z(Z<0)=0;
% Z(Z>1)=1; this is for efficiency only

% [r,c]=size(Z);
% for i=1:r
%     for j=1:c
%         if Z(i,j)<0
%             Z(i,j)=0;
%         end
%     end
% end
```

9.3 Simulation blocks and flowcharts

9.3.1 Summary of Cylinder Block

An overview of the Cylinder block is presented in Figure 135. Mass flow rate and engine speed are the inputs, engine torque, mass flow rate-out and temperature are the outputs of the system. Figure 136 shows the cylinder flow-charts .

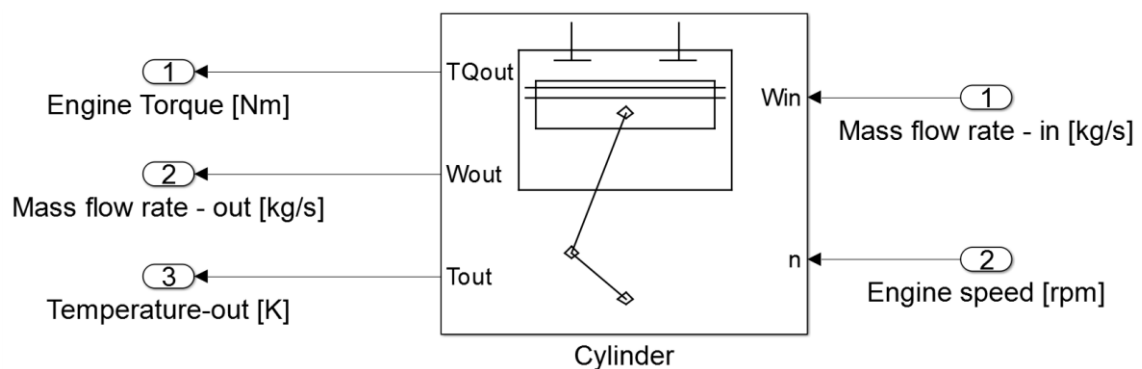
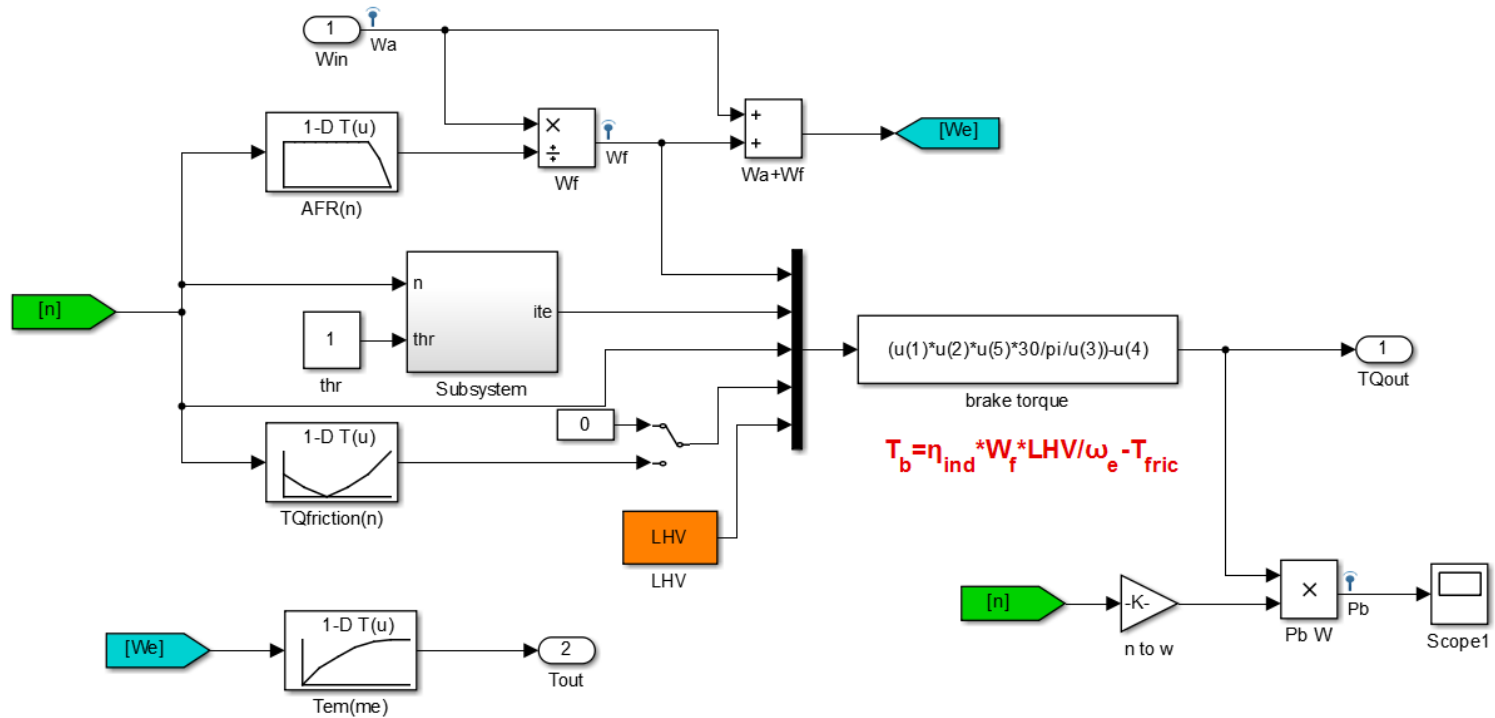


Figure 133: Cylinder block overview



Where:
 Tout: Output temperature
 TQout: Torque
 Win: Input massflow rate
 We: Engine output mass flow rate
 n: Engine speed
 thr: Throttle position, 1 is fully open and 0 is fully closed
 LHV Net calorific value

Figure 134: Cylinder flow-charts

9.3.1.1 Summary of Throttle Block

An overview of the throttle block is shown in Figure 137. Effective throttle area, inlet pressure, outlet pressure and inlet temperature are inputs, mass flow rate and temperature are the outputs of the sub-system. The throttle flow-charts can be seen in Figure 138.

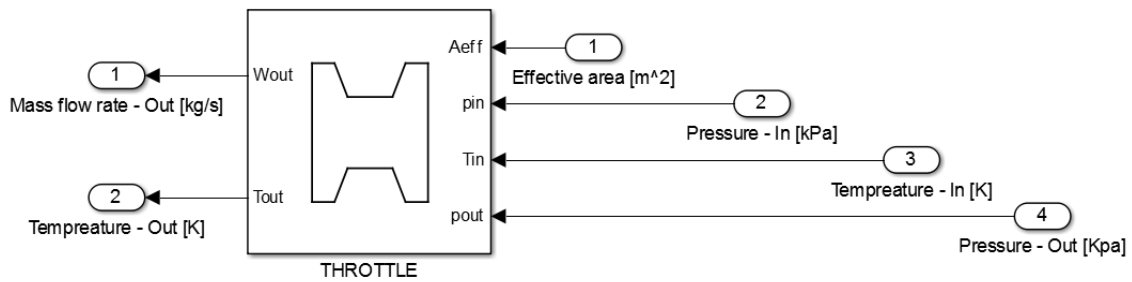
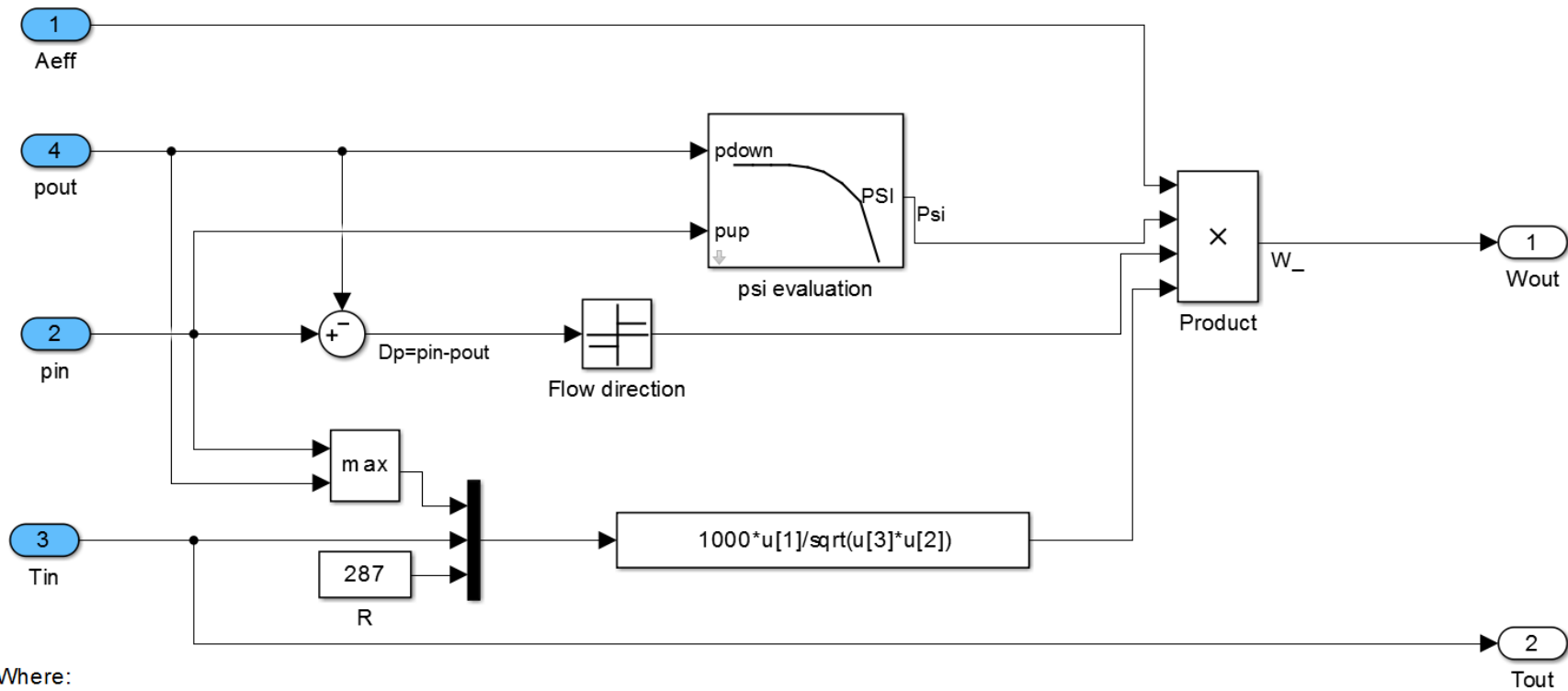


Figure 135: Throttle block overview



Where:

R: Gas constant

pin: Inlet pressure

Tin: Inlet temperature

Tout: Outlet temperature

pout: Outlet pressure

Aeff: Effective area = $\pi/4 \cdot 0.05^2$ [m²]

Wout: Outlet mass flow rate

Note that temperature is assumed to be constant during throttle

Figure 136: Throttle valve flowchart

9.3.2 Summary of Connecting Volume Blocks

The inputs of the sub-system are mass flow rate of the previous block, temperature of the previous block, output temperature of the pipe (as shown in Figure 139) and the mass flow rate of the next block fed in the system. The outputs of the sub-systems are pressure and temperature where the temperature is fed back to the pipe as an inlet temperature 2 (T2).

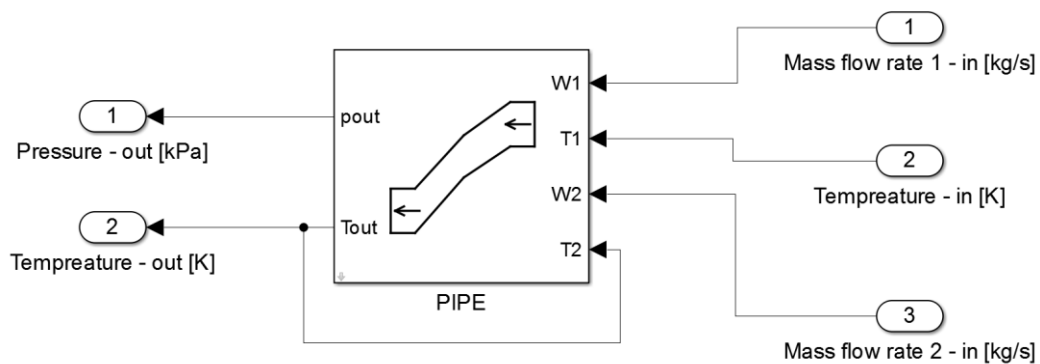


Figure 137: Connecting volumes (adiabatic pipe) block overview

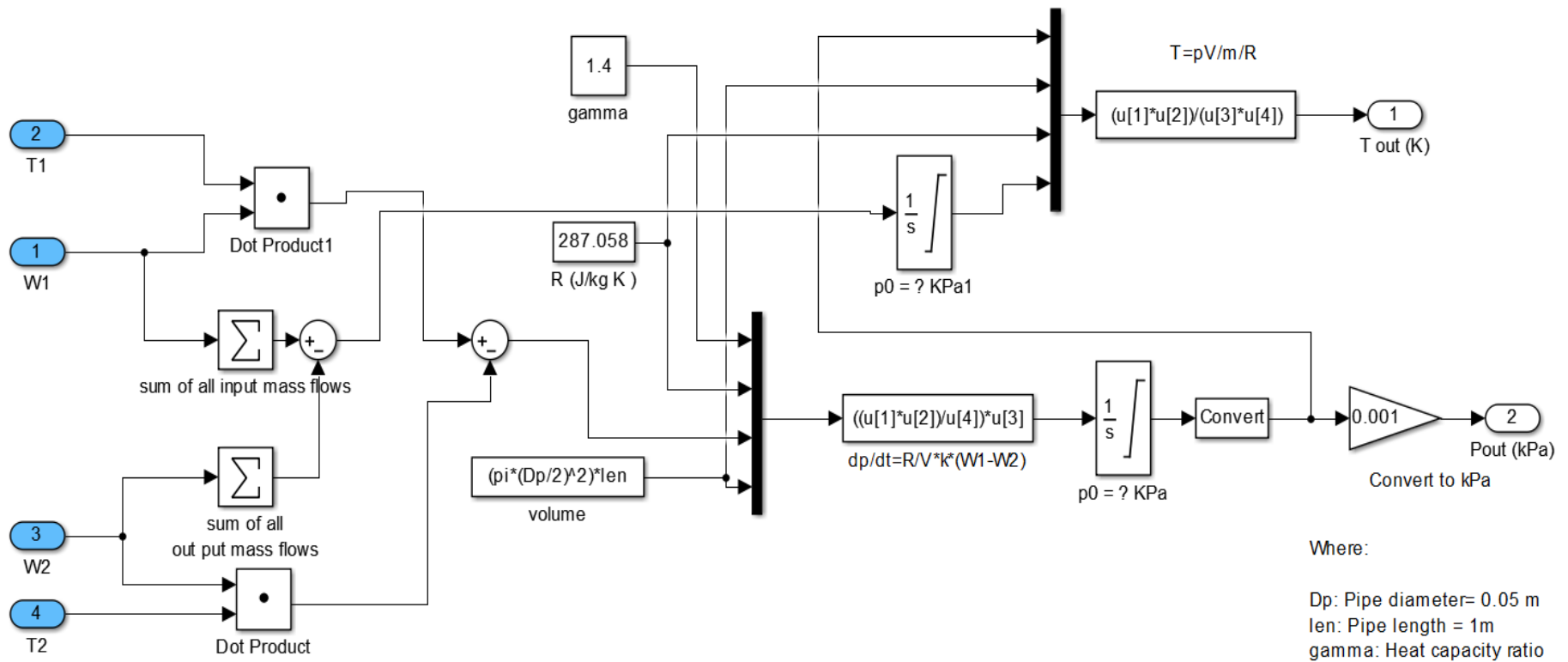


Figure 138: Connecting volumes (adiabatic pipe) flow-chart

4.2.1.1 Summary of Electric Supercharger Compressor Block

Figure 141 shows an overview of electric supercharger compressor block. The same methodology is also taken towards designing the turbocharger compressor. The main differences between two blocks are the look-up tables; the TurboClaw data was used for eSC unit while the turbo-compressor was chosen based on the TurboClaw performance. Figure 142 displays the eSC compressor flow-charts.

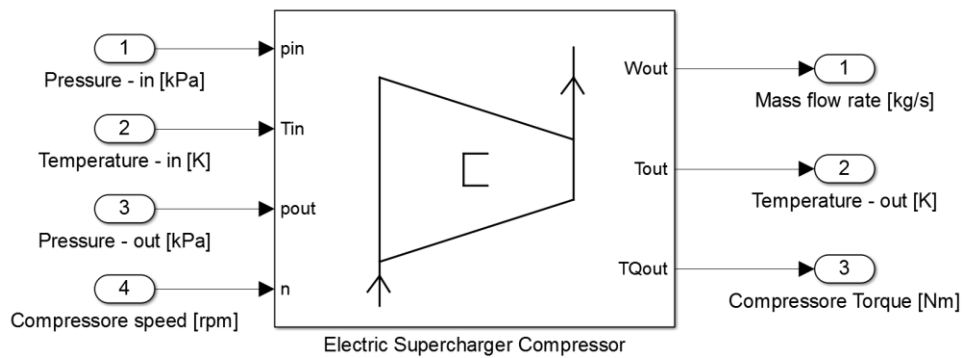


Figure 139: eSC compressor block overview

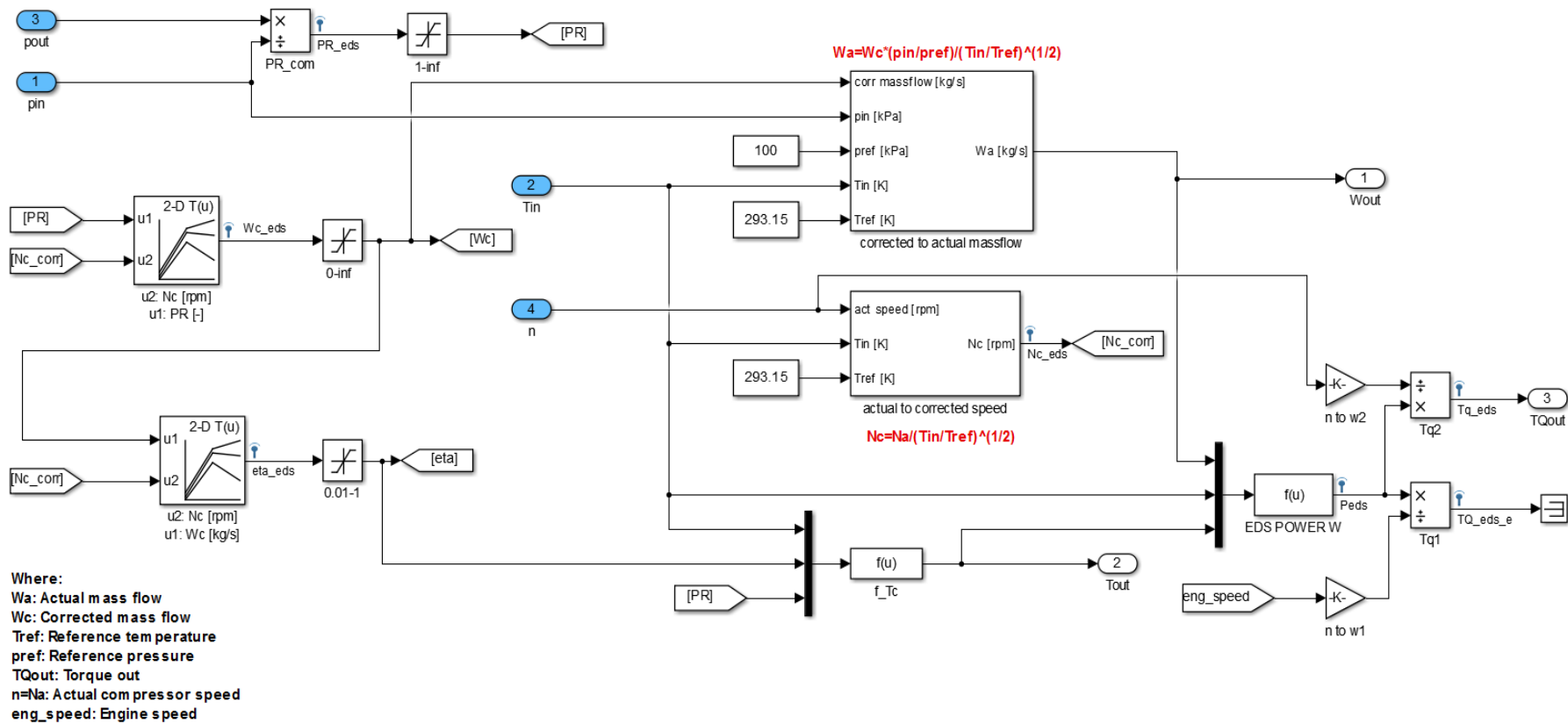


Figure 140 : eSC compressor flow-chart

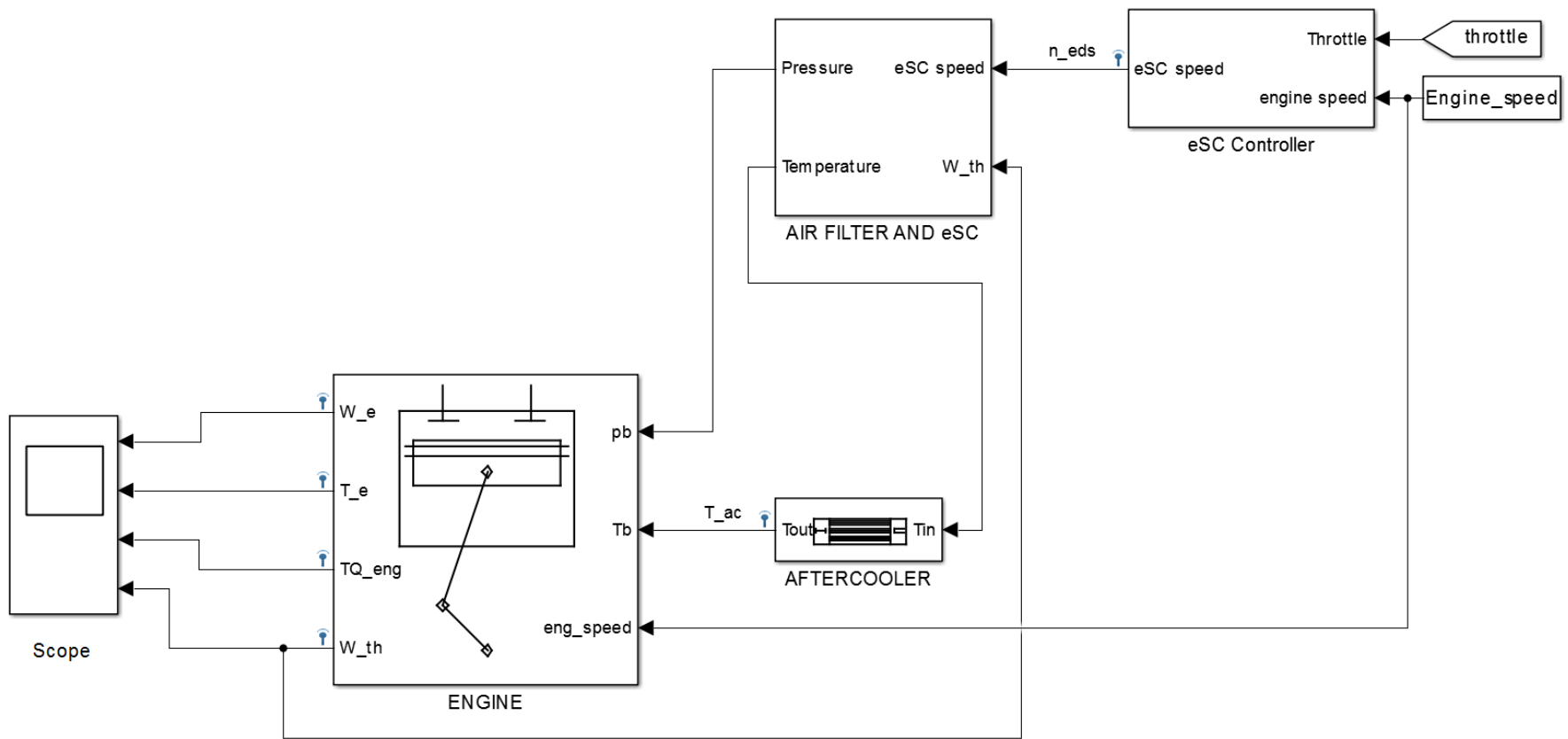


Figure 141 : eSC Engine simulation layout

	1000	1500	2000	2500	3000	3500	4000	4500	5000	5500	6000
40	0.673944181...	0.665961036...	0.670054596...	0.673855558...	0.702241745...	0.719871332...	0.747400209...	0.784899061...	0.823465624...	0.838137590...	0.841124118...
63.3333...	0.685823580...	0.643808926...	0.660845749...	0.724273180...	0.758753536...	0.786514036...	0.795577690...	0.825485527...	0.846316798...	0.865421706...	0.878557897...
86.6666...	0.803761066...	0.783906746...	0.784077020...	0.834910451...	0.869442333...	0.873741947...	0.870969236...	0.882132040...	0.892968490...	0.893229544...	0.893130360...
110	1.039871996...	1.029724117...	1.007541208...	0.968422118...	0.964501323...	0.950622249...	0.946746962...	0.933627692...	0.929131312...	0.911873751...	0.892950658...
133.3333...	1.198680208...	1.132045527...	1.084311775...	1.034428940...	1.008227550...	0.988374225...	0.972520624...	0.954748743...	0.935267526...	0.921521895...	0.903835841...
156.6666...	1.282822316...	1.197209718...	1.087328363...	1.039842729...	1.011973798...	0.997426998...	0.981462219...	0.959522400...	0.940054845...	0.931771662...	0.925894415...
180	1.281483065...	1.192251543...	1.079883099...	1.034739204...	1.015588468...	0.991779358...	0.973724868...	0.954739890...	0.938648986...	0.938604301...	0.947666592...
203.3333...	1.219553352...	1.129325877...	1.072883708...	1.032709645...	0.999730178...	0.975247046...	0.960655040...	0.946927631...	0.937278781...	0.931628566...	0.946916211...
226.6666...	1.145060994...	1.092432085...	1.055725556...	1.024610604...	0.995634205...	0.968743902...	0.950718569...	0.933284465...	0.936092188...	0.902620946...	0.887950639...
250	1.072248503...	1.055427641...	1.036926913...	1.015177103...	0.990249490...	0.963549810...	0.937772542...	0.914303111...	0.897536499...	0.870226195...	0.835950479...

Table 14: Volumetric efficiency as a function of Manifold pressure and engine speed

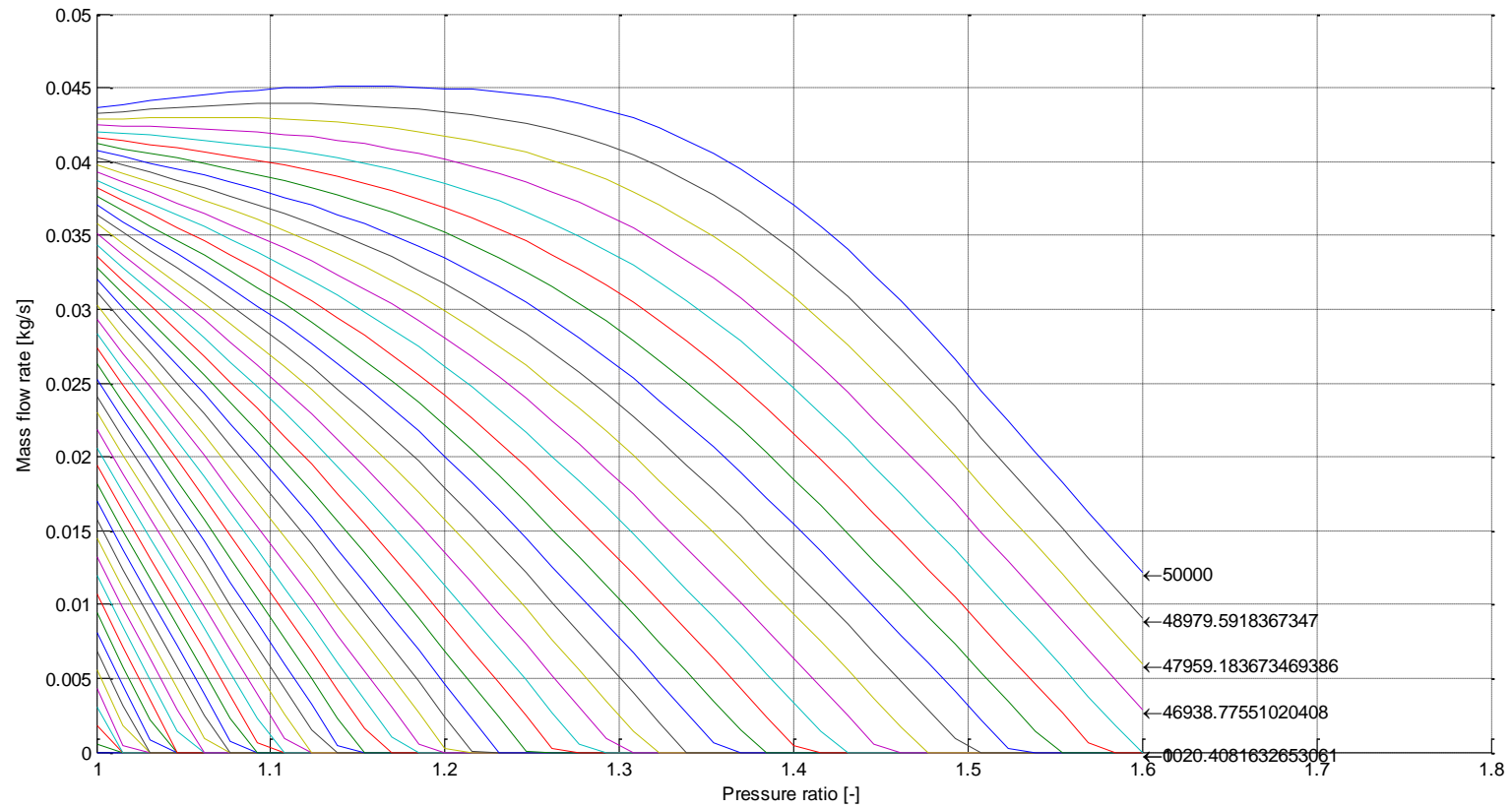


Figure 142: TurboClaw 2-D mass flow rate map as a function of compressor speed and pressure ratio

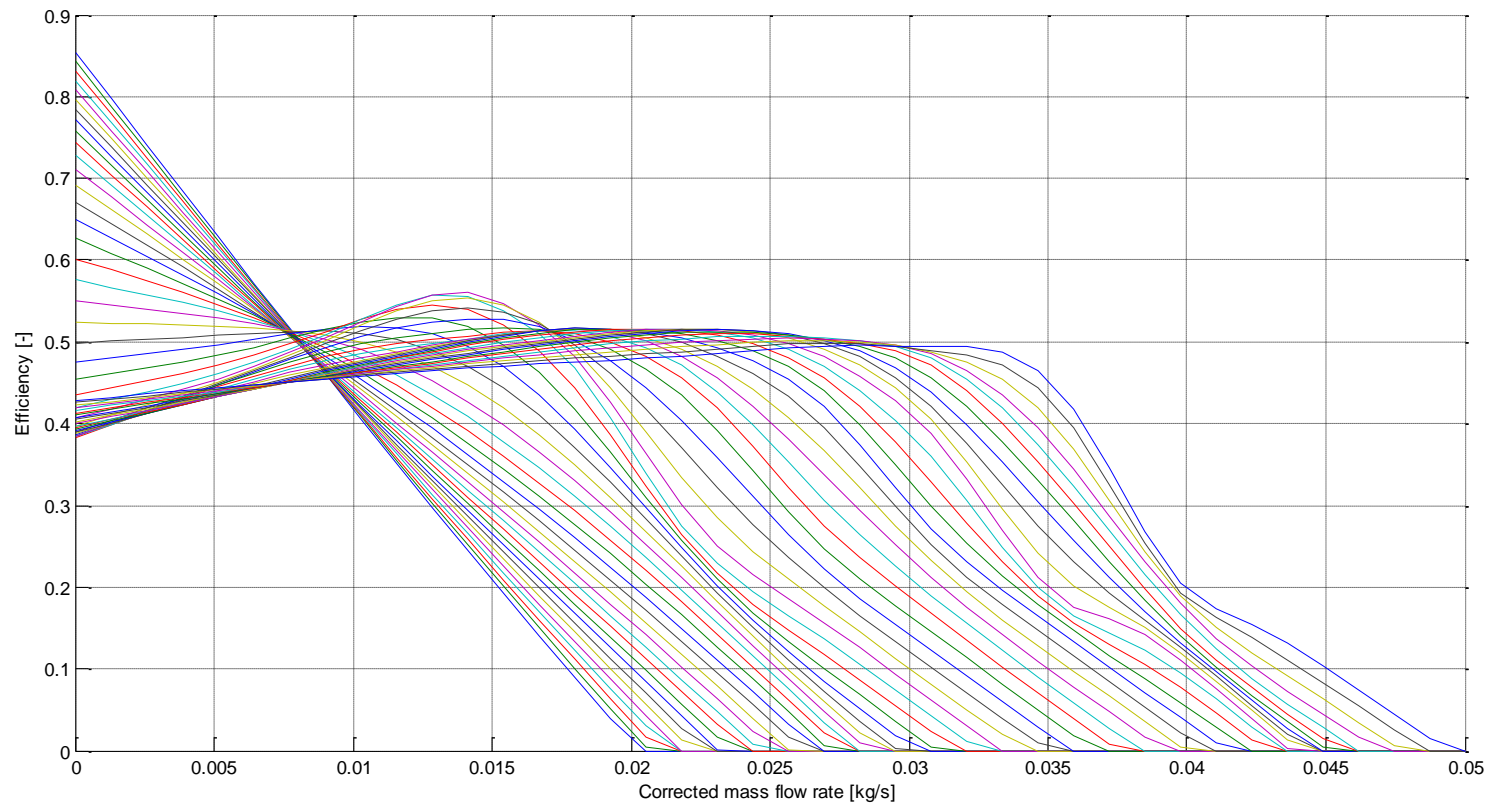


Figure 143: Figure 144: TurboClaw 2-D efficiency as a function of compressor speed and pressure ratio- 2D map

Wheel						
Engine capacity of vehicle [L]	1	1.2	1.4	1.6	1.8	2
Wheel inertia [kgm ²]	0.815	0.815	0.815	0.815	0.815	0.815
Rolling resistance coefficient	0.009	0.009	0.009	0.009	0.009	0.009
Tyre radius [m]	0.317	0.317	0.317	0.317	0.317	0.317
Wheel coefficient of friction	0.7	0.7	0.7	0.7	0.7	0.7

Table 15: Wheel parameters

Transmission (manual)					
Gear number	1st	2nd	3rd	4th	5th
Gear ratio	3.25	1.81	1.21	0.86	0.64
Final drive	4.06	4.06	4.06	4.06	4.06

Table 16: Manual transmission parameters

Engine + Vehicle						
Engine capacity [L]	1	1.2	1.4	1.6	1.8	2
Max power [kW]	50	60	70	80	90	100
Thermal efficiency	0.3	0.3	0.3	0.3	0.3	0.3
Drag coefficient	0.29	0.29	0.29	0.29	0.29	0.29
Frontal area [m ²]	2.07	2.07	2.07	2.07	2.07	2.07
Kerb mass [kg]	1274	1301	1328	1356	1383	1410
Vehicle centre of gravity height [m]	0.5	0.5	0.5	0.5	0.5	0.5
Drive axle weight distribution	0.6	0.6	0.6	0.6	0.6	0.6
Wheel base [m]	2.59	2.59	2.59	2.59	2.59	2.59
Driver mass [kg]	80	80	80	80	80	80
Mass of vehicle + driver [kg]	1354	1381	1408	1436	1463	1490

Table 17: engine and vehicle parameters

